Modelling dispersal and connectivity of broadcast spawning corals in the Western Indian Ocean

Majambo J. Gamoyo

Department of Oceanography
University of Cape Town

Thesis Presented for the Degree of
Doctor of Philosophy

University of Cape Town October 2018

I would like to dedicate this thesis to my loving mum ...

Declaration

I hereby declare that except where specific reference is made to the work of others, the contents of this dissertation are original and have not been submitted in whole or in part for consideration for any other degree or qualification in this, or any other university. This dissertation is my own work and contains nothing which is the outcome of work done in collaboration with others, except as specified in the text and Acknowledgements.

Majambo J. Gamoyo
October 2018

Acknowledgements

First and foremost, I would like to thank the Almighty for giving me the strenght, good health and insight to persue this PhD. I would also like to acknowledge and thank my supervisor Professor Chris Reason for the opportunity and for his continued support and guidance, your critical eye has improved this work to the end, and I am most grateful for all the opportunities that you afforded me. Dr. David Obura, the exceptional scope of your knowledge on coral reefs, your imagination and enthusiasm has been nothing short of inspiring, while your constructive and honest feedback (especially with regard to manuscript drafts!) has been invaluable. I am grateful to Dr. Issufo Halo and Dr. Charine Collins, for all the assistance they provided while setting up the Regional Ocean Modelling System (ROMS) and validation process. All the valuable discussions we had have undoubtedly enhanced the quality of this work. I am extremely grateful to all of them for patiently sharing their expertise and for tolerating my constant barrage of questions. To my friends of the square (Daneeja Mawren, Obadius Cossa, Catherine and Jerome 'General'), thank you for all the animated discussions we shared and for playing an integral part in keeping me motivated and excited about coding. Last, but definitely not least I want to thank my family for their support. I am especially grateful to my mom and sisters for believing in me even when I did not and for always being there when needed. To my dear wife 'Schamim' who has been largely responsible for preserving my sanity, at considerable cost to her own; without your unerring encouragement, inexhaustible patience, I would never have made it this far. Lastly to my beautiful daughter 'Siti', though I was away part of your first year, I can't wait to see you follow your fathers footsteps.

Abstract

Coral reef degradation is happening at an alarming rate all over the world due to multiple stressors with elevated sea surface temperature being the root cause. Using the Regional Ocean Modelling System and an individual-based model for the western Indian Ocean, this thesis explored the general circulation patterns (both large and mesoscale) important to dispersal and connectivity of broadcast corals while identifying regions that act as a source of larvae and those that receive larvae. Because habitat destruction and fragmentation through severe bleaching and mortality threaten coral reef health, projected thermal stress from Global Climate Models was explored to quantify future bleaching scenarios that might impact the reproductive timing and larval dispersal.

Evaluation of the ROMS configuration for the western Indian Ocean shows that the basin-scale circulation patterns of the region are appropriately captured with the mean volume transports consistent with those derived from observation. Using the eddy detection algorithm, a description of the Southern Gyre as a key aspect of the Somali Current system was identified. The Southern Gyre is associated with barotropic instabilities associated with the northward flowing Somali Current. Rossby waves arriving at the East African coast and the strength of the monsoon winds are also responsible for the evolution and intensification of the gyre.

The aggregated trajectories from the Lagrangian model highlight the dominant dispersal pathways and barriers to dispersal following release. The general circulation plays an important role in the dispersal of reef larvae over the study region. At a short pelagic larval duration, most of the released larvae settle back to or near natal reefs, but as the pelagic duration increases, the number of isolated reefs and islands decreases. Even with increased pelagic duration, some reefs (e.g., Agalega and Tromelin) are completely isolated. The mean dispersal distance from release to settlement varied across the region with larvae released along the East African coast dispersed an average of 405 km before settling while those in the Seychelles archipelago dispersed about 101 km. Different blocks of clusters were observed with 16 clusters observed when

the pelagic duration is shorter (5 days), compared to seven clusters when the pelagic duration is longer (60 days).

The warming trends and bleaching thermal stress shows that among the 636 reef pixels in the study region, about 56% showed positive sea surface temperature trends during the study period (1985-2016). The frequency of bleaching level thermal stress has also increased over the same period, a tendency that climate models project to continue. Even under optimistic scenarios (such as the Representative Concentration Pathway RCP 4.5), most coral reefs are projected to experience severe bleaching and possible mortality by the 2050s. Low to moderate thermal stress are projected over reefs along the East African coast and near the northwest tip of Madagascar and thus these regions may act as potential climate refugia while increasing the potential of reefs to cope with climate change.

Table of contents

List of figures

List of tables

Chapter 1

Introduction

The Western Indian Ocean (WIO) region is a province of the Indian Ocean encompassing the African east coast and the island states, comprising the marine and coastal environments of Somalia, Kenya, Tanzania, Mozambique, and South Africa belonging to the mainland countries and the Seychelles, Comoros, Reunion, Mauritius and Madagascar being the Island States (Figure 1.1). These countries are politically, geographically, and demographically diverse. The region encompasses two of the world's 64 identified Large Marine Ecosystems (LMEs), i.e., the Agulhas Current LME and the Somali Current LME.

The Agulhas Current LME is located in the southwestern Indian Ocean, encompassing the continental shelves and coastal waters of mainland states Mozambique and eastern South Africa, as well as the archipelagos of the Comoros, the Seychelles, Mauritius and La Reunion (France). At the centre of the LME is Madagascar, the world's fourth largest island, with an extensive coastline of more than 5000 km (McKenna et al., 2005). The dominant large-scale oceanographic feature of the LME is the Agulhas Current, a swift, warm western boundary current that forms part of the anticyclonic gyre of the South Indian Ocean (Lutjeharms, 2006). Large parts of the system are characterised by high levels of mesoscale variability, particularly in the Mozambique Channel and south of Madagascar. On the other hand, the Somali LME extends geographically south to north from the Comoros Islands and the northern tip of Madagascar to the Horn of Africa. The monsoons dominate the climate of the Somali LME and influence the wind-driven general circulation including the South Equatorial Current (SEC), the North East Madagascar Current (NEMC), the East

African Coastal Current (EACC) and the Somali Current (SC).

The WIO region is considered to be a distinct biogeographic province within the larger Indo-West Pacific region with low levels of regional endemism and a high diversity of marine life (Obura, 2012). The main ecosystems that constitute the major support for biodiversity and living resources in the WIO region include mangroves, salt marshes and seagrass beds to beaches, rocky shores and reefs, coral reefs, near-shore sandy substrata, the offshore shelf and deep-sea environments. Thirty-five Ecologically or Biologically Significant Marine Areas (EBSAs) have been identified in this region, including the Agulhas Front, the Mozambique Channel, the Walters Shoal, and the Mahe, Alphonse and Amirantes Plateau (Secretariat of the Convention on Biological Diversity, 2015). Over a quarter of the population (about 60 million) in the western Indian Ocean, live within 100km of the shoreline with an annual "gross marine product" GMP of at least US$ 20.8 billion while total "ocean asset base" is about US$ 333.8 billion (Obura et al., 2017).

1.1 Indian Ocean overview

The Indian Ocean is the third largest of the world's oceans with a unique geographical setting. Unlike the Pacific and Atlantic Oceans, the Indian Ocean is landlocked in the north due to the Asian continent extending from the northern tropics to the high latitudes. As a result, the circulation patterns north of the equator do not mirror those south of the equator. According to the International Hydrographic Organization (International Hydrographic Organization and Sieger, 2012), the Indian Ocean spans the tropical and southern mid-latitude wind systems and is bounded by land on three sides. In the north, the Red Sea, Persian Gulf, Arabian Sea and the Bay of Bengal, collectively termed the marginal seas, lie adjacent to the Asian continent. In the South, the basin is open to the Southern Ocean but is bounded by the Subtropical Front. In the East, the maritime continent and Australia form a semi-continuous barrier to the Pacific Ocean, broken only by the Indonesian Seas equatorward of 40°S. Continental Africa separates the Indian Ocean from the Atlantic Ocean along the entire western boundary to the shelf at Cape Agulhas at 35°S. The presence of the Asian continent results in a strong meridional land-sea contrast leading to a seasonal reversal of the winds, known as the monsoon and is the strongest monsoon system on earth (Schott,

Fig. 1.1 Geographic map of the Indian Ocean showing existing mooring and sensors locations, as well as those planned for future deployment: ACT is Agulhas Current Time-series, LOCO is Low-Cost Internal Wave Mooring, UTR is Underwater temperature recorder, ARC is Agulhas Return Current reference station, ADCP is the Acoustic Doppler Current Profiler and proposed moorings and sensors locations. Source: http://www.sea-seek.com/images/7/7c/Indian_ocean.jpg

.

1983) generating large seasonal variations in ocean circulation.

1.1.1 Winds over the Indian Ocean

The presence of the Asian continent results in a strong meridional land-sea contrast leading to a seasonal reversal of the winds, known as the monsoon. The Asian monsoon is the strongest monsoon system on earth and generates large seasonal variations in ocean circulation north of about 15°S (Schott, 1983). The monsoon system also leads to strong surface variations in heat fluex exchange on the North and tropical South Indian Ocean.

During austral summer, high surface pressure builds up over the Indian subcontinent as a result of rapid cooling of the landmass as the sun is retreating south while the Indian Ocean and surrounding atmosphere still holds its heat. This causes a north-south pressure gradient from the Indian subcontinent to the South Indian Ocean (Tomczak and Godfrey, 1994). The cold wind from the Himalayas is forced towards East Africa and is known as the Northeast monsoon. The prevailing winds over the North Indian Ocean during this period are northeasterlies (Figure 1.2a) which upon crossing the equator converge with the southeast trade winds of the South Indian Ocean at about 10∘S (Hastenrath and Greischar, 1991) forming the ITCZ. The rising branch of the Walker circulation is located over the maritime continent and as a consequence the Indian Ocean lacks steady equatorial easterlies (Schott et al., 2009).

During austral winter (from June to September), Asia heats up resulting in a low pressure system over the northern and central Indian subcontinent and a pressure gradient between this landmass and the South Indian Ocean (Tomczak and Godfrey, 1994). The pressure gradient force combined with Coriolis and the effect of the East African highlands causes southwesterly winds to blow from the tropical Indian Ocean and Arabian Sea towards the Indian subcontinent landmass (Figure 1.2b). This season is known as the southwest monsoon and dominates the annual cycle over the Indian Ocean (Yamagata et al., 2004). The surface winds during this season peak in July-August, and fade away in September-October (Schott and McCreary Jr, 2001; Schott et al., 2009). During this season, a low-level atmospheric jet of intense southwesterlies, known as the Findlater or Somali Jet (Findlater, 1969a, 1978) exists along the Somali coast. Pulses and the strength of this jet lead to strong upwelling filaments along the Somali coast (Mafimbo and Reason, 2010).

The monsoon transition periods occur for about four to six weeks during April through May for the northeast monsoon, and October through November for the south-

west monsoon. They are characterized by a strong westerly winds that dominate in the equatorial region. During the inter-monsoon periods, the winds along the Somali coast weaken which, in turn, decreases the upwelling giving rise to warmer SSTs. The warmer water is transported eastward by strong equatorial currents known as the Wyrtki jet (Wyrtki et al., 1971) generated by the strong equatorial westerlies (Yamagata et al., 2004).

In addition to the seasonal reversal of surface winds, the monsoon is also characterized by a distinct seasonality of precipitation in the Greater Horn of Africa Region with heavy rains during the Southwest monsoon from March through May known as long rains and less rain during northeast monsoon from October through December known as short rains (Ogallo, 1988; Kijazi and Reason, 2012; Gamoyo et al., 2015).

1.1.2 Basin-scale circulation

The oceanic wind-driven circulation in the western Indian Ocean north of about 15°S is mainly influenced by the monsoon winds and as such undergoes a seasonal reversal (Schott and McCreary Jr, 2001; Shetye and Gouveia, 1998; Shetye et al., 1994). There are, however, some distinct differences between the depth-integrated flow and that at the surface. A schematic representation of the major current systems in the upper Indian Ocean is shown in Figure 1.3.

Driven by the southeasterly winds, zonal flow in the tropical South Indian Ocean is characterized by the South Equatorial Current (SEC), augmented by transport contributions from the Pacific via the Indonesian Throughflow (ITF). The Indonesian Throughflow flows westward in a broad band between the subtropical gyre and the tropical monsoon system to the north (Schott and McCreary Jr, 2001). While predominantly a geostrophic current, the zonal flow the SEC during the austral winter is dominated by a wind-induced Ekman component (Hastenrath and Greischar, 1991). In the eastern Indian Ocean (East of ∼105°E), the SEC has been observed in a broad band between 7°S and 15°S (Quadfasel et al., 1996). In the west Indian Ocean, this current has been observed between 10°S and 20°S. Hydrographic measurements suggest that the volume transport of the SEC, measured around Mascarene Plateau, between 10°S and 16°S, is about 50 Sv - 55 Sv (New et al., 2007) which is consistent with the volume transport reported by previous studies (Schott and McCreary Jr, 2001; Swallow et al., 1988). Collins et al. (2014) reported a mean vol-

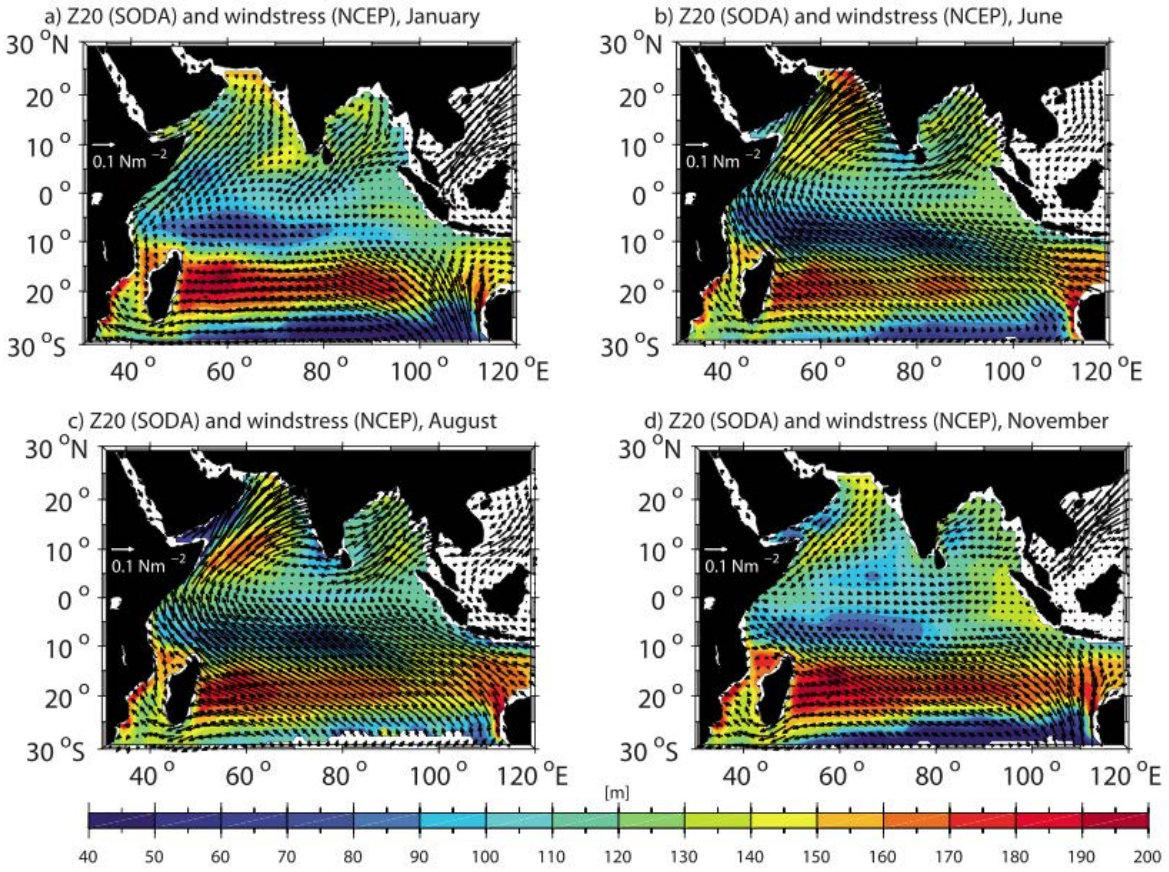

Fig. 1.2 Monsoon wind stress fields from the 1990-1998 National Center for Environmental Prediction (NCEP) climatology (vectors) (Kalnay et al., 1996) and depths of 20°C isotherm (Z20) from Simple Ocean Data Assimilation (SODA) (mean for 1992-2001, colour shaded) for (a) January, (b) June, (c) August, and (d) November. Obtained from Schott et al. (2009)

ume transport of 50.19±10.41 Sv from model simulation integrated in the upper 1500m.

On reaching the east coast of Madagascar, the SEC branches into two opposite flowing current, as the Northern and Southern extension of the East Madagascar Current (Schott et al., 1988; Chapman, 1983; Schott and McCreary Jr, 2001) (Figures 1.3a). The northward extension is known as the North East Madagascar Current (NEMC) and carries about 30 Sv (Swallow et al., 1988; Schott et al., 1988) flowing across the northern tip of Madagascar (Cape-Amber) before flowing towards the African continent. The estimated 30 Sv from observations is in good agreement with estimates calculated from model data (Collins et al., 2014; Manyilizu et al., 2016). Past the northern tip of Madagascar, the NEMC current split into two branches at about 11°S.

The northward branch forms the East African Coastal Current (EACC), along the Tanzanian - Kenyan coast (Schott et al., 1988) , while the southward branch flows through the Mozambique Channel in form of mesoscale eddies (de Ruijter et al., 2002; Ridderinkhof and De Ruijter, 2003; Schouten et al., 2003; Halo et al., 2014c). The mean annual volume transport through the Mozambique Channel in ROMS model simulations was about 20 Sv (Collins et al., 2014; Halo et al., 2014c) which is in good agreement with transport estimates (16–18 Sv) based on a long-term moored array (Ridderinkhof et al., 2010; Ullgren et al., 2012). This agreement between ROMS simulations and observations provide confidence in using the model in this thesis.

The EACC is the western boundary current of a cyclonic tropical gyre, which comprises the SEC to the south and the South Equatorial Counter Current (SECC) in the north during the North-East Monsoon season and the Wyrtki jets in the transition seasons (Schott and McCreary Jr, 2001). The strong southwesterly winds that dominate over the North Indian Ocean strengthen the EACC with velocity of upto 2 ms^{-1} (Newell, 1957; Leetmaa et al., 1982; Schott and McCreary Jr, 2001). The EACC supplies water to the northward flowing Somali Current where a set of different cells and gyres develop depending on the driving wind field and the time of season (Schott et al., 2009). At about 4°N, a part of the Somali Current turns offshore forming a cold upwelling wedge on its left shoulder; the other part forms the 'Southern Gyre' through recirculation across the equator (Schott and McCreary Jr, 2001). A second gyre, the 'Great Whirl', is formed in the north, while a third, the 'Socotra Eddy', forms northeast of Socotra while the southward (Beal and Chereskin, 2003; Schott and McCreary Jr, 2001).

During the NE monsoon, the circulation changes, when the Northeast Monsoon Current flows westward across the Indian Ocean basin carrying water from the Bay of Bengal to the Arabian Sea (Schott and McCreary Jr, 2001). Upon reaching the coast of Africa this flow turns south as the Somali Current and converges, in a confluence zone at 2-4°S, with the northward flowing East Africa Coastal Current (EACC) to supply water to the eastward flowing South Equatorial Counter Current (SECC; Schott and McCreary Jr, 2001; Swallow et al., 1988; Schott et al., 2009). During this period the EACC is weakened to average velocities of less than 0.2ms^{-1} (Newell, 1957). Comparison of volume transport of the EACC show seasonality where Swallow et al. (1991) estimated transport of ∼10 Sv in the upper 100 m for April at 5°S, while Schott et al. (1990) similar transport in the upper 500 m during the northeast monsoon and

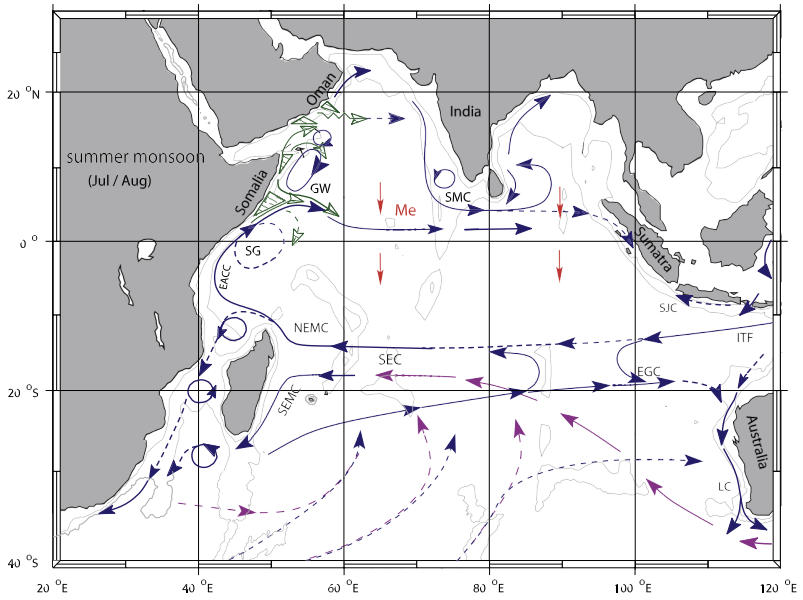

(a) Summer Monsoon currents

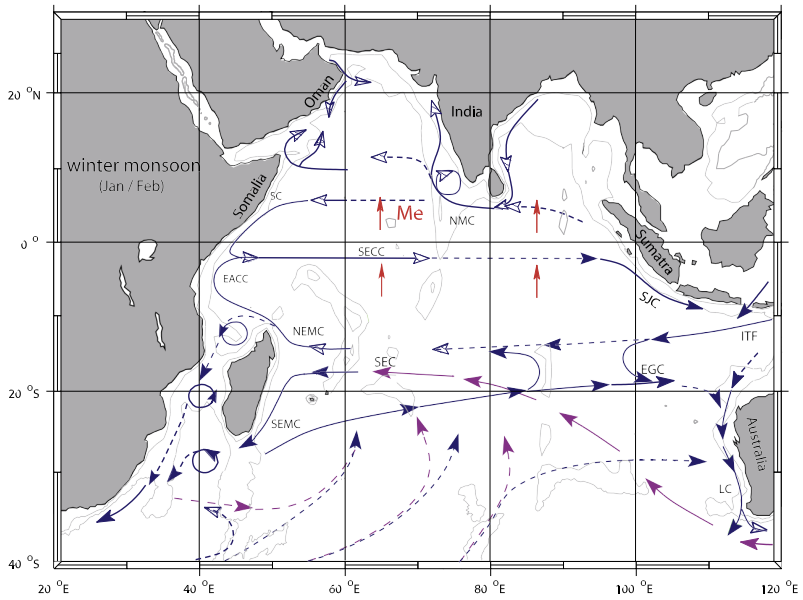

(b) Winter Monsoon currents

Fig. 1.3 Schematic diagram of the large scale surface circulation of the Indian Ocean. (a) portrays the currents during the summer monsoon, and (b) the winter monsoon. The inserted acronyms indicates the main currents studied by Schott et al. (2009)

21 Sv during the southweat monsoon. Modelling work of Gabriela Mayorga-Adame et al. (2016) reported ∼15 Sv while Manyilizu et al. (2016) reported ∼40 Sv.

During the monsoon transition periods, the equatorial Indian Ocean experiences eastward flowing equatorial currents driven by the relatively strong westerly winds along the equator that produce Ekman convergence (McPhaden et al., 2009). The strong eastward surface jets are known as Wyrtki Jets (Wyrtki et al., 1971). The Wyrtki Jets play an important role in the seasonal heat balance of the Indian Ocean basin (McPhaden et al., 2009). Schott and McCreary Jr (2001) observed that two months after the onset of the Wyrtki Jets, upper surface waters are transported from west to east which then results in decrease of the thermocline and mixed layer, sea surface level and surface temperature in the west while increasing in the east. Remote forcing such as Rossby and Kelvin waves modulates the impacts of the Wyrtki Jets beyond the Indian Ocean equatorial region (Schott et al., 2009).

1.2 Western Indian Ocean Marine Ecosystems

The Western Indian Ocean region is a province of the Indian Ocean encompassing the African east coast from Somalia to South Africa. There are 10 states situated in the area of which Somalia, Kenya, Tanzania, Mozambique, and South Africa belong to the mainland countries and the Seychelles, Comoros, Reunion, Mauritius and Madagascar are the Island States. A mosaic of different habitats and substrates runs along the coastline, e.g. estuaries, coastal lagoons, mangrove forests, coral reefs, seagrass beds, mud flats, algal beds, barrier islands, and sandy and rocky beaches (Ngoile and Linden, 1997; Obura, 2012). The region encompasses two of the world's 66 identified Large Marine Ecosystems (LMEs), the Somali Current LME and the Agulhas Current LME (Duda and Sherman, 2002; Sherman, 2006).

The Somali LME extends geographically south-north from the Comoros Islands and the northern tip of Madagascar to the horn of Africa while the Agulhas LME in the south includes a western boundary current system along the east coast of South Africa, as well as its source regions in the Mozambique Channel and east of Madagascar (Vousden et al., 2008). However, many of the ecosystem-related functional areas, such as upwellings, larvae recruitment zones, nurseries and breeding grounds, areas that demonstrate resistance to coral bleaching are generally poorly known, despite their great ecological and economic importance for the region.

The marine and coastal ecosystems of the western Indian Ocean islands reflect a high degree of biodiversity and endemism (Obura, 2012). This diversity of habitats provides a variety of ecosystem services to the human populations along the coast as well as to pelagic and deep-sea organisms. Coral reefs, seagrass and mangrove ecosystems are highly productive and support a huge diversity of organisms as well as provide critical coastal protection and ecosystem maintenance services.

1.2.1 Coral reefs

Corals are marine invertebrates within the class Anthozoa of the phylum Cnidaria and the most diverse ecosystems in the world comprising over 6000 known species with Scleractinia (stony corals) making up the largest order of anthozoa and are principle reef building organisms (Barnes, 1989). Corals have limited degree of organ development with almost all having hundreds of individuals, called polyps. Each polyp consists of three layers: an outer epidermis, an inner layer of cells lining the gastrovascular cavity which acts as an internal space for digestion (Figure 1.4), and a jelly layer called the mesoglea in between (Barnes, 1989).

There are also two basic structural features found within the polyp. The first is a gastrovascular cavity that opens at only one end, commonly called the mouth, where food is consumed and some waste products are expelled. A second feature all corals possess is a circle of tentacles, extensions of the body wall that surround the mouth. Tentacles help the coral to capture and ingest plankton for food, clear away debris from the mouth, and act as the animal's primary means of defense (Barnes et al., 1987; Levinton and Levinton, 1995).

Most corals, like other Cnidarians, contain symbiotic algae called *zooxanthellae* of the genus *Symbiodinium* embedded in the outer layer of the epidermis in high densities ($> 10^6$ cm^2), and are typically 8 -2 µm in diameter giving the coral its color (Levinton and Levinton, 1995). Zooxanthellae provide up to 90% of a coral's nutrition including glucose, glycerol, and amino acids (Berkelmans and Van Oppen, 2006; Sumich, 1996). Coral's utilize these compounds as building blocks in the manufacture of proteins, fats, and carbohydrates, as well as the synthesis of calcium carbonate (Barnes, 1989; Lalli and Parsons, 1995; Sumich, 1996; Barnes and Hughes, 1999). In return, the coral provides the algae with a protected environment and the compounds necessary for photosynthesis including carbon dioxide and inorganic nutrients such as nitrates, and phosphates.

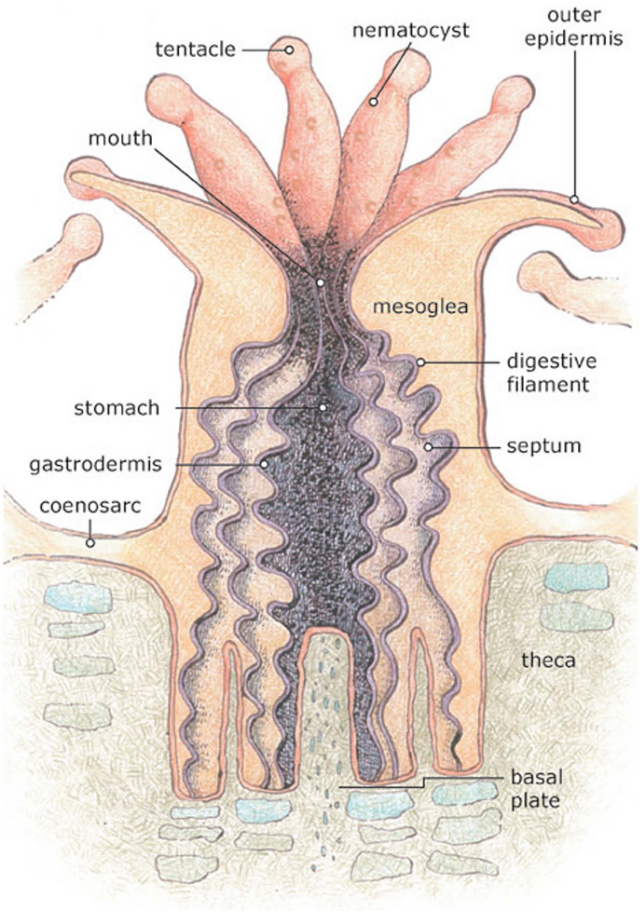

Fig. 1.4 Detailed diagram and description of a coral poly's anatomy

Based on early morphological studies, *zooxanthellae* in corals and other Cnidarians were believed originally to belong to a single specie, *Symbiodinium microadriaticum* (Muller-Parker et al., 2015). *Zooxanthellae* of corals and other invertebrate hosts are grouped into nine phylogenetic types (clades A-I) distinguished based on nuclear ribosomal DNA and chloroplast DNA (Rowan and Powers, 1991; Carlos et al., 1999; LaJeunesse and Trench, 2000; LaJeunesse, 2001; Pochon et al., 2004; Pochon and Gates, 2010). Although members of a clade are more closely related to each other than to members of other clades, taxa within each clade exhibit broad genetic diversity. These genetically distinct clades have different environmental, ecological and geographic characteristics which influence the resistance and resilience of corals to thermal stress (Baker et al., 2004; Rowan, 2004; Berkelmans and Van Oppen, 2006). Therefore, various combinations of host and symbiont may provide ecological advantages in different

ecological niches.

Fig. 1.5 Tissue of corals with zooxanthellae
Image source: https://www.thoughtco.com/zooxanthellae-photosynthetic-algae-3960574

Uptake of zooxanthellae depends on whether the coral reproduces asexually or sexually. The mechanism of acquisition of zooxanthellae may affect zooxanthellae diversity in the host species as well as within a single colony. In asexually reproduced coral colonies, zooxanthellae transmission takes place through coral budding or fragmentation which form a new coral. The zooxanthellae are directly transmitted in coral fragments that form the basis of new colonies (Muller-Parker et al., 2015). In sexually produced corals, acquisition of zooxanthellae is either direct: from the parent, or indirect: from the environment. During direct transmission, parental zooxanthellae are transferred to the eggs or to larvae brooded by the parent (Muller-Parker et al., 2015; Padilla-Gamiño et al., 2012). Coral larvae that was borne from eggs without zooxanthellae may take up their parent's algae at any time prior to release. But if they do not have this opportunity, they have to absorb them from the environment a process called indirect or horizontal transfer. The presence or absence of zooxanthellae in eggs and planulae may affect their ability to persist in the plankton, as it appears that the photoautotrophic contributions of the zooxanthellae are potentially important

factors in explaining the large distance of dispersal of some species (Richmond and Hunter, 1990).

1.2.1.1 Thermal stress and coral bleaching

Despite coral reefs being the richest repositories of marine biodiversity (Spalding et al., 2001), they are also highly susceptible to environmental changes (e.g.change in temperature, pH (ocean acidity), sedimentation, pollutant concentrations and light availability, as well as changes in the reef community due to unsustainable fishing practices and the impacts of recreational tourism (Hughes et al., 2003). Roughly a quarter of coral reefs worldwide are considered damaged beyond repair, with another quater under serious threat. For the last two decades, coral reef biologists have attributed much of the increase in coral mortality to coral bleaching subsequent to elevated sea surface temperatures both at regional and global spatial scales persisting over several weeks (Glynn and D'Croz, 1990; Glynn, 1993; Brown, 1997; Hoegh-Guldberg, 1999b; Hughes et al., 2003; Obura, 2005, 2009). Bleaching can occur when corals are subject to sea surface temperatures only 1 to 1.5 °C above the seasonal maximum mean temperature (Atwood et al., 1992; Baker et al., 2008; Boylan and Kleypas, 2008; Veron et al., 2009; Donner, 2011). Coral bleaching, a stress response of reef-forming corals, results in the loss of their symbiotic algal partners that supplies a large percentage of the nutritional requirements of the coral host and causes the corals to appear white (Figure 1.6) (Lalli and Parsons, 1995; Barnes and Hughes, 1999; Hoegh-Guldberg, 1999b).

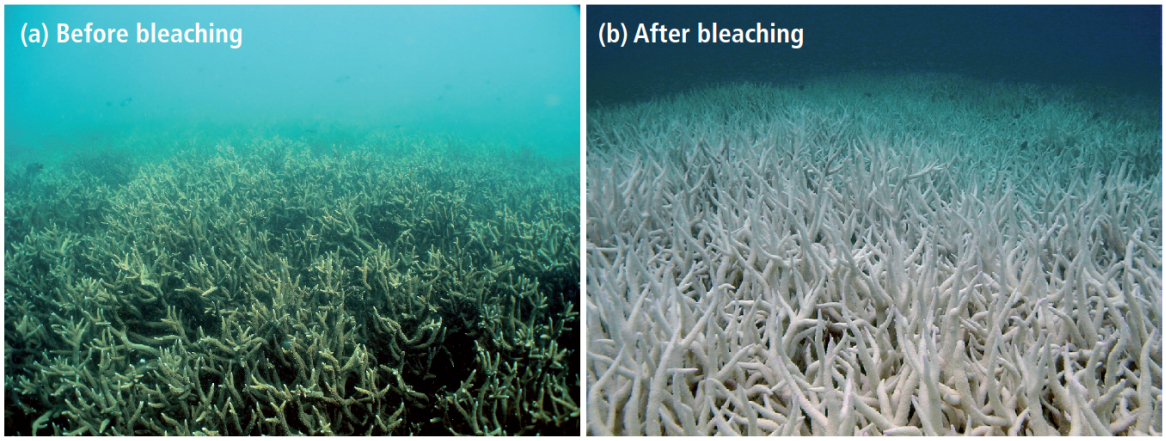

Fig. 1.6 Underwater photograph of coral reef taken before and after bleaching event in 2005, Great Barrier Reef. Source: Mark Eakin

The effects of bleaching are not uniform as bleaching tolerance is variable both within the colony and between species of coral. Flexibility in the relationship between hosts and symbionts occurs where coral species may have more than one type of symbiont (Trench, 1988; Thornhill et al., 2006) or are able to switch or shuffle these symbionts in response to environmental change (Rowan et al., 1997; Rowan, 1998; Baker, 2003). Research to date has shown that distribution of different clades of zooxanthellae in the Western Indian Ocean region have a high dominance of clade C Symbionts, particularly in the cooler southwestern Indian Ocean region Macdonald et al. (2008); Sebastián et al. (2009); LaJeunesse et al. (2010), while clade D symbionts is frequently found in higher abundances in marginal regions, such as shallow Kenyan reefs, the Persian Gulf and the far eastern tropical Pacific (Baker et al., 2004). Clade D symbionts offer coral colonies some advantages for example tolerance to unusually warm conditions and slower growth which increases survival in stressful warm temperature environments (Berkelmans and Van Oppen, 2006; Jones et al., 2008; Jones and Berkelmans, 2010). Berkelmans and Van Oppen (2006) noted that knowledge of the role of zooxanthellae in the thermal tolerance is central to understanding how coral colonies will cope with increased thermal challenges in an era of global warming.

Before thermal stress becomes too severe, corals can survive a bleaching event and return to their normal colour (Grimsditch et al., 2008). However, this stress is likely to cause decreased coral growth and reproduction, and increased susceptibility to disease. Bleached corals often die if the stress persists. Coral reefs that have high rates of coral death following bleaching can take many years or decades to recover (Hughes, 1999; Hoegh-Guldberg, 1999a; Hoegh-Guldberg et al., 2008; Wilkinson and Hodgson, 1999; Obura et al., 2006). Studies in the western Indian Ocean revealed a coral cover decline of over 50% (McClanahan, 2000; Quod and Bigot, 2000; Mohammed et al., 2002; Sheppard, 2003; McClanahan et al., 2007). Mass coral bleaching and mortality as a result of elevated SST is the most widespread and conspicuous impact of climate change (Hoegh-Guldberg et al., 2008). Some corals, like many branching corals, cannot survive for more than 10 days without zooxanthellae. Others, such as some massive corals, are capable heterotrophs and can survive for weeks or even months in a bleached state (Obura, 2009; Mackinson et al., 2009; McField et al., 2005)

Reefs that suffer substantial mortality face different challenges than those where the majority of corals manage to survive the bleaching event. The biggest difference is

the need for a much longer time period until returning to pre-bleaching structure. How long it takes a coral community to recover from bleaching related mortality depends on a variety of factors, including:

- **Favorable recruitment conditions:** These include good water quality, open hard substrate for settlement, presence of coralline algae (provide settlement substrate and chemical cues to facilitate coral settlement), and healthy herbivore populations.
- **Larval supply:** Regardless of how good recruitment conditions are (e.g., availability of substrate, presences of important herbivores), reefs require a robust supply of larvae from source reefs to recover following a disturbance event.
- **Connectivity:** Reefs with high mortality after bleaching depend on connectivity to other sources of live corals for re-seeding. For example, it is possible for reefs receiving great numbers of larvae from other source reefs to recover in a relatively short time span (∼10 years), provided that recruitment conditions are favorable.

1.2.2 Reproduction

Corals are known to have two modes of reproduction that is, asexual and sexual. However the precise mechanism by which coral reproduce vary greatly among taxonomic groups. In asexual reproduction, new clonal polyps bud off from parent polyps as a consequence of external disturbances e.g. storms to expand or begin new colonies. This process continues throughout the animal's life (Barnes and Hughes, 1999).

In sexual reproduction, two main reproductive patterns have been described that is gonochoric broadcast spawner's or gonochoric brooders. Hermaphroditic corals produce female and male gametes within the same polyp and colony, while gonochoric species produce female and male gametes in separate colonies. Broadcast spawners are corals that release gametes into the sea for external fertilization and larval development, while brooders undergo internal fertilization and planula larvae develop within polyps prior to release. Recent findings have shown that broadcast spawning to be the dominant (∼70%) mode of reproduction in Scleractinian corals (Harrison and Wallace, 1990; Richmond and Hunter, 1990; Carroll et al., 2006; Mangubhai and Harrison, 2009). Based on *Acropora* spp. the life cycle of corals is illustrated in Figure 1.7

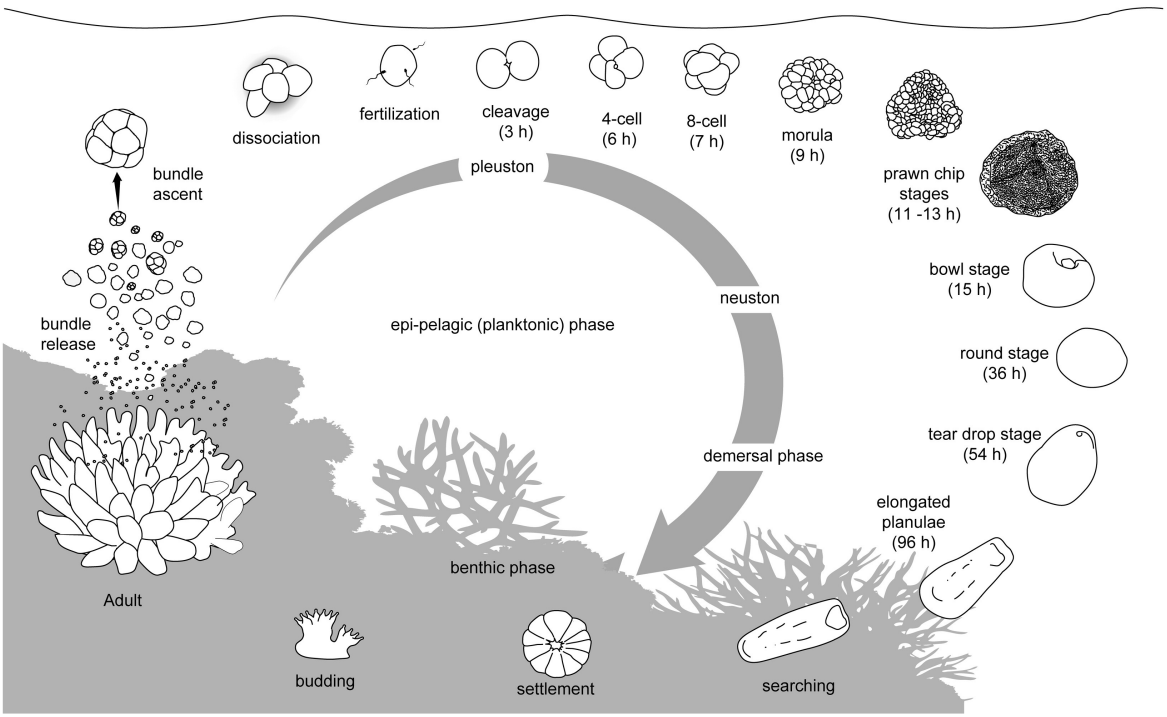

Fig. 1.7 A stylized depiction of the reproductive cycle of the broadcast spawning Acropora species. Image from Jones et al. (2015)

The timing of gametogenesis and spawning is thought to be controlled by a number of factors, that is evolutionary causes and proximate cues responsible for controlling reproductive patterns (Harrison and Wallace, 1990). Evolutionary cues are selective pressures that govern the timing of spawning within each species including physiology, enhanced fertilisation and predator avoidance, and which result in increase fitness or survival (Oliver et al., 1988; Hoegh-Guldberg and Pearse, 1995; Olive, 1995). Proximate cues are environmental regulatory mechanisms such as sea surface temperature, day length, moonlight, tidal cycles, diel (light and dark) cycles, rainfall and food abundance that 'fine-tune' or 'constrain' the timing of reproduction in marine invertebrates (Harrison and Wallace, 1990; Richmond and Hunter, 1990; Olive, 1995).

Spawning patterns have been described for coral communities in a number of different regions including the Great Barrier Reef (Harrison et al., 1984; Willis et al., 1985; Babcock et al., 1986), French Polynesia (Carroll et al., 2006), Galapagos Islands (Glynn et al., 1991), Red Sea (Shlesinger et al., 1998; Bouwmeester et al., 2016) and the Western Indian Ocean (Schleyer et al., 1997; Mangubhai et al., 2007; Mangubhai and Harrison, 2008, 2009). The degree and scale of reproductive synchrony varies

within and among coral species and assemblages (Harrison and Booth, 2007). On the Great Barrier Reef, more than 130 species of coral from 36 genera and 11 families have been observed to synchronize their spawning and release eggs and sperm over a few nights after full moon periods in the austral spring and summer (Harrison et al., 1984; Willis et al., 1985; Babcock et al., 1986). This contrasts markedly with corals in the Red Sea where synchrony between different species is less pronounced, and spawning or planulae release occurs in different seasons, months or at different lunar phases despite a high degree of synchrony within individual species (Shlesinger et al., 1998). In the equatorial region, Mangubhai and Harrison (2008, 2009) reported asynchrony of coral reproduction in Kenya with some level of 'temporal reproductive isolation' occurring between species in relation to the lunar month and lunar phase when the main spawning occurred. Oliver et al. (1988) hypothesized that the breakdown in mass spawning at the equator due to weaker variations in environmental cues such as temperature and tides influencing the onset and timing of spawning events.

1.2.3 Larval dispersal and connectivity

Following successful spawning, subsequent fertilisation and embryo development, larvae of most broadcast spawning corals remain in the water column for a minimum of 2-6 days (Harrison and Wallace, 1990; Miller and Mundy, 2003; Harrison and Booth, 2007). Large numbers of larvae are produced to compensate for the many hazards, such as predators, that they encounter as they are carried by water currents. The time between planulae formation and settlement is a period of exceptionally high mortality among corals (Barnes and Hughes, 1999). This planktonic development period is followed by settlement, which occurs after metamorphosis of larvae and permanent attachment to the substratum (Harrison and Wallace, 1990; Connolly and Baird, 2010; Graham and Nash, 2013). The success of coral larvae to grow into adult corals (known also as coral recruitment) is critical to the health of coral reef ecosystems. Recruitment is dependent on the interaction of recruits with biotic (e.g. predation, competition) and abiotic (e.g. environmental variation, disturbance) factors (Richmond and Hunter, 1990), and plays an important role in determining community structure and dynamics (Gaines and Roughgarden, 1985; Connell et al., 1997; Hughes et al., 2002).

The rate of recovery of a reef following disturbances will depend, in part, on whether reefs are largely 'self-seeding' or reliant on larvae transported from other source reefs (Wilson and Harrison, 1998). The extent to which coral communities and reefs are

self-seeding or interconnected by larval dispersal depends on the mode of development, competency periods, mortality rates, oceanography, and the location and topography of reefs (Harrison and Wallace, 1990; Harrison and Booth, 2007). The process of larval dispersal and subsequent recruitment of individuals into a receiving population influences coral biogeography, genetic structure and population dynamics (Treml et al., 2008; Cowen et al., 2006; Cowen and Sponaugle, 2009; Selkoe and Toonen, 2011; Treml et al., 2012) and has for example been hypothesized as the main driver of patterns of coral species richness (Veron, 1995).

Quantifying the connectivity of populations is fundamental to understanding the dynamics of populations and meta-populations (Botsford et al., 2009), and how species might cope with a changing climate (Hughes et al., 2003). Dispersal and connectivity also provide valuable insights into the geographic distribution of species (Lester et al., 2007; Paris et al., 2007; Crochelet et al., 2016; Mayorga-Adame et al., 2017), patterns in genetic divergence (Palumbi, 2003; Jones et al., 2009; Otwoma and Kochzius, 2016), and endemism (Meyer et al., 2005). Therefore integrating dispersal patterns and connectivity into marine ecosystem management is important (Almany et al., 2009; Planes et al., 2009). The spatio-temporal scale of individual movement can range from much less than a meter and minutes to thousands of kilometres and many months depending on the species' life-history characteristics and the environment (Kinlan et al., 2005; Trakhtenbrot et al., 2005; Gilmour et al., 2009).

Due to the difficulty in empirically measuring dispersal of larvae in the open ocean, two indirect methods are generally used to determine population connectivity. The first uses genetic markers to identify degrees of differentiation between populations, from which inferences regarding the scale of dispersal and levels of exchange can be derived (Warner et al., 2005; Hellberg, 2007; Thorrold et al., 2007). The use of genetics-based approaches provides a view of genetic connectivity taking place over many generations making it difficult to link patterns to processes that drive the direction and scale of exchange (Hedgecock et al., 2007). Results of population genetic studies of reef associated organisms in the Indian Ocean display a wide variety of population structure (Huyghe and Kochzius, 2018). For example, Visram et al. (2010) concluded that populations of the blue barred parrotfish (*Scarus ghobban*) are genetically diverse and have relatively high gene flow. Huyghe and Kochzius (2017) found highly restricted gene flow of skunk clownfish (*Amphiprion akallopisos*) between the Eastern Indian Ocean

and Western Indian Ocean. The comparative genetic analysis of the coral reef sea star (*Linckia laevigata*) in the Western Indian Ocean and Indo-West Pacific by Otwoma and Kochzius (2016) revealed a strong genetic differentiation suggesting that Indo-West Pacific populations of *L. laevigata* can be grouped into four biogeographic regions (Western Indian Ocean, Eastern Indian Ocean, Indo-Malay-Philippines Archipelago, and Western Pacific. While investigating the genetic structure of the stony coral (*Acropora tenuis*), van der Ven et al. (2016) found moderate but significant genetic structure grouped into (a) Kenya and northern Tanzania, (b) southern Tanzania and (c) sample sites located in the Zanzibar and Pemba channels.

Given the extensive effort that often must be expended to complete the tracking of a single reproductive event from a single source location, Cowen et al. (2006) described alternative means to identify realistic dispersal kernels. This approach to estimate dispersal distances, with the potential to calculate dispersal kernels, is based on the utilization of high-resolution biophysical models (Cowen et al., 2006; Paris et al., 2005; Lett et al., 2008; Kool et al., 2013). The modelling approach allows repeated measures through time and space, thereby capturing the expected environmental variability and allowing construction of a connectivity matrix (Cowen and Sponaugle, 2009). Recent studies have shown the importance of physiological and behavioral characteristics of larvae on influencing the connectivity and dispersal of species with a planktonic larval stage. For example, Cowen et al. (2000) used a simple advection-diffusion model that incorporated larval mortality to demonstrate the significant dilution and loss of larvae with distance from source locations, and concluded that biophysical mechanisms must be operating to reduce the loss of larvae from the vicinity of the source location. Wood et al. (2014) provided a global view of connectivity that complements genetic and biogeographic views. In her study, she found that the central Indo-Pacific is a dispersal source while Johnston Atoll is the sole 'stepping-stone' into Hawaii. Recently, Crochelet et al. (2016) and Mayorga-Adame et al. (2017) have modelled reef larvae dispersal in the Western Indian Ocean using individual based models. Results from Crochelet et al. (2016) showed high interconnectivity in the Mozambique Channel and Mascarene archipelago and lower connectivity across the other Western Indian Ocean region.There conclusion was that the MPA implementation in the region has to be designed as a network and planned at the regional scale to maintain connectivity nodes and the health of spawning stocks. Mayorga-Adame et al. (2017) on the other-hand

observed approximately 8% of *Acropora* larvae that successfully settled, recruited to their source reef (self-recruitment)

1.3 Motivation

Coral reef degradation is happening at an alarming all over the WIO region due to multiple stressors with elevated sea surface temperature being the root cause (Brown, 1997; Hoegh-Guldberg, 1999b; Hoegh-Guldberg and Bruno, 2010). While some components of climate change have received researcher's attention, there are fewer studies done in the WIO region to understand how well marine populations are connected especially coral reef and how thermal history trends and projected thermal stress will impact coral reef. The mechanisms controlling larval dispersal and their response to the changing environmental conditions will dictate how connectivity will change in the future. Although the implications of connectivity have long been acknowledged and explored in terrestrial organisms, variable connectivity patterns are only beginning to be recognized as an important driver of present-day population dynamics in the marine realm. It has long been assumed that, due to the lack of visible barriers and the presumed ability of larvae to passively disperse great distances by riding ocean currents, marine organisms dispersed freely and had high levels of population connectivity throughout their ranges. However, recent studies in coastal habitats, have revealed that larvae of many marine species actually settle much closer to their natal reefs than previously thought (Almany et al., 2007; Jones et al., 1999; Kingsford et al., 2002; Planes et al., 2001; Swearer et al., 1999; Taylor and Hellberg, 2003).

Therefore, not only do we need to understand the regional ocean circulation, estimates of dispersal potential and connectivity patterns to understand recovery and reef processes, but we also need to understand how future thermal stress may affect the ability of corals that disperse from one reef to another to withstand conditions at their destination reefs. Such information on connectivity and future bleaching patterns are necessary to improve the design of reserve networks or marine protected networks to facilitate the mitigation and recovery measures and to safeguard biodiversity. This is critical to any projections of how the goods and services of marine species especially coral reefs change.

The overall objective of this thesis is to examine the temporal and spatial, physical and ecological processes influencing connectivity in the region by developing a high-resolution eddy-resolving ocean model for the western Indian Ocean region and coupled to individual-based model (IBM) that track particles (virtual larvae) released from each reef location. The results from this work will provide a regional view of connectivity that complements previous biogeographic work (e.g., Obura, 2012; Otwoma and Kochzius, 2016). With mass coral bleaching among the greatest threats to coral reefs, it is also imperative to understand future projections in coral bleaching thermal stress to predict future bleaching patterns, estimate the potential for adaptation and design effective networks of protected areas.

In order to achieve this broad objective, specific research objectives are formulated as follows:

1. To develop a high-resolution model for the Western Indian Ocean region to resolve both large and mesoscale oceanographic features that are important in dispersal and connectivity..

2. To identify temporal and spatial patterns in larval dispersal from broadcast spawning coral reefs and inter reef connectivity networks within the western Indian Ocean region while identifying reefs that act as source of larvae and those that act as settlements for coral larvae.

3. To assess thermal history trends, generate downscaled projections for severe annual bleaching at the approximate scale of reefs ($\sim$ 4-km) and quantify the potential for connectivity to bring immigrants from different temperature regimes to inform conservation planning and climate policy.

The outcome of this research may enhance the understanding of both the dynamics of the regional circulation and its role in the dispersal and connectivity of reef larvae and also quantify the exposure of coral reefs to key climate threat (coral bleaching conditions) which might lead to changes in community structure and ecosystem function.

This introductory chapter **Chapter 1** is followed by data and methods **Chapter 2** providing detailed description of the numerical and the Lagrangian models. **Chapter 3** discusses the regional oceanographic features with focus on the Southern Gyre that forms off the coast of Somalia. **Chapter 4** focusses on the dispersal and connectivity

of broadcast coral reefs larvae in the study region using an offline coupled biophysical model while **Chapter 5** investigates future projections of coral bleaching thermal stress using an ensemble of Coupled Model Inter-comparison Project phase 5 models. Finally, **Chapter 6** summarizes the conclusions of this work and presents avenues that warrant further investigation.

Chapter 2

Data and Methods

2.1 Numerical Modelling

A review of the current knowledge of the western Indian Ocean presented in Chapter 2 illustrates the seasonal variability as a result of the monsoon winds. The western Indian Ocean is the least studies compared to the other oceans partly due to lack of sufficiently dense observations. Despite the increase in interest in the western Indian Ocean, majority of research efforts have focused further south of 10°S (e.g. Hermes and Reason, 2008, 2009; Collins et al., 2014; Halo et al., 2014a,c) while others focused further north in the Arabian Sea (e.g. Beal and Chereskin, 2003; Brandt et al., 2002; Cox, 1979). As a result of insufficient data, resolving mesoscale features and seasonal dynamics of the region, numerical ocean models could be used to provide insight into some processes in the western Indian Ocean. Therefore, this chapter describes in detail the model choice.

The Regional Ocean Modelling System (ROMS) (Shchepetkin and McWilliams, 2005) has been previously used to study ocean circulation off East Africa (e.g. Manyilizu et al., 2014, 2016; Gabriela Mayorga-Adame et al., 2016). ROMS employs higher order numerics, allowing for increased precision at a given resolution at relatively low computational costs. In addition, the vertical sigma co-ordinate of the model capture topographical interactions effectively.

2.1.1 The Regional Ocean Modelling System (ROMS)

ROMS is a split-explicit, free surface, topographic following coordinate model that solves barotropic and baroclinic momentum equations separately, important for computational efficiency (Shchepetkin and McWilliams, 2003, 2005). In separating the solutions to the barotropic and baroclinic modes of the momentum equations, the split-explicit approach reduces the number of time-stepping operations required as discussed in detail by Shchepetkin and McWilliams (2005). The associated gain in computational efficiency allows for simulations to be performed at higher resolution, advantageous for studies that focus on the mesoscale features. ROMS solves the incompressible primitive equations under the Boussinesq and hydrostatic approximations. The hydrostatic approximation assumes that the buoyancy force is balanced by the vertical pressure gradient. ROMS is coupled with a non-linear equation of state and advective/diffusion schemes for potential temperature and salinity. A non-local, K-Profile Parameterization (KPP) boundary-layer scheme (Large et al., 1994) is used to parameterize the sub-grid scale vertical mixing. Good representation of oceanic processes at the upper layers of the ocean column is important, especially for the biology, and climate studies. At the ocean bottom, a good representation of the processes is important especially for the deep flows, benthic life, and some geological processes (e.g, sediment transports). These features make the model code suitable to expand its applications in order to simulate several processes such as ecosystem dynamics, and biogeochemical cycling (Gruber et al., 2006). The primitive equations of motion under Boussinesq and hydrostatic approximations can be discretized in the Cartesian coordinate system as the time evolution of potential temperature and salinity which is governed by the advective-diffusive equations:

$$\frac{\delta u}{\delta t} + \vec{v}.\nabla u - fv = -\frac{\delta \varnothing}{\delta x} + F_u + D_u \tag{2.1}$$

$$\frac{\delta v}{\delta t} + \vec{v}.\nabla u - fu = -\frac{\delta \varnothing}{\delta x} + F_v + D_v \tag{2.2}$$

the time evolution of potential temperature and salinity which is governed by the advective-diffusive equations:

$$\frac{\delta T}{\delta t} + \vec{v}.\nabla T = f_T + D_T \tag{2.3}$$

$$\frac{\delta S}{\delta t} + \vec{v}.\nabla S = f_S + D_S \tag{2.4}$$

the hydrostatic and mass balance:

$$\frac{\delta \varnothing}{\delta Z} = \frac{-\rho g}{\rho_o} \tag{2.5}$$

the continuity equation for an incompressible fluid

$$\frac{\delta u}{\delta x} + \frac{\delta v}{\delta y} + \frac{\delta w}{\delta z} = 0 \tag{2.6}$$

and the equation of state

$$\rho = \rho(T, S, P) \tag{2.7}$$

In the above equations, u, v, w are the components of vector velocity $\vec{v}$, in the x, y (horizontal coordinates) and z (vertical coordinate) directions respectively. t is time in seconds, f is the Coriolis parameter and g is the acceleration due to gravity. D_u and D_v is the lateral momentum dissipation terms while T and S are potential temperature (°C), and salinity (psu) respectively while ρ is density. f_T represents the surface forcing term for temperature and includes short and longwave radiation as well as latent and sensible heat fluxes. D_T, and D_S describe the diffusion of temperature and salt. The dynamic pressure $\varnothing$ is calculated as $\frac{P}{\rho_o}$, where P is pressure and ρ_o is the reference density of sea water ($1024\ \mathrm{kg \cdot m^{-3}}$)

2.1.2 Boundary condition schemes

As a regional model, ROMS requires boundary information at the surface, bottom and, (typically) four lateral boundaries, where it may connect to an external solution. The effects of external forcing at the surface and ocean floor through vertical viscosity and diffusivity in the free-surface and bottom boundary layers can be illustrated as follows:

$$K_m \frac{\delta u}{\delta z} = \frac{\delta u}{\rho_o}(x, y, t) \tag{2.8}$$

$$K_m \frac{\delta v}{\delta z} = \frac{\delta u}{\rho_o}(x, y, t) \tag{2.9}$$

In the above equations, z is surface elevation (m), with equations (3.8) and (3.9) expressing the horizontal momentum transfered into the ocean by atmospheric wind stress at the sea surface.

2.1.3 Nesting approach

High resolution simulation can be expensive in-terms of computational resources therefore, nesting technique is used to obtain higher grid resolution at a reduced computation cost. In ROMS this is achieved by through the use of the Adaptive Grid Refinement in Fortran routines (AGRIF; Debreu et al., 2008). The AGRIF approach facilitates for the low resolution grid simulation to supply boundary conditions for the high-resolution grid simulation, a technique referred to as one-way nesting (Mason et al., 2010). In two-way nesting, the high resolution grid also feeds information back to the low-resolution grid (Debreu et al., 2012). In order to preserve the CFL (Courant Friedrichs Lewy) criterion, for a typical coefficient of refinement, for each parent time step the child must be advanced by the number of time steps necessary to reach the time of the parent (Figure 2.1).

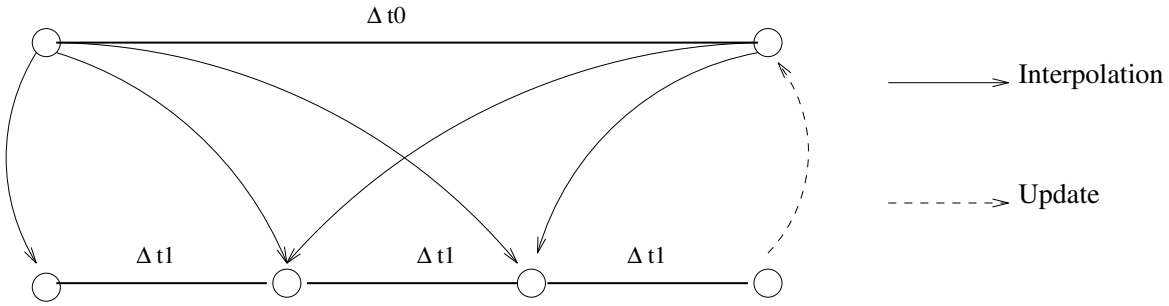

Fig. 2.1 Baroclinic time-step coupling between a parent △t0 and a child grid △t1, for a refinement factor of 3

2.2 Domain specifics

The experimental approach outlined in the objectives of this thesis require that the model is able to resolve both the large-scale circulation observed in the region and some of the mesoscale features that play an integral role in dispersal or larvae.

The model configuration was built using ROMSTOOLS (Penven et al., 2008) utilizing nesting capabilities to resolve small scale processes. Geographically the large domain (herein called 'parent grid') lies between 31 - 85°E and 24°N - 30°S (Figure 2.2) designed to simulate the prominent oceanographic features of the Indian Ocean and provide boundary condition for the higher resolution small domain (herein called

'child grid'). The parent grid configuration has a spatial resolution of 1/4° and considered eddy permitting and is comparable to the first Rossby radius of deformation at this latitude, ∼230 km (Chelton et al., 1998). Vertical resolution of the parent grid is defined by 40 σ-coordinate levels, distributed according to $\theta_b = 0$ and $\theta_s = 6$ resulting in an increased resolution towards the surface. The transition depth between the horizontal surface layers and the bottom σ-levels, was set to hc = 20 m which ensures a good representation of outflows in shallow straits as well as in the interior basin. Bathymetry is derived from the 1' General Bathymetric Chart of the Oceans (GEBCO) global topography data set, and bi-linearly interpolated onto the grid. As discussed in the previous section, pressure gradient errors are reduced by smoothing the bathymetry such that the smoothing parameter, r, is less than a critical value of 0.2 (Haidvogel and Beckmann, 1999). As shelf dynamics are not accurately represented at this resolution, the minimum depth at the shore is set to 150 m. In addition, to prevent the establishment of large coastal walls, the maximum depth at the shore is set to 500 m. To remove steep topographic features in the deep ocean that could possibly induce some numerical instabilities into the system, a selective hanning filter was applied.

The embedded child domain was designed to cover north of Mozambique Channel, northeast Madagascar and north along the East Africa coast. Geographically the domain lies between 34 - 58°E and 5°N - 18°S (Figure 2.2) designed to resolve the mesoscale circulation by refining the model solution by a factor of three (coefficient of refinement (r_{coef})=3) resulting to model results of 1/12° (∼ 9 km). Similar to the parent configuration, the child grid has 40 stretched vertical levels with the bathymetry interpolated from the original GEBCO dataset and not from the coarser parent topography in order to obtain finer resolution bathymetry. To prevent discontinuities between the parent and child domains, a smooth connection between the different grid levels is needed. The topography of the child domain is smoothly connected to the bathymetry of the parent domain using the equation below:

$$h_{child} = \alpha h_{parent} + (1 - \alpha) h_{fine} \tag{2.10}$$

Where the bottom topography of the child and the parent domains are defined by h_{child} and h_{parent} respectively. h_{fine} is the high-resolution bathymetry, and α is a parameter that ranges from zero to 1 within a number of grid points at the lateral parent-child boundary.

The surface forcing as well as the initial and boundary conditions of the child domain are interpolated from that of the parent domain. Vertical re-interpolation of the initial conditions for the child domain is necessary due to the different topographies of the child and the parent domains. Mass and energy conservations through the three open boundaries of the child domain, which are forced by the parent solution, are obtained through the open boundary conditions described by Penven et al. (2006). The time evolution of the child domain takes place within the time step of the parent domain through a recursive integration procedure (Penven et al., 2006). To maintain the CFL criteria, it is necessary to decrease the time step of the child domain by the same factor as the coefficient of refinement (r_{coef})

2.2.1 Surface forcing

At the surface, the parent is forced with monthly climatology fluxes: heat and freshwater fluxes are at 0.5° spatial resolution derived from the Comprehensive Ocean-Atmosphere Data Set (COADS; da Silva et al., 1994). To improve the model representation of the of the air-sea interaction, the COADS data is reinforced with satellite derived SST climatology from the Pathfinder Advanced Very High Resolution Radiometer (AVHRR) as a restoring term for the boundary layer. This SST climatology data has a resolution of 9 km and was generated from version 4 NOAA-NASA AVHRR Oceans Pathfinder fields from 1985 to 1995 (Casey and Cornillon, 1999). Wind forcing comes from the 0.5° spatial resolution QuikSCAT climatology data (Liu et al., 1998a) constructed from 2000 to 2007) of data. Compared to lower resolution NCEP-II and ERA-interim reanalysis products, the high-resolution QuikSCAT wind data provide a better representation of the small-scale wind features such as wind jets and wind shadows or coastal upwelling (Collins et al., 2012; Mafimbo and Reason, 2010).

2.2.2 Lateral boundaries and initial conditions

The model configuration has its physical lateral boundaries opened in the east, north and south. The eastern boundary is characterized by the inflow of the South Equatorial Current (SEC) while the northern boundary is characterized by the East Africa Coastal Current (EACC) and Somali Current (SC). The southern boundary is mainly characterized by the outflow of the Mozambique Channel eddies. At these boundaries, a mixed passive-active implicit radiation condition connects the model solution to the surrounding oceanic environment (Marchesiello et al., 2009). In an outflow condition,

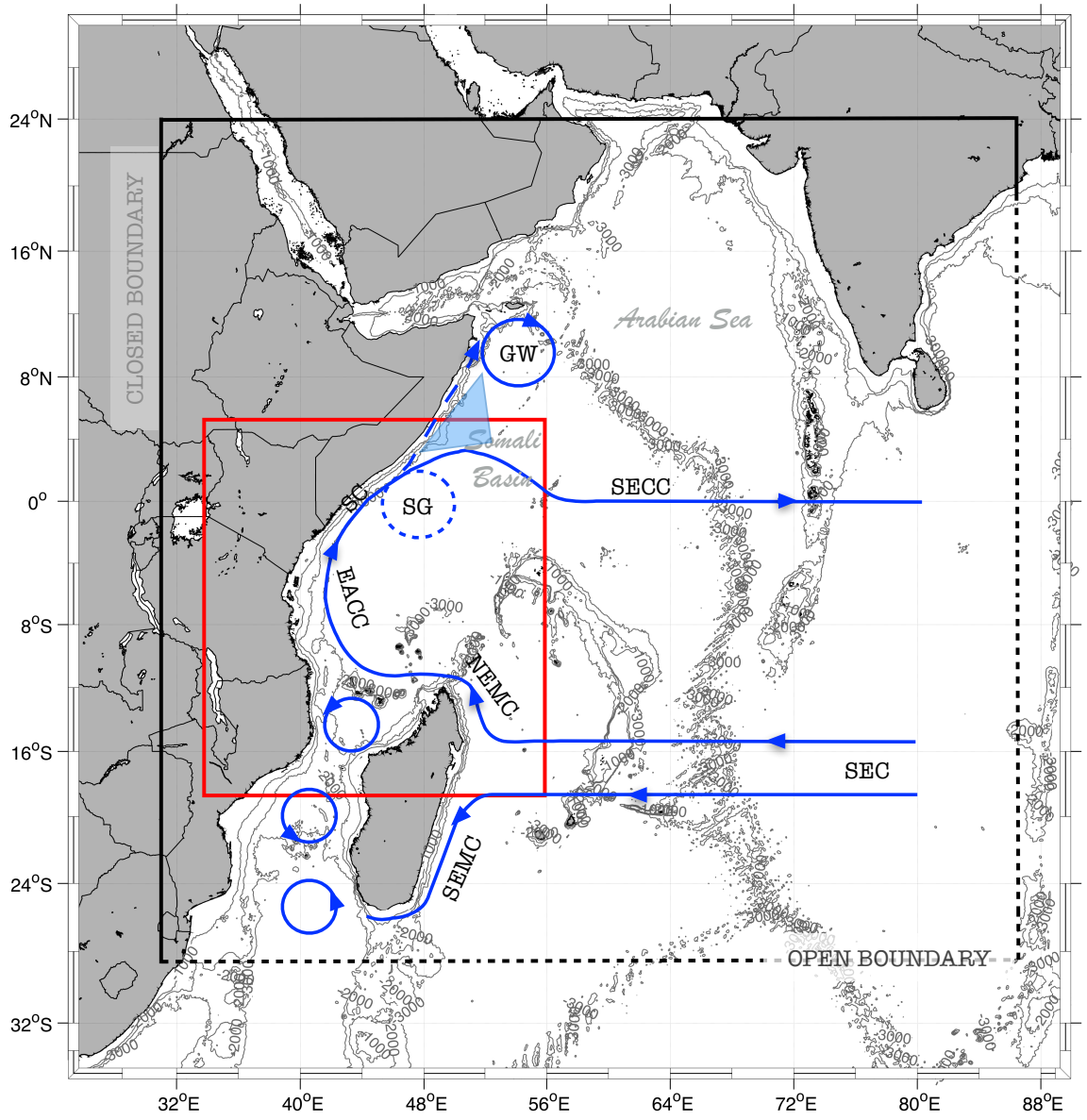

Fig. 2.2 Schematic for boreal summer surface circulation in the western Indian Ocean adapted from Schott and McCreary Jr (2001). The major currents illustrated include; the South Equatorial Current (SEC), Northeast Madagascar Current (NEMC) and Southeast Madagascar Current (NEMC), East African Coastal Current (EACC), Somalia Current (SC), and its northern extension during the SW monsoon (dashed), and South Equatorial Counter Current (SECC). Also included are the quasi-steady eddies; the Southern Gyre (SG) and Great-whirl (GW) with its corresponding wedges of upwelling as shaded blue triangle. The black lines represent the boundaries of the parent configuration used, while the red box represent the boundaries of the child domain.

the outward solution is allowed to escape the model domain, whereas, in an inflow case (inward fluxes), the model solution is nudged towards the external dataset: monthly climatology, gridded at 1° x 1°, World Ocean Atlas 2009 (WOA09; Conkright et al., 2002). Temperature and salinity for January are used to initialize the model, which is started from rest. Furthermore, geostrophic velocities at the open boundaries are calculated from temperature and salinity at a reference level of 1000 m while Ekman velocities are estimated from the wind field.

2.3 Individual Based Modelling

Over the past two decades, ecological models have shifted away from models governed by the general equations towards those that incorporate individual characteristics in an ecological system to generate the dynamics of that system as a whole. This shift reflects the implications that even the simplest non-linear equations can have complex and more Importantly chaotic dynamics (May, 2001). The variability of recruitment, population connectivity, the spread of invasive species and of marine diseases, the transport and fate of atmospheric dust and pollutants, all are examples of phenomena that can be investigated using a particle-tracking framework. Individual Based Models (IBM) are indeed the best tools available to learn how dynamic marine ecosystems operate by testing hypotheses and teasing apart the role of often non-linear factors (Railsback, 2001). Most IBMs use outputs from hydrodynamic models (e.g. ROMS, Hybrid Coordinate Ocean Model (HYCOM; Bleck, 2002), Model for Applications at Regional Scale (MARS; Lazure and Dumas, 2008) to determine particle movement through space and time.

For many marine species, life histories are characterized by a planktonic larval stage and a sessile, or sedentary, adult existence. Their spatially distributed adult populations are thought to be connected primarily through the dispersal of larvae by ocean currents, often over great distances (Scheltema, 1986; Shanks et al., 2003; Kinlan et al., 2005; Trakhtenbrot et al., 2005). Population connectivity, defined as the exchange of individuals among marine populations, is important for the persistence of isolated populations (Roughgarden et al., 1988; Gaylord and Gaines, 2000; James et al., 2002), re-establishment of sites following disturbances, and the flow of genetic information Palumbi et al. (2003). In addition, larval dispersal determines the rate and spatial patterns of population spread a key factor in determining how species might

cope with global climate change (Gaylord and Gaines, 2000; Trakhtenbrot et al., 2005).

2.3.1 Ichthyop

This subsection describes the overall structure of the Lagrangian model used and provides details about the model component.

Ichthyop is a free Lagrangian model developed using Java to study the effects of physical and biological factors (Lett et al., 2008) of marine particles (available at http://www.ichthyop.org/downloads). The model is an updated version of of previous modelling experiments investigating the effects of physical and biological factors on the dynamics of anchovy and sardine ichthyoplankton in the Benguela (Mullon et al., 2002, 2003; Huggett et al., 2003; Lett et al., 2006) and in the Humboldt upwelling systems (Lett et al., 2007; Brochier et al., 2008).

The model description follows the Overview-Design-Details (ODD) protocol for describing individual- and agent based models (Grimm et al., 2006). It operates either as off-line or online using archived ocean velocity, temperature and salinity fields from different hydrodynamic models (e.g. ROMS, MARS) which forms the physical environment. Individuals are characterized by age, length, stage (egg, yolk-sac larva or feeding larva), location and status (alive or dead). Larval dispersal in the model consists in updating the individuals' position $\vec{x}$ using the following equation:

$$d\vec{x}/dt = \vec{u} + \vec{u}' \tag{2.11}$$

The deterministic advection term $\vec{u}$ is derived from spatial and temporal interpolations of the flow fields provided by the hydrodynamic model. $\vec{u}'$ is a stochastic term added to take into account the small-scale fluctuations in the currents that are lost due to the grid resolution of the hydrodynamic model and temporal averaging of the hydrodynamic model outputs. The stochastic term is often represented using an ad-hoc diffusion term (i.e., a random walk process) or using a random displacement process if a spatially non-uniform diffusivity is used (North et al., 2006). Equation 3.11 is numerically integrated using schemes such as a forward Euler or a Runge-Kutta.

Larval mortality is an important parameter that can change the dispersal distance of an organism, influencing the structure of the meta-population. Mortality has been

represented in early life stage models in a variety of ways, including constant rates (Brown et al., 2005; Tilburg et al., 2005), and depending on life stage (Miller et al., 1998), temperature (Mullon et al., 2003), and growth rate (Hinrichsen et al., 2002). In Ichthyop, individuals die when they are in waters at a temperature below a certain value (lethal temperature) which may be different for eggs and larvae (Lett et al., 2008). Individuals are considered as recruited when they have reached a minimum length (or age) and spent a minimum amount of time within a "recruitment area". Recruitment areas are defined in the same way as spawning areas.

Having described the models used in this thesis, the next chapter uses ROMS to investigate the dynamics of the Southern Gyre as a key aspect of the Somali Current system. This oceanic circulation feature is an important component of the western Indian Ocean during boreal summer and may play an important role in larval dispersal.

Chapter 3

A numerical investigation of the Southern Gyre using ROMS

This result chapter is based on the work published as:
Gamoyo, M., Reason, C.J.C. & Collins, C. 2017. A numerical investigation of the Southern Gyre using ROMS. Journal of Marine Systems 169:11-24.
http://dx.doi.org/10.1016/j.jmarsys.2017.01.002

Abstract

A numerical model (The Regional Ocean Modeling System - ROMS), configured over the western Indian Ocean and driven by monthly climatology winds and heat fluxes, is applied to examine the Southern Gyre in the Somali Current system during the Southwest Monsoon. Despite the Southern Gyre playing a role in transporting water masses and other properties northwards across the equator, it has not been much studied. The model results indicate that the Southern Gyre appears in early June in the upper ocean as a result of instability in the northward flowing Somali Current. The arrival of downwelling Rossby wave energy at the East African coast intensifies the recirculation of the Southern Gyre and causes its northward movement. The Southern Gyre is characterized as a shallow feature which deepens from 100 m in June to 300 m in July-August. The average spatial scale of the gyre is about 400 km with subsequent development of positive vorticity bursts which are identified as potential contributors to the decay of the Southern Gyre. Cool and fresh waters observed in the gyre resulted from advection via the South Equatorial Current and then through the Somali Current (SC).

3.1 Introduction

The circulation of the western Indian Ocean is influenced by the seasonally reversing monsoon winds, blowing mainly from the southwest in boreal summer (SW Monsoon from June to August) and from the northeast in boreal winter (NE Monsoon from December to February) (Bruce, 1979) (Figure 2.2). The best studied of the seasonally reversing currents is the Somali Current (SC), which is a western boundary current along the East African coast. The Somali Current flows poleward (equatorward) during the SW Monsoon (NE Monsoon) (Schott, 1983; Shetye and Gouveia, 1998; Schott and McCreary Jr, 2001). Strong winds during the SW Monsoon strengthen the East African Coastal Current (EACC) which reached a maximum speed of 2 ms^{-1}, and then supplies the northward flowing SC to its north (Schott, 1983; Schott and McCreary Jr, 2001; Manyilizu et al., 2014). Throughout this phase of monsoon winds, the waters largely originate from the South Equatorial Current (SEC), flowing across the equator into the EACC which then feeds the SC (Figure 3.1). Water properties in the western Indian Ocean are influenced by the Indonesian Through Flow (ITF) which provides the pathway for substantial transfer of heat and freshwater budgets from the Pacific Ocean to the Indian Ocean (Rochford, 1964; Wyrtki et al., 1971; Warren et al., 1976; Gordon, 2001).

During the NE Monsoon from December through February, the SC flows southward between 10°N and the equator but with speeds weaker than the northward flow during SW Monsoon. This current meets the northward flowing EACC, which is driven by the Southern Hemisphere trade winds, and this results in a confluence of the EACC and SC to form the eastward-flowing South Equatorial Counter Current (SECC) (Newell, 1957; Leetmaa et al., 1982; Schott and McCreary Jr, 2001). The western Indian Ocean basin circulation mainly follows the large-scale wind stress curl pattern, which shows mainly positive curl during the NE Monsoon (Figure 3.1a) and mainly negative curl during the SW Monsoon (Figure 3.1c). In the former, the positive wind stress curl mainly exists as a basin-scale band across the 8°N - 8°S zone.

However, during the inter-monsoon periods (Figure 3.1b & d) the winds over the equatorial Indian Ocean are mainly westerly and thereby generate strong eastward flowing equatorial jets, known as Wyrtki Jets (Wyrtki et al., 1971). The Wyrtki Jets during spring and autumn are comparable in transport magnitude (Jensen, 1991; Han

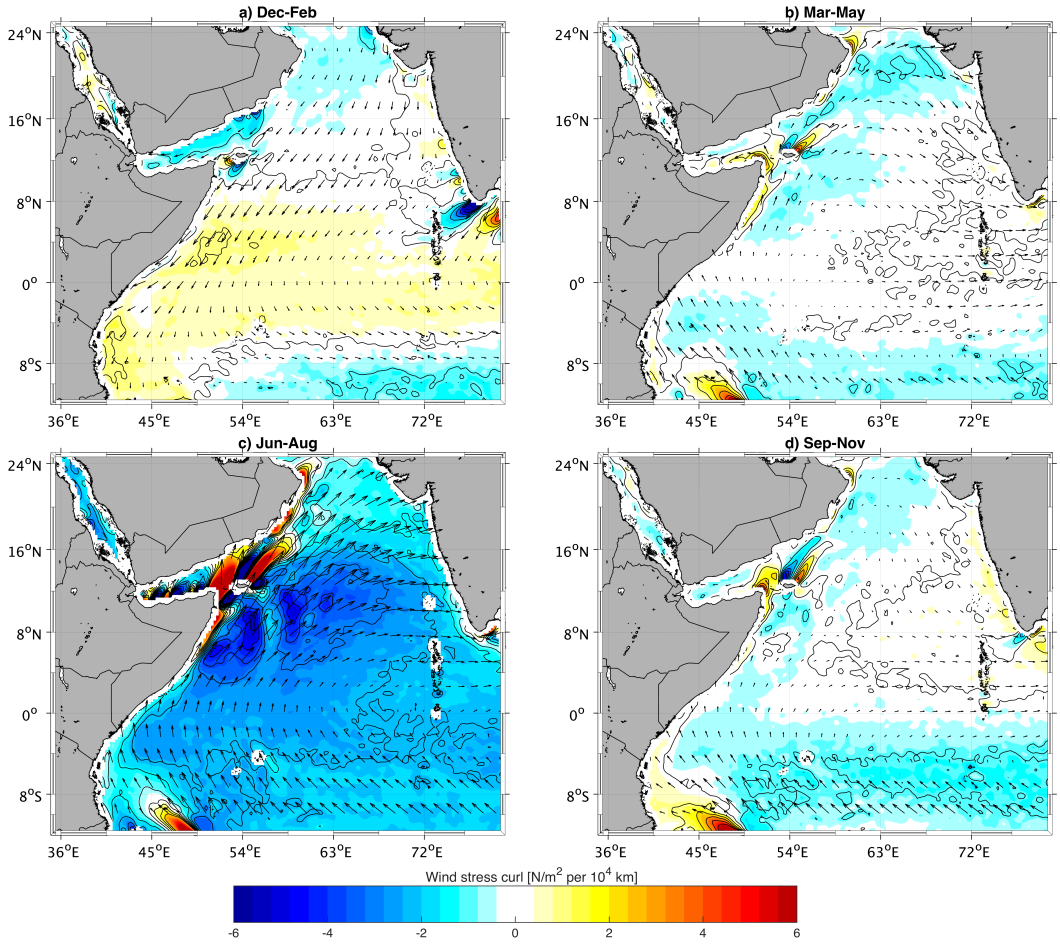

Fig. 3.1 Wind stress curl (shaded) and wind stress (arrows) derived from SCOW climatology (Risien and Chelton, 2008) and averaged for the periods (a) December February (NE Monsoon), (b) March May (Inter-Monsoon), (c) June August (SW Monsoon), and (d) September November (Inter-Monsoon).

et al., 1999). However, the jet is faster and more intense in autumn than in spring.

Jet speeds reported in the literature vary in the range 0.5 - 0.9 ms^{-1} in spring and from 0.75 - 1.2 ms^{-1} in autumn (Knox, 1976; McPhaden, 1982; Han et al., 1999).

Unlike other steady western boundary currents (WBCs), the SC is associated with two quasi- stationary eddies that are separated from the East African coast namely, the Southern Gyre and Great Whirl (Figure 2.2). As south westerly winds build in June, the northward flowing SC reaches about 3°N, where it separates from the coast and flows back across the equator, forming a shallow clockwise feature known as the

Southern Gyre (Düing and Schott, 1978; Jensen, 1991). Awedge-shaped region of upwelling forms along the northern flank of this gyre driven by upwelling favorable winds (Mafimbo and Reason, 2010). According to Beal and Donohue (2013), this cell recirculates southward across the equator to feed into the South Equatorial Counter Current (SECC). At this time, there is also a continuation of the SC farther north, driven by the local alongshore winds. Beal and Donohue (2013) and Akuetevi and Wirth (2015) in their studies on the Great Whirl showed that the generation mechanism involved the arrival of remotely forced Rossby waves and amplification by the monsoon winds.

In July, the monsoon winds strengthen, with strong southwesterlies (up to 14 m^{-1}) extending offshore at about 9°N (Findlater, 1969b) and a large anticyclone, the Great Whirl, spins up between 5°N and 10°N (Leetmaa et al., 1982; Beal and Chereskin, 2003). Subsequently, a component of the SC continues northward, past the recirculating Great Whirl, to flow through the Socotra passage (Fischer et al., 1996). During the months of August and September, the SC and the Great Whirl strengthen while the Southern Gyre weakens (Fischer et al., 1996). There is some observational and model evidence (e.g. Evans and Brown, 1981; Swallow et al., 1983; Luther and O'Brien, 1989) that suggests that the Southern Gyre migrates northward in September (before the monsoon winds weaken) to coalesce with the Great Whirl but it is not clear how typical this behaviour is. According to Akuetevi and Wirth (2015), the interaction between the Southern Gyre and Great Whirl is a collision without merging. During the collision, the Great Whirl is pushed to the east coast of Socotra Island, which then sheds several smaller patches of anticyclonic vorticity which can then evolve into the Socotra Eddy in the northwest Indian Ocean.

Although there have been several studies done on the broader Indian Ocean e.g. in the southwest Indian Ocean (Collins et al., 2014; Halo et al., 2014a,c; Hermes and Reason, 2008, 2009) and further north in the Arabian Sea (Beal and Chereskin, 2003; Brandt et al., 2002; Cox, 1979). Few modelling efforts and observational studies have been performed along the East African coast (Manyilizu et al., 2014, 2016; Gabriela Mayorga-Adame et al., 2016). Overall, the analyses on the Southern Gyre have not been comprehensive and understanding of the related mechanisms is still inadequate. Insufficient in-situ observations over the past two decades have occurred as a result of Somali piracy and thus there is limited data to resolve its evolution and characteris-

tics. Therefore, the current paper focuses on the characteristics (position and radius) of the Southern Gyre and related mechanisms (role of Rossby waves and vorticity bursts) addressing aspects of generation, persistence and to provide a description of the subsurface structure. To achieve this, an eddy resolving Regional Ocean Modelling System(ROMS) configuration is used which allows for a consistent spatial and temporal view.

The intent is to update and provide a detailed description of the Southern Gyre as a key aspect of the large-scale circulation of the Somali Current and its dynamics which are important for the Somali upwelling system observed on its northern boundary and the meridional transport of fresh water northwards along the East African coast. This work may then be helpful for the new phase of the Second International Indian Ocean Experiment (IIOE-2) which started in late 2015 and is planned to continue through 2020.

3.2 Data and Methods

Version 3.0 of The Regional Ocean Modelling System (ROMS) (Shchepetkin and McWilliams, 2005) developed by the Institut de Recherché pour le Development [IRD] is used. ROMS solves the primitive equations on an orthogonal curvilinear coordinates system. Its vertical component is terrain following to better represent the effect of topography on the fluid. The advection scheme is third-order and the diffusive part of the advection scheme is rotated along iso-geopotential surfaces to avoid spurious diapycnal mixing (Marchesiello et al., 2009). In order to maximize computing efficiency at a higher resolution over the study area, the Adaptive Grid Refinement in Fortran (AGRIF) embedding capabilities (Debreu et al., 2008, 2012) of ROMS is used. In this study, the two-way nesting approach was preferred as it allows for the coarse resolution outer domain to provide boundary conditions for the higher resolution embedded inner domain (child) and additionally allows the inner domain to feed back into the outer domain (parent).

The parent domain in this study lies between 31 - 85°E and 24°N - 30°S and was designed to simulate the large oceanographic features in the western Indian Ocean region with the horizontal resolution set at 1/4°. The embedded inner domain designed to resolve the circulation and mesoscale features near the East African coast and extends

from 34 - 58°E and 5°N - 18°S at a horizontal resolution of 1/12° with 40 vertical sigma levels with increased resolution towards the surface. The stretching parameters $h_s = 6$ for the surface and $h_b = 0$ for the bottom (Haidvogel and Beckmann, 1999) are used. The minimum depth at which stretching occurs is defined with the parameter $h_c = 20$ m which ensures a good representation of outflows in the shallow straits as well as in the interior basin. Bathymetry is taken from Global Earth Bathymetric Chart of the Oceans (GEBCO1; Carpine-Lancre and Bv, 2003) and linearly interpolated onto the grid. Pressure gradient errors are reduced by smoothing the bathymetry such that the smoothing parameter is less than a critical value of 0.2 (Haidvogel and Beckmann, 1999).

At the surface, the parent domain is forced with monthly climatological heat and fresh-water fluxes at 0.5° spatial resolution derived from the Global Comprehensive Ocean-Atmosphere Dataset (COADS; da Silva et al., 1994). To improve the model representation of the air-sea interaction, the COADS heat-flux product is augmented with the 9 km Pathfinder Advanced Very High Resolution Radiometer (AVHRR) SST climatology as a restoring term for the boundary layer. The Pathfinder data was generated from version 4 NOAA-NASA AVHRR Oceans Pathfinder fields for the period 1985–1995 (Casey and Cornillon, 1999).

The wind forcing used in this study is the 0.5° resolution QuikSCAT climatology (Liu et al., 1998a) constructed from 8 years (2000–2007) of data. Compared to lower resolution NCEP II and ERA-interim reanalysis products, the high-resolution QuikSCAT wind data provide a better representation of the small-scale wind features such as wind jets and wind shadows or coastal upwelling (Collins et al., 2012; Mafimbo and Reason, 2010). Initial and boundary conditions are obtained from World Ocean Atlas 2009 (WOA09; Conkright et al., 2002) gridded at 1° x 1°. Temperature and salinity for January are used to initialize the model, which is started from rest. Furthermore, geostrophic velocities at the open boundaries are calculated from temperature and salinity at a reference level of 1000 m while Ekman velocities are estimated from the wind field.

The nested simulation was run for a total period of 10 years and the integrated properties show that statistical equilibrium is reached after a spin-up of 36 months (Figure A.1). The results presented in the following sections are based on the remaining 7 years' model output. Comparison of the model solution with observed and satellite

fields are performed to evaluate the degree of confidence. The datasets used for this purpose include those described previously section as well as published information (e.g. Schott and McCreary Jr, 2001; Bruce, 1979; Beal and Chereskin, 2003; Cox, 1979; Düing and Schott, 1978; Donohue and Toole, 2003). In conjunction with the model simulation, absolute dynamic topography (ADT) obtained from the SSALTO/DUACS-gridded data products www.aviso.oceanobs.com is used to investigate the Southern Gyre. The product combines sea level anomaly observations merged from satellites Jason-1, Envisat, GFO, ERS-1, ERS-2, and Topex/Poseidon with the CNES-CLS09 mean dynamic topography (MDT) binned into 7-day averages from 14 October 1992 to 31 March 2010 globally gridded at 1° x 1° (Ducet et al., 2000).

3.3 Results and discussion

3.3.1 Model evaluation

As discussed in the introduction, the regional dynamics are highly seasonal due to the influence of monsoonal wind forcing. Figure 3.2 compares the climatology of sea surface temperature (SST) computed from 7 years of model output and optimally interpolated SST derived from microwave and infrared (MW-IR) from2002 to 2015. The optimally interpolated SST product combines the through cloud capabilities of the microwave data (MW) with the high spatial resolution of the IR SST data.

The general distribution of the model and satellite-derived SSTs agree well in the interior of the domain during all seasons. The seasonal cycle is well represented in the model compared to observations with large-scale patterns of warmer SST during boreal winter (Figure 3.2a & e) in the range of ∼27 – 30 °C but the model tends to overestimate SSTs value north of 5°S by ∼0.3 °C. North of the equator, a zone of cooler waters of ∼27 – 28°C is evident with warm waters further south. In boreal spring (inter-monsoon), there is warming north of 5°S (Figure 3.2b and f) due to weaker winds (Figure 3.1) compared to the previous season while east of Madagascar there is cooling. The cooling is more pronounced in the model which has a negative bias of ∼0.9 – 1.5 °C for most parts of the region south of about 5°S (Figure 3.2j). With the onset of the SW Monsoon in boreal summer, the tropical western Indian Ocean cools significantly in both the model and satellite observation (Figure 3.2c and g). The coldest SSTs (25 – 26 °C) occur in the central and southeast of the domain while in the northeast

of the domain warm SSTs (27 – 28 °C) are evident. The occurrence of cool waters near Madagascar is more pronounced in the model compared to what is observed from satellite, resulting in a negative bias of between 0.3 and 0.6 °C (Figure 3.2k). A similar size bias exists along the equator whereas a small warm bias is apparent northeast of Madagascar. The cooling during boreal summer and spring in the west and south of the domain may be attributed to the strong monsoon winds which then increase the surface latent heat flux and vertical mixing.

In boreal autumn (inter-monsoon) (Figure 3.2d & h), warmer SSTs become evident in both the model and observation with values ranging between 26 and 28 °C. This increase in SST can be attributed to weaker inter-monsoon winds (Figure 3.1d) leading to reduced evaporative heat loss and vertical mixing. The model shows a positive bias in SST of 0.3 °C south of about 3°S. The magnitude of the model bias is smaller and more spatially confined than what is observed in (Figure 3.2b & c).

In summary, the model displays a negative bias over lower parts of the domain in boreal spring and the SW Monsoon. Near Madagascar there are negative biases in all seasons except boreal autumn and generally the SST biases are weakest for the NE Monsoon season.

To represent the simulated seasonal mean circulation (Figure 3.3) shows the volume transport integrated over the upper 1500 m. The main currents described by (Wyrtki et al., 1971; Schott and McCreary Jr, 2001; Leetmaa et al., 1982) are present in this depiction. In the model, the South Equatorial Current extends from about 12 – 18°S and flows westward before splitting near the east coast of Madagascar at around 17°S (Figure 3.3a) into the Northeast Madagascar Current (NEMC) and the Southeast Madagascar Current (SEMC). The NEMC flows north of Madagascar where it splits into the northward flowing EACC and a southward flow which is largely made up of anti-cyclonic eddies in the Comoros Basin (Backeberg and Reason, 2010; Collins et al., 2014; Manyilizu et al., 2014, 2016). The SEC transports about 50 Sv during the SW Monsoon and spring similar to the transport estimate of 52.3 Sv in June and July of Manyilizu et al. (2016) followed by weaker volume transport of about 45 Sv during the autumn and the NE monsoon similar to what Manyilizu et al. (2016) calculated for September. The annual mean volume transport of 39 Sv from the model is lower than the 50 Sv estimated by Schott and McCreary Jr (2001) and considerably higher than volume

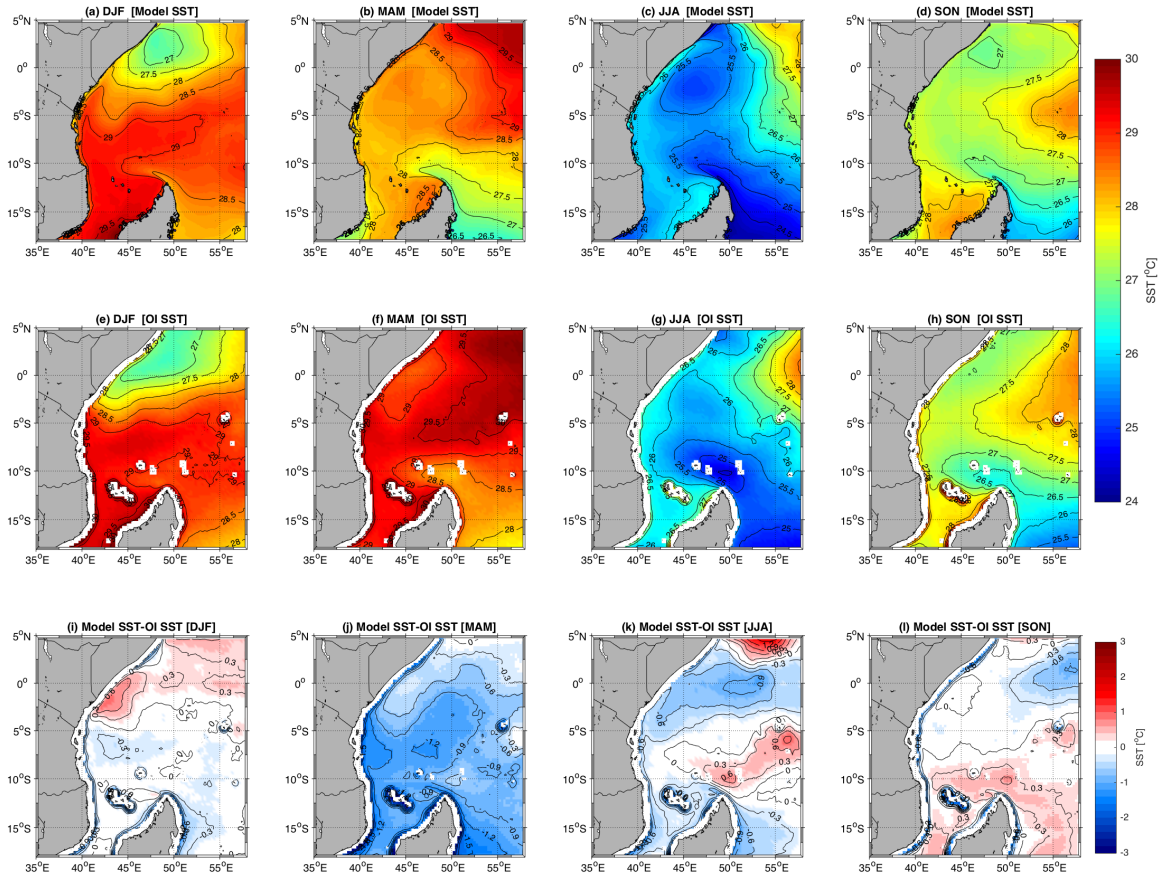

Fig. 3.2 Seasonal cycle of mean sea surface temperature from model (a-d) and OI SST (e-h) over the tropical western Indian Ocean where the contour interval is 0.5°C. The difference between the model and satellite are shown in (i)-(l) with contour interval at 0.3°C. Positive (negative) values indicate over-estimation (under-estimation of SSTs by the model)

transport estimates of 25 Sv reported by Stramma and Lutjeharms (1997) in the upper 1000 m. The reason for the lower annual mean volume transport estimated in the model than that of Schott and McCreary Jr (2001) is because the southern boundary of the model extends only to 18°S and thus excludes part of the southern most part of the SEC.

The NEMC supplies the northward flowing EACC along the East African coast with transport estimate of 35 Sv past the tip of Madagascar at 49°E between 8 and 12°S. This value is in good agreement with a transport value of 38 Sv of Manyilizu et al. (2016) calculated in April and May. The annual volume transport calculated for this section is 36 Sv which is fairly close to the 30 Sv estimated by Swallow et al.

(1988) and Donohue and Toole (2003) using hydrographic data. The EACC flows steadily north and turns offshore just south of the equator forming the South Equatorial Counter Current (SECC) during the NE Monsoon and boreal spring (inter-monsoon) respectively (Figure 3.3a and b) During the SW Monsoon and boreal autumn (inter-monsoon) period (Figure 3.3c and d), the EACC tends to flow faster and merges with the northward flowing SC. The northward flowing SC diverges from the coast turning eastward at about 3 – 5°N. Further offshore (48 – 52°E), it turns southward and then back towards the coast forming the Southern Gyre. Consequently, the volume transport in the EACC is highest during the SW Monsoon with values of about 30 Sv in the model as compared to the 22 Sv calculated in June 1979 by Swallow et al. (1991) and a value of 40Sv in the climatological model output of Manyilizu et al. (2016) for June.

3.3.2 Rossby wave propagation in the tropical Indian Ocean

In this section, the propagation of Rossby waves in the Southern Gyre region is considered. The variability of winds north of 10°S in the Indian Ocean is dominated by the annual cycle. The alternating southwest/northeast monsoons provide a strong annual and semi-annual forcing that drives a basin-scale sea-level response involving both equatorial wave dynamics and coastal wave propagation around the perimeter of the equatorial Indian Ocean McCreary et al. (1993) Therefore, given the inherent variability of the western Indian Ocean region, a better understanding of remote forcing and its contribution to the dynamics of the Southern Gyre need to be investigated. To investigate the effect of Rossby waves on the Southern Gyre, a longitude time cross-section of SSH anomalies at 4°S from 40 - 80°E is illustrated in (Figure 3.4a and b). This transect is defined on the basis of the first meridional mode Rossby waves typically having SSH maxima centered around 4°S Chelton et al. (2003).
Note that (Figure 3.4 b) is computed from 2000 to 2009 Aviso data and therefore shows inter-annual variability whereas (Figure 3.4a) is derived from 7 years of model output forced by monthly mean surface winds and fluxes (as discussed in Section 2). Thus, the only inter-annual variability in (Figure 3.4a) is that arising from internal ocean processes. (Figure 3.4c) shows the QuikSCAT zonal wind stress from 40 - 120°E for the same period as the Aviso plot.

At this latitudinal band, the model shows a strong annual cycle in SSH that is essentially driven by the seasonally reversing winds over the tropical Indian Ocean (Figure 3.1). Westerly winds in the eastern equatorial Indian Ocean during the boreal

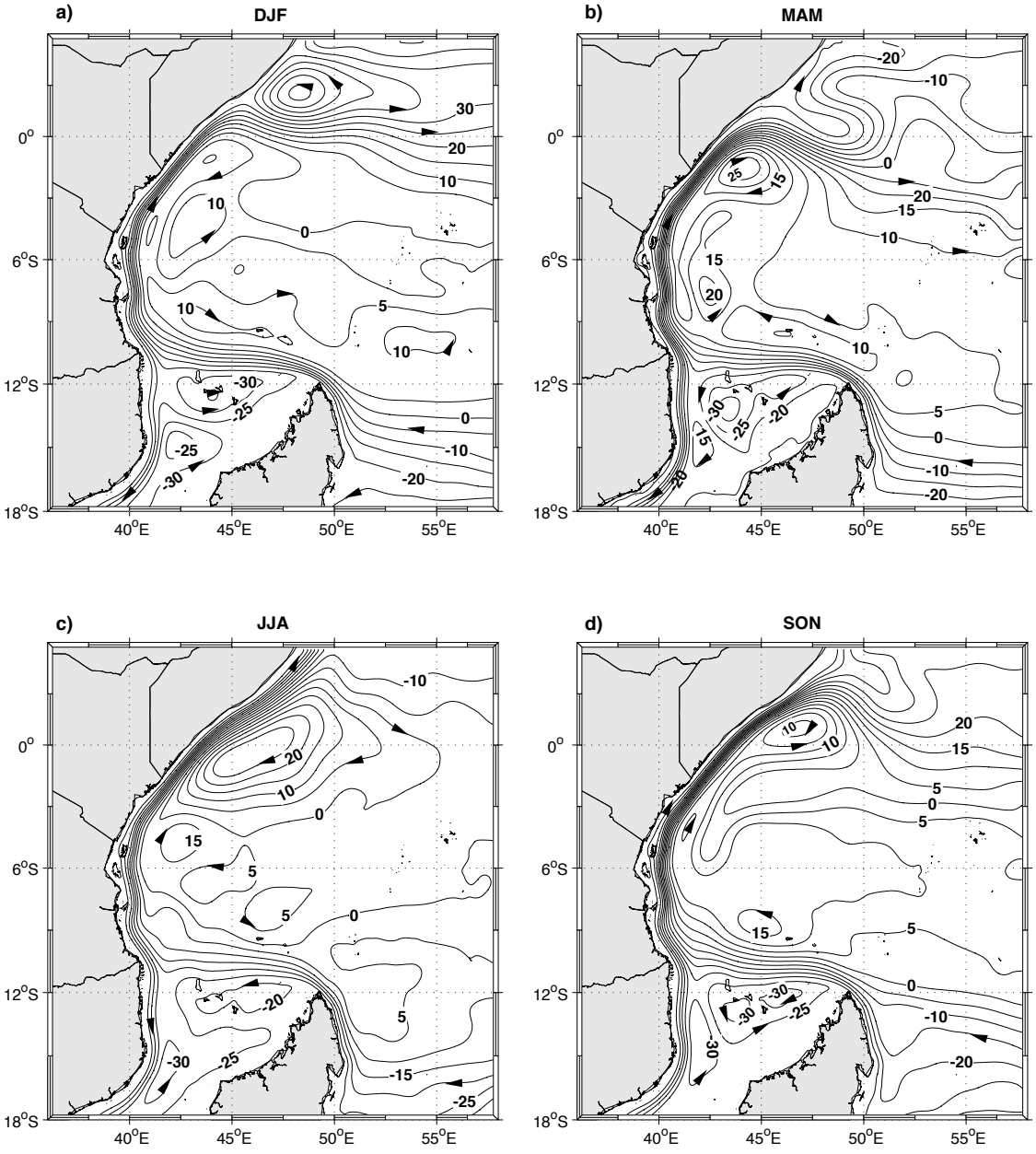

Fig. 3.3 Volume transport (Sv) calculated for the upper 1500 m derived from 7-year model output. The arrows indicate the direction of the flow.

autumn and boreal winter drive downwelling Rossby waves that propagate westwards towards East Africa. During boreal spring and summer, there are strong easterlies extending from Java / Sumatra across the equatorial belt which drive upwelling Rossby waves. (Figure 3.4c) shows this seasonal variation in QuikSCAT wind stress but modu-

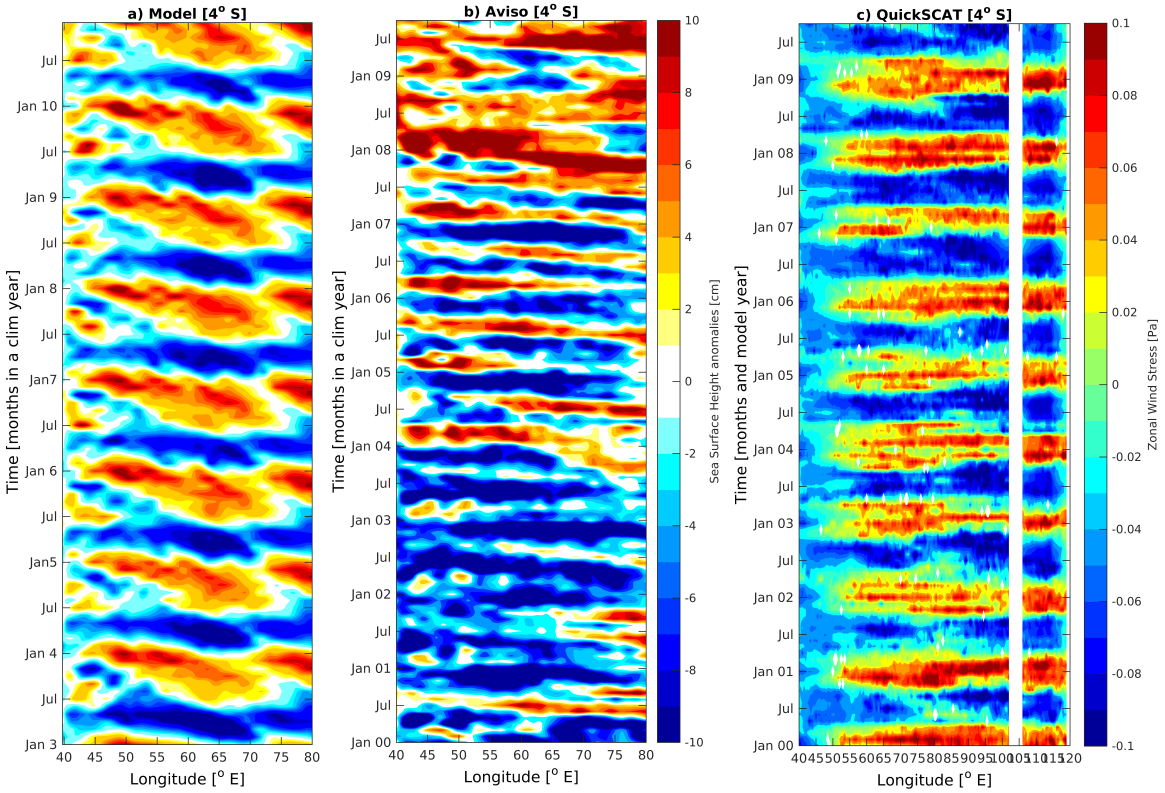

Fig. 3.4 Hovmöller plot of sea surface height anomalies froma) 7 years ofmodel output, b) Aviso computed from1999 to 2009 (same period as forcingwindstress in the model), and c) zonal windstress from QuikSCAT.

lated from year to year by interannual variability arising from ENSO (Reason et al., 2000) or the Indian Ocean Dipole (Saji et al., 1999) for example. Near the East African coast (west of 47°E), the seasonal signal in the zonal wind is just evident in magnitude as the winds here always have an easterly component (Figure 3.1) oscillating between southeasterly during SW Monsoon and northeasterly during the NE Monsoon. The seasonal variability in the Aviso SSH anomalies (Figure 3.4b) is strongly modified by interannual variability with the first few years mainly dominated by upwelling Rossby waves and the last few by downwelling Rossby waves propagating into the domain from the east.

Figure 3.4b suggests that it takes 4–6 months for the Rossby waves to reach the East African coast from 80°E while, in the model (Figure 3.4a) the propagating signal appears slower. Because the model was forced with climatological data, the seasonal SSH signal is essentially repeated each year with only small variations. The Hovmöller

plots (Figure 3.4a and b) suggest that the propagating SSH anomalies along 4°S will reach the location of the Southern Gyre and hence could influence its evolution and intensification. However, this is dependent on the strength of the monsoon winds as described in Subrahmanyam et al. (2001). Through modelling studies and use of altimetry data, Rossby waves in the southern Indian Ocean have been studied by Wang et al. (2001) and Hermes and Reason (2008, 2009) who found the influence of localized forcing between 70° and 80°E causes the waves to breakdown. It is evident from (Figure 3.4a) that there is a change in propagation characteristics near 75°E where another Rossby wave starts to propagate in the model. However, in the Aviso data (Figure 3.4b) a possible breakdown near this longitude only seems clearly apparent in 2002, 2004 and 2008 at longitudes similar to what was observed in Wang et al. (2001) and Hermes and Reason (2008) while another wave forms at 65°E. Wang et al. (2001) suggested that the second wave west of 65°E is a continuation of the Rossby wave in the east and the apparent breakdown is due to interaction with the local winds.

The phase speed associated with the model and Aviso is calculated by estimating an optimal line on the Hovmöller plot of SSH anomalies computed from lag correlation at each longitude. The highest correlation coefficient at each longitude is then used to calculate the phase speed from the slope of the line. The resulting phase speeds from the model and Aviso are 0.18 ms^{-1} and 0.5 ms^{-1} respectively assuming that the propagating signal is a Rossby wave. The estimated speeds are slower than the theoretical and observed Rossby wave speeds of between 0.26 and 0.31 ms^{-1} calculated by Subrahmanyam et al. (2001) for the tropical Indian Ocean. However, the estimate is within the range of typical phase speeds of Rossby waves identified in several other studies (White, 2000; Rao et al., 2002). A slower wave speed than the theoretical value suggests that the ocean signal may be retarded through coupling with the atmosphere or that interactions with the mean flow or topography may be important. For example, Subrahmanyam et al. (2001) showed that Rossby wave amplitude and speed tended to change when these waves crossed the Ninety East Ridge or due to interactions with the Indonesian through-flow and the SEC.

In summary, the effect of remotely forced Rossby waves may accelerate the Somali Current whereas local wind forcing dominate right after the monsoon onset. In addition, along the East African coast, smaller-scale signals are particularly evident during mid boreal winter at periods between 30 and 50 day (Figure 3.4a) These signals contribute

energy to the Southern Gyre resulting in the intensification of the Southern Gyre and its northward movement.

3.3.3 Sea surface height variability

To evaluate both the mesoscale and large scale circulation in the region, the variance of sea surface height from the 7 years of model output and Aviso derived absolute dynamic topography were computed. Since the model domain includes the equator where geostrophy is no longer valid, the enhanced variance of SSH is used as a proxy for available potential energy (Vic et al., 2014), and to assess mesoscale variability (Collins et al., 2014)

The patterns of SSH variance show a strong seasonality in both the model and Aviso with broadly similar patterns except along the Somali coast and in the eastern equatorial region during the SW Monsoon and in the far south of the domain during the NE Monsoon (Figure 3.4a and b). In general, the model shows a larger area of high variability during the SW Monsoon, particularly over the Somali Basin. During this season, the SSH variance ranges from 10 to 50 cm^2 extending north from 3°S along the Somali coast and further offshore near the locations of the SC, the Southern Gyre, and the Great Whirl. The zonal strip of SSH variance in the open ocean between 0 and 5°S in the model and 2 – 8°S in Aviso reflects the propagating Rossby waves from the eastern Indian Ocean consistent with (Webber et al., 2012). During the NE Monsoon, the eddy activity is lower over most of the basin than for the SW Monsoon with the SSH variance ranging from 5 to 20 cm^2. However, the model shows much higher variance values in the northern Mozambique Channel which are not evident in the satellite data. The lower values in SSH variance during this season may result from the weaker currents in this season compared to what is observed during the SW Monsoon

To quantify mesoscale activity observed in the region and the characteristics of the Southern Gyre, an automated eddy identification and tracking scheme (Penven et al., 2005; Halo et al., 2014c) was applied. The mesoscale activity in the region is important because mesoscale eddies carry water masses that are different from their surrounding enhancing mixing as the eddies dissipate. It would be great to investigate the interaction of these mesoscale eddies and the Southern Gyre.

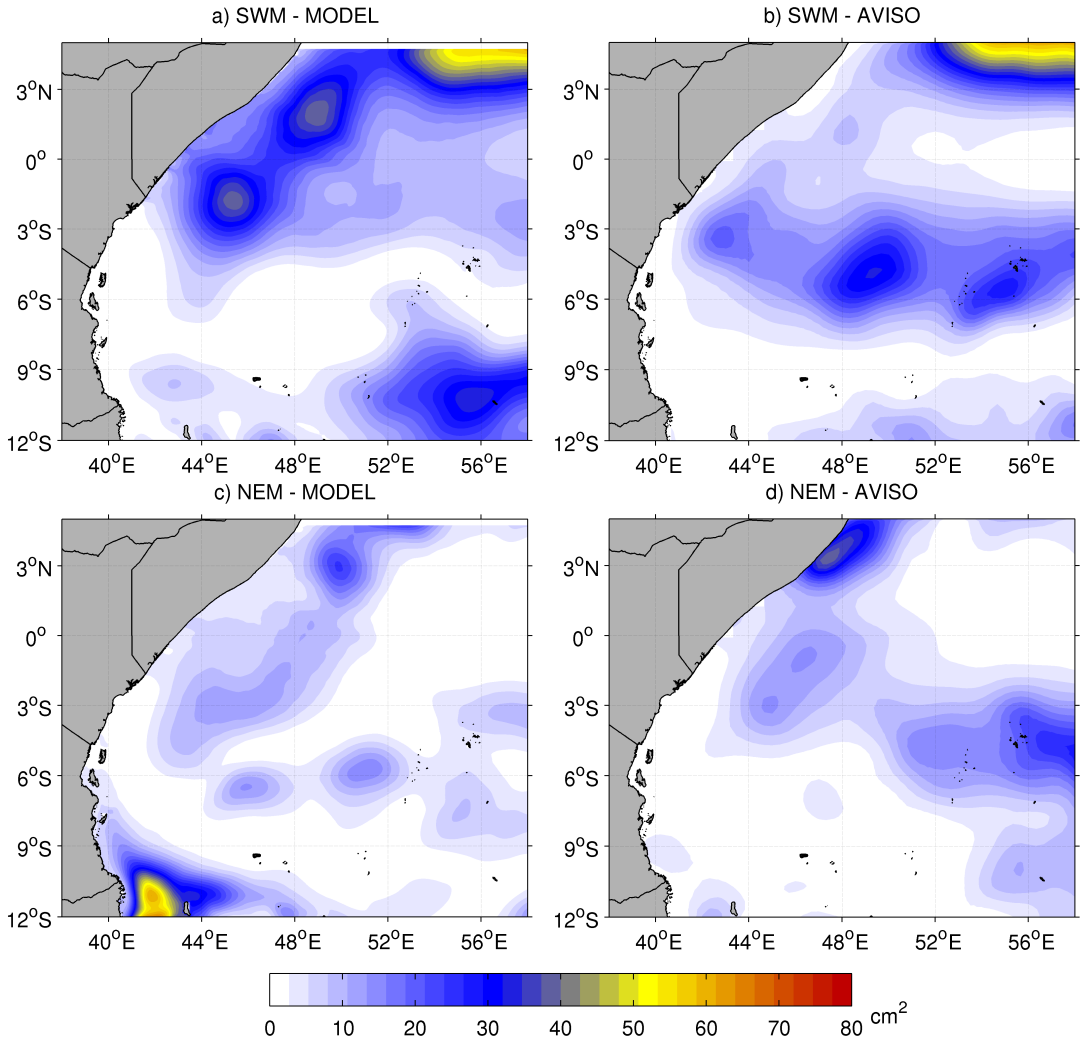

Fig. 3.5 Sea surface height (SHH) variance calculated from the 7-years of model run and 17 years of MADT Aviso data.

This scheme which was applied to both the Aviso data and the model output uses physical criteria as well as geometric techniques to identify and track eddies. A combination of positive values of the Okubo-Weiss parameter and the largest closed contour is used by the eddy identification scheme to detect both cyclonic and anticyclonic eddies. This parameter aims to separate the velocity field into regions of high deformation and high vorticity (Okubo, 1970; Weiss, 1991). As demonstrated by Halo et al. (2014c), this hybrid method is more robust than using the closed contours and Okubo-Weiss criteria independently.

In this study, the scheme is used to track both eddies and the gyre scale feature (here the Southern Gyre) by setting the maximum radius as a closed loop of SSH to 600 km. The algorithm was applied to both weekly maps of absolute dynamic topography from Aviso (14 October 1992 to 31 March 2010) and 7 years' model output. Only eddies with a lifespan longer than 20 days were tracked. To assess the general characteristics of the eddies and the gyre found within the basin, an inspection of relevant mean geometric and dynamical properties is presented in (Table 3.1).

Table 3.1 The mean characteristics of the Eddies and Southern Gyre generated in the study region.

Characteristics	AVISO		MODEL	
	Eddies	Southern Gyre	Eddies	Southern Gyre
Number of Eddies	140	1	60	1
Life span (days)	52	70	35	98
Eddy scale (km)	101	358	97	400
Rotational speed (m/s)	0.31	0.55	0.25	0.72
Eddy amplitude	0.63	0.51	0.77	0.80
Total integrated energy (m^4 s^{-2})	9.33 x 10^{11}	6.63 x 10^{11}	8.32 x 10^{11}	11.15 x 10^{11}

During this period, the scheme identified 140 eddies from Aviso and 60 eddies from the model with 95% of eddies tracked being cyclonic with 5% of tracked eddies being anticyclonic. Table 3.1 only gives the mean characteristics of the tracked cyclonic eddies and the Southern Gyre which is of relevance to this study. The number of eddies found in the model is lower than in the altimetry data because only 7 years of model output was analyzed. The observed and simulated cyclonic eddies have an average lifespan of 52 and 35 days respectively (Table 3.1) and remain in the domain for their entire lifespan. The same definition as Halo et al. (2014a) was used to define the eddy life span which is the difference between the date when the eddy makes its first appearance and the date since it was last seen. Given the 18 years of altimeter data and 7 years of model output, the estimates in Table 3.1 suggest that about 8 eddies are generated per annum in the study domain in both Aviso and the model. In the observations and model, the majority of the cyclonic eddies generated in the study domain have lifespans shorter than 40 days (Figure 3.6a and b). Life-spans greater than 90 days are attained by 5% of the eddies generated.

The tracked Southern Gyre has a mean lifespan of about 70 days from Aviso and 98 days from the model with the eddy radius being similar in the observed data and model. The mean rotational speed associated with the gyre calculated from the model and Aviso is 0.72 ms^{-1} and 0.55 ms^{-1} respectively. The rotational speed is a measure of the eddy currents that characterizes the strength of the eddy with faster (slower) rotational speeds implying stronger (weaker) (Collins et al., 2014). The spectrum of the eddy energy distribution with respect to size is eddies ∼9.55 x10^{11} m^4 s^{-2} from Aviso and ∼11.15 x10^{11} m^4 s^{-2} from the model. The Southern Gyre remains in the domain over its entire lifespan as it moves northward to about 4°N and its spatial dimension is similar in the model and Aviso.

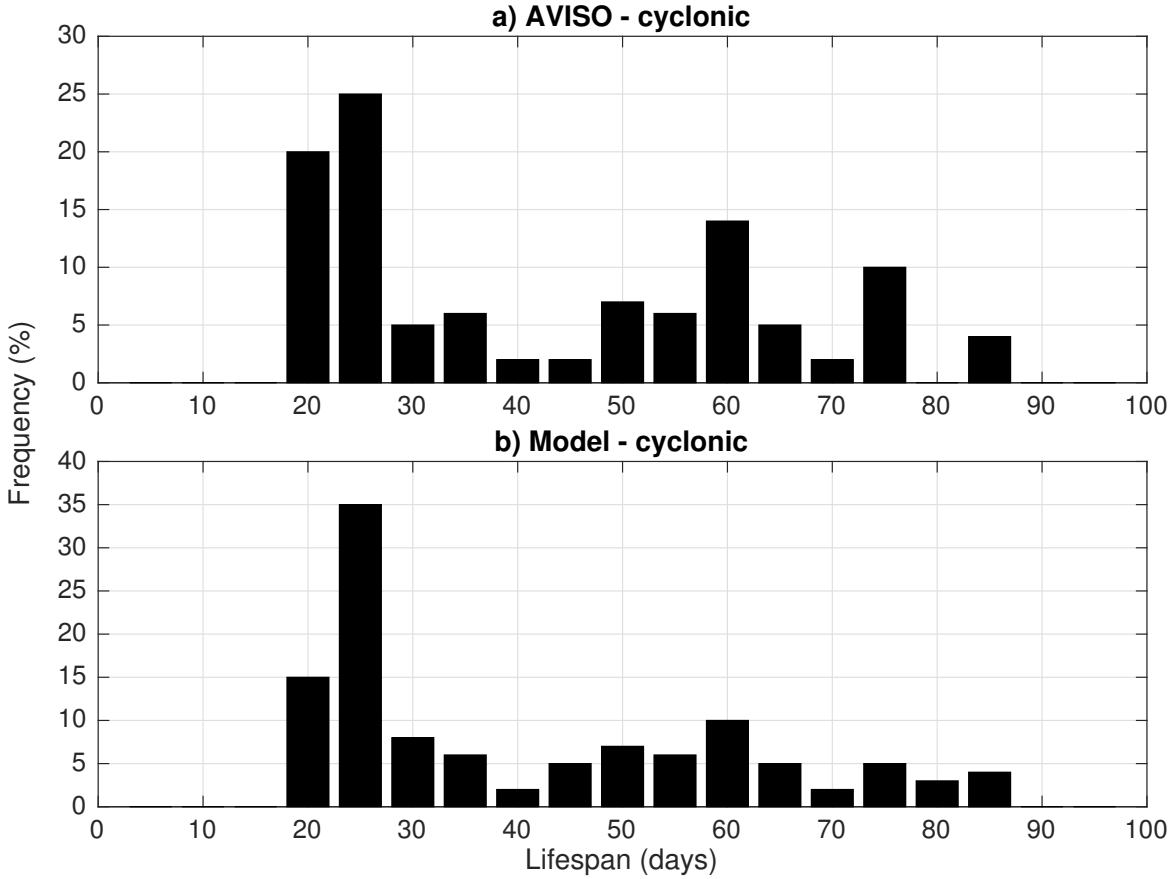

Fig. 3.6 The distribution of the lifespan of eddies (days)generated and residing in the study domain as tracked (a) Aviso and (b) ROMS.

Energy conversion terms are used to investigate the dominant eddy forcing mechanisms through either baroclinic (PeKe) or barotropic (KmKe) instabilities. (Figure 3.7 shows the spatial distribution of energy conversion terms (KmKe and PeKe) associated

with the Southern Gyre. The transfer terms were integrated vertically through the upper 500 m. Figure 3.7a portrays a dynamical process in which the kinetic energy of the system is directly converted from its mean state to its turbulent form which represents a barotropic instability of the flow. Over the Southern Gyre region, the PeKe is largely negative suggesting dissipation at this location (Figure 3.7b). However, the mixed signals of positive and negative PeKe further north suggest that this area may also contribute to the dissipation of eddy kinetic energy towards its potential form. Regions of shear production (positive conversation rate) occur along the East African coast with eddy formation appearing to be driven by both barotropic and baroclinic instabilities of the northward flowing SC. The strongest positive conversion rate for mean potential energy to eddy potential energy occurs along the Somali coast from the equator to about 3°N indicating an increasing barotropic nature of the Southern Gyre due to barotropic instabilities associated with the northward flowing SC as it crosses over the equator. A pure barotropic instability process initially involves horizontal shear, although later it may evolve into a mix of barotropic and baroclinic instabilities. Part of the resulting variability is subsequently converted into a barotropic component by a geostrophic turbulence cascade (Rhines and Holland, 1979; Rhines and Young, 1982) or a topographical coupling between Rossby wave modes (Straub, 1994).

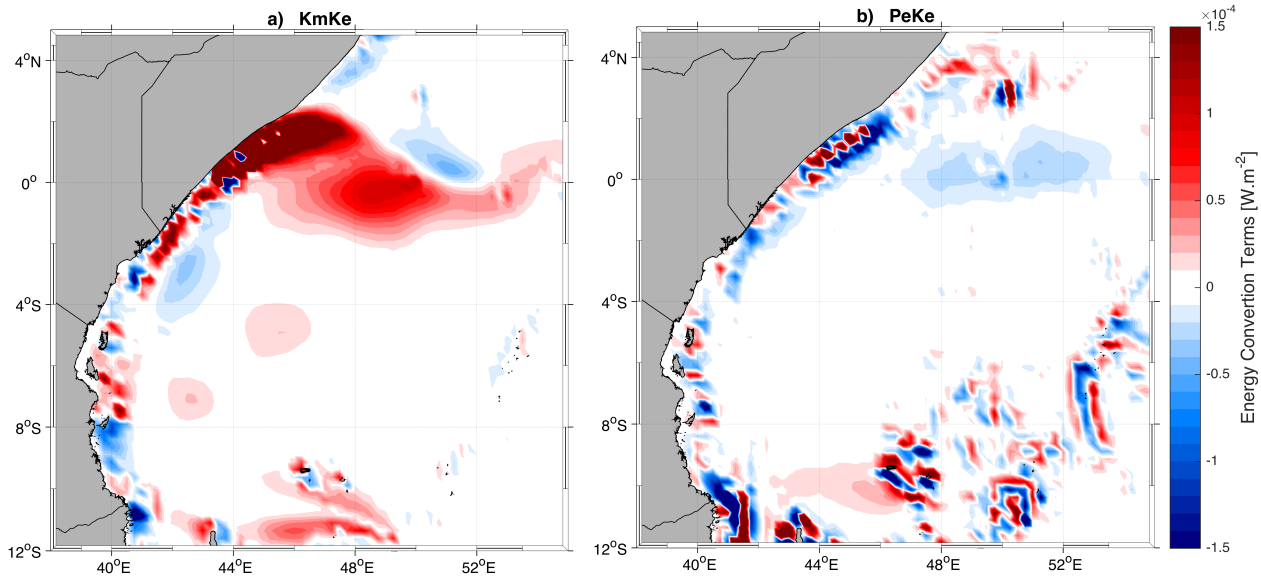

Fig. 3.7 Spatial distribution of the energy transfer terms associated with a) mean kinetic to eddy kinetic (KmKe) and b) eddy potential to eddy kinetic (PeKe) computed from the 7-year climatology model simulation.

3.3.4 Southern Gyre vertical structure

Because limited in-situ data are available in the region, model outputs are used to investigate the vertical structure of the Southern Gyre which is known to be quasi-stationary near the equator. In order to investigate the vertical structure, snapshots of the Southern Gyre are randomly selected from the model output as case studies. In an attempt to characterize the dynamical aspect of the Southern Gyre, relative vorticity (ζ) (Figure 3.8a - c) and vertical profiles of meridional velocity at the equator, 1°N and 2°N (Figure 3.8d - f) were computed from the model outputs. In June, the Southern Gyre is positioned near the equator with maximum surface velocities of 0.2 ms^{-1} and penetrates to about 100 m depth (Figure 3.8a and d). This recirculation is relatively strong because there is substantial negative vorticity input from the wind stress curl. A northward flow occurs further offshore around 55°E that crosses the equator.

The intensification of the SW Monsoon in July amplifies the intensity of the Southern Gyre. Simultaneously, the northward flowing alongshore SC which is part of the gyre strengthens with a maximum velocity of 1.4 ms^{-1} and deepens to over 1000 m resulting in a V-shaped structure between the East African shelf and 43°E (Figure 3.8d - e) similar to other western boundary currents. The strong off shore flow observed in (Figure 3.8b) which is part of the Southern Gyre northern boundary (positive vorticity) extends northward to about 2°N coinciding with an increase in wind stress.

During this period, the typical flow speed in the Southern Gyre is approximately 0.6 ms^{-1} which widens and deepens to about 200 m compared to June. Between the SC and the Southern Gyre, there is a southward flowing undercurrent observed at between 300 and 500 m depth at 46° to 48°E Ewith velocities ranging between 0.4 and 0.6 ms^{-1} (Figure 3.8e) connected to eastward undercurrents along the equator similar to what was observed by Jensen (1991). By mid-August, the Southern Gyre occupies almost the entire width of the Somali Basin from 44°E to about 52°E, and extends to about 200 m depth (Figure 3.8f) and is strongly surface intensified with maximum northward and southward velocities reaching 1.2 ms^{-1}. At this time, the SW Monsoon winds are just beginning to decrease and the northern boundary of the Southern Gyre has reached about 4°N (Figure 3.8c). What triggers the northward migration is not yet known but it may be related to the decrease in the westerly component of the near-equatorial SW Monsoon winds and arrival of Rossby wave energy at the East African coast. This energy helps to intensify the recirculation of the Southern Gyre and causes it to move northward. Note that the timing of the northward movement of the Southern Gyre coincides with the arrival of downwelling Rossby waves which take

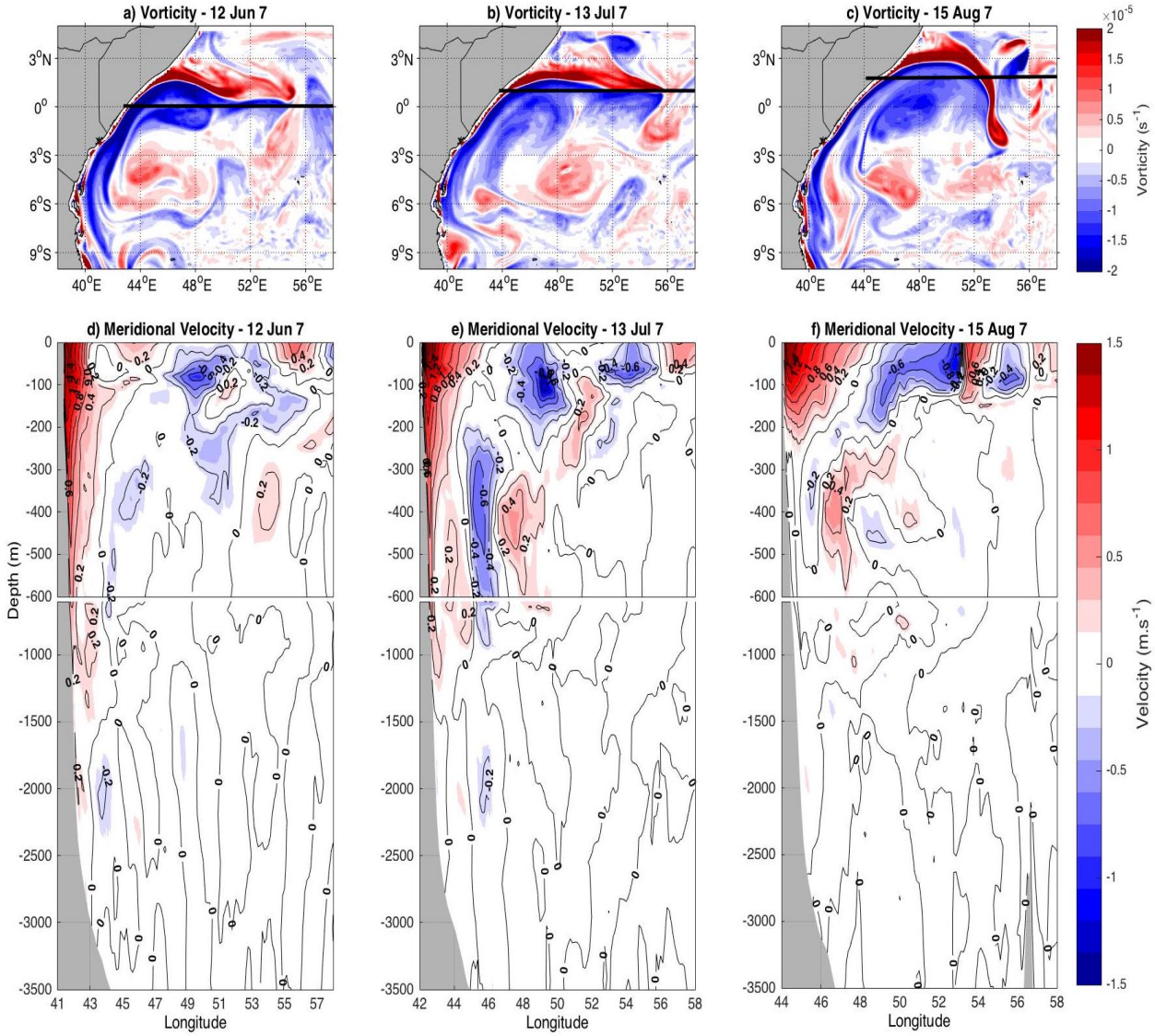

Fig. 3.8 Sequence of relative vorticity (ζ) and vertical profile of meridional velocity averaged at 10 days and centered on each date marked above figures. The large pool of negative (blue) vorticity is the Southern Gyre while the filaments of positive (red) vorticity representing bursts. The contour interval for the meridional velocity is 0.2m/s. Negative (positive) velocities indicate southward (northward) flow. (For interpretation of the references to colour in this figure legend, the reader is referred to the web version of this article.)

approximately 30–50 days to travel from 75°E to the East African coast.

The evolution of the gyre is also dominated by chaotic interactions with detachments of positive vorticity near 53–56°E. These detachments are intense phenomena and exhibit strongest velocity and vorticity gradients near the east of the Southern Gyre. Beal and Donohue (2013) also observed similar flanking positive vorticity bursts attached to the Great Whirl. In Figure 3.8a, b and c, there is a thin sheet of positive vorticity that stretches along the western boundary at the inner edge of the SC and the EACC. Akuetevi and Wirth (2015) explained this phenomenon as resulting from the lateral shear of the SC whose circulation is intensified by the growth of the Southern Gyre and Great Whirl. Entrained by the swirling motion of the larger Southern Gyre, the filament of positive vorticity is torn off the boundary near 3°N and moves offshore towards the open ocean. The ejected positive vorticity anomalies pair with the negative vorticity of the Southern Gyre to form dipoles. In August (Figure 3.8c), the positive vorticity get absorbed into the northward flowing Somali Current injecting positive vorticity into the Southern Gyre which is hypothesized to weaken the recirculation of the Southern Gyre prompting its decay. The bursts of positive vorticity entrain the upwelled water masses from the cold wedge as illustrated on (Figure 2.2) which then contribute to water properties of the Southern Gyre once absorbed.

The water mass signatures of the Southern Gyre are of interest in terms of their connectivity to the SEC which is known to bring relatively low salinity water from the Indonesian Through Flow (ITF). Figure 3.9 shows vertical sections of potential temperature and salinity over the Southern Gyre taken along the equator, 1°N and 2°N. Above the thermocline (∼200 m), a layer of high potential temperature and low salinity surface water in the upper 100 m is observed (Figure 3.9a and d). Near the surface, the low salinity water flows north and then returns southward near 51°E (Figure 3.9d). Further offshore, between 55° - 57°E, higher salinity water extends deeper to about 100 m depth.

These temperature and salinity characteristics are due to seasonal heating and advection of low salinity waters from the east during the SW Monsoon (Schott and McCreary Jr, 2001). It has been shown that the ITF transports Pacific waters into the Indian Ocean, mostly within the upper ocean and dominantly composed of North Pacific water (Gordon, 2005). The ITF transport also has a subsurface core at intermediate depths, most of which comes from the South Pacific (Gordon, 2005; McCreary et al., 2007). The water masses entering through the Indonesian passages become transformed by strong vertical mixing as they flow over the bottom topography (Ffield

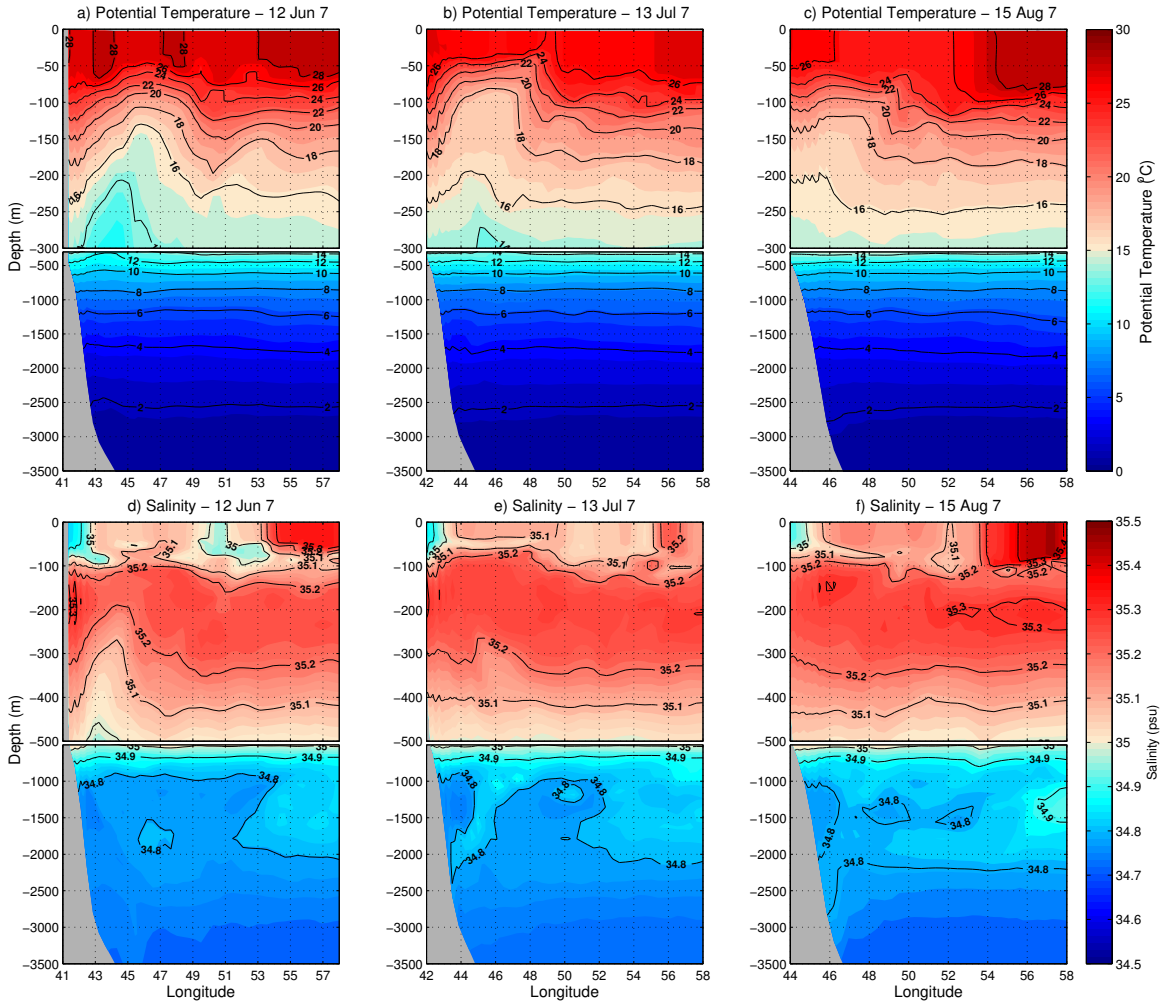

Fig. 3.9 Vertical section of potential temperature and salinity of the Southern Gyre at time averages. The contour interval for the potential temperature is 2 °Cwhile that of salinity is 0.1 psu

and Gordon, 1992), and so assume new characteristics, showing a relative salinity minimum along the SEC (Koch-Larrouy et al., 2007) which points towards fresher waters in the Southern Gyre and SC. Below 1000m, Indian Deep Waters are observed with salinities around 34.8 psu as described by Tomczak and Godfrey (2013).

During July and August (Figure 3.9b, c, e and f), conditions in the upper ocean remain relatively similar and the Southern Gyre is characterized by slightly cooler (∼26 °C) and fresh water. The most pronounced feature of the thermocline is the dome between 44° - 46°E, associated with the boundary current turning offshore and then south forming the Southern Gyre. A trough in the 20 °C isotherm between 47° - 49°E suggests a northward loop. Further east, there is little variation in the thermocline

although larger changes can be seen in the salinity field. Close to the coast, the 20 °C isotherm shoals to 100 m (Figure 3.9c) presumably in response to weaker southwesterly winds compared to June.

It is evident that the water properties of the SC are fresher compared to those in the Southern Gyre. The reason for fresher water in the SC is due to upwelling along the path of the monsoon wind jet,which follows the Somali coast and extends offshore from the Horn of Africa (Findlater, 1969b).

3.4 Summery and conclusion

This study examined the dynamics and characteristics of the Southern Gyre in the western Indian Ocean. The work was motivated by the fact that few studies investigate the Southern Gyre and previous efforts to understand it have mainly focused on the role of the seasonal monsoon winds in its establishment. This paper presents an analysis of the Southern Gyre based on a high resolution regional ocean model. The region is very energetic and influenced by seasonal monsoons characterized by the Southern Gyre during the SW Monsoon.

The pre-conditioning effect of the annual downwelling Rossby wave and amplification by the SW monsoon winds may result in the intensification of the Somali Current and retroflection forming the Southern Gyre. The Rossby wave, originating in the eastern equatorial Indian Ocean, takes ∼30 – 60 days to travel from 75°E to the East African coast and plays a key role in the generation of the Southern Gyre as proposed by McCreary and Kundu (1988); Schott and McCreary Jr (2001). In addition to arrival of downwelling Rossby waves, there are smaller scale signals in late summer and autumn at periods between 30 and 50 days that induce energy on the Southern Gyre intensifying the recirculation.

Besides the influence of remote forcing and local forcing, internal instabilities play a key role in generation of the Southern Gyre. An examination of the different energy conversion terms (barotropic and baroclinic instabilities) reveals that barotropic instabilities related to the EACC/Somali Current is primarily responsible for the Southern Gyre development.

With the turbulent nature of the Somali Current, positive vorticity bursts are observed from the Southern Gyre that later pair with the negative vorticity of the Southern Gyre to form dipoles (Figure 3.8b). Towards the end of SW Monsoon season (around August), the positive vorticity detachments get absorbed into the northward flowing Somali Current injecting positive vorticity causing its decay.

From the eddy tracking algorithm, the Southern Gyre has a mean diameter of ∼400 km with a lifespan of about 3 months and lies more or less quasi-stationary near the equator for roughly 80% of its life before moving slightly north. This movement of the Southern Gyre can be attributed to it being situated in a turbulent western boundary region which is affected by interactions with the continental shelf and smaller-scale signals of Rossby waves observed along the East African coast.

There appears to be no sequence of events attributed to the collapse of the Southern Gyre, other than an initiation by the change in seasonal wind forcing and absorption of the positive vorticity bursts that contribute to its decay. However, to separate the role of different forcing on the Southern Gyre and its variability, it would be necessary to perform a longer run with inter-annually varying forcing and extend the northern boundary to investigate if the Southern Gyre coalesce with the Great Whirl. The new generation SWOT satellite observations and hopefully in-situ measurements from the on-going Second International Indian Ocean Expedition (IIOE-2) may also shed further light on this highly variable and complex region.

Having described the general circulation of the study region, the next chapter uses the ocean state variables of the ROMS to drive the Lagrangian Individual Based Model (IBM).

Chapter 4

Modelling dispersal and connectivity of corals at regional scale

This result chapter is based on the work submitted to Journal of Geophysical Research - Biogeosciences as:
Gamoyo, M., David, O., & Reason, C.J.C. (2017). Estimating connectivity through larval dispersal in the Western Indian Ocean.

Abstract

The health and functioning of coral reef ecosystems in the western Indian Ocean are in decline due to anthropogenic stress and the rate of decline is set to accelerate with mounting anthropogenic pressures. Marine reserves have become important tools in mitigating these pressures and one of the most critical factors in determining their spatial design is the degree of connectivity among different populations. However, the spatial scale and strength at which populations are potentially connected by dispersal remain uncertain. This study used a biophysical model incorporating a high-resolution ocean current to quantify the seascape-wide dispersal potential. Potential larval density, connectivity metrics, and graph theory showed that connectivity varied with pelagic larval duration and influenced by both large-scale and mesoscale ocean circulation. Dispersal was mostly westwards towards East African coast and northwards from Tanzania towards Kenya. Six reef nodes (Tanzania-22, Mozambique-49 & 60, Comoros-71 & 77, and Glorieuses-86) emerged as crucial nodes for ensuring multi-generational

connectivity while Tromelin was completely isolated based on larval dispersal that also corresponded to genetic studies. The identification of reef nodes that act as a stepping stone would guide the selection of priority conservation areas and support resilience.

Keywords: Regional Ocean Modelling System, Individual Based Model, Graph theory, Connectivity

4.1 Introduction

Coral reefs are one of the most diverse ecosystems in the world, providing essential ecosystem services to millions of coastal communities (Done et al., 1996; Moberg and Folke, 1999). However, combined myriad of large-scale (related to global warming) and local stressors (over-fishing, pollution, and disease) have reduced coral populations worldwide (Loya et al., 2001; Hughes et al., 2003; Wakeford et al., 2008) with about 30% of world corals seriously degraded (Wilkinson et al., 2004). With the Western Indian Ocean (WIO) being the peak of biodiversity (species and genus distributions) within the larger Indo-Pacific region (Obura, 2012; Hoareau et al., 2013; Parravicini et al., 2013; Borsa et al., 2016), managing this ecosystem and associated resources is crucial. A very efficient and much used conservation instrument is the establishment of marine protected areas (MPAs).

Biogeography patterns in the region are determined by the past and present circulation that define connectivity and barrier to dispersal (Obura, 2012). The westward flow of the South Equatorial Current (SEC) between 10 and 20°S transports water from the Indonesia Through-flow across the Indian Ocean. (Swallow, 1984; Gordon et al., 2010). The zonal flow of the SEC creates a boundary between Seychelles and Mascarene Islands. On reaching the east coast of Madagascar, the SEC splits into two opposite flowing currents, the Northern and Southern extension of the east Madagascar Current (Schott and McCreary Jr, 2001). The northern extension of the current (North East Madagascar Current) flows past the tip of Madagascar, resulting in the formation of the Comoros eddies due to instabilities (Collins et al., 2014). On reaching the East African coast, the current flow northwards as the East African Coastal Current (EACC) that flows along the Tanzania and Kenya coasts and southwards as a net flow of the mesoscale eddies (Ridderinkhof and De Ruijter, 2003; Schouten et al., 2003; Halo et al., 2014b). The Mozambique Channel eddies join up the flow from the East Madagascar

Current to form the Agulhas Current that flows south (Lutjeharms, 2006). In the north, the reversal of the Somali Current southwards during the northeast monsoon, meets the northwards flowing EACC resulting in a confluence of the EACC and the Somali Current to form the eastward-flowing South Equatorial Counter Current (Schott and McCreary Jr, 2001) that flows towards the Seychelles archipelago.

Understanding biogeographic patterns and their causal mechanisms provide the foundation for conservation planning (Obura, 2012). With most reef species having a bipartite life history, a planktonic larval stage and a benthic associated adult life, how far and to what extent larvae disperse from their natal sites remains an intriguing question. Larvae are dispersed in the open ocean via an interplay between physical e.g. ocean currents and temperature and biological processes e.g. the timing of spawning, pelagic larval duration (PLD), larval behaviour, and mortality (Cowen and Sponaugle, 2009). The combined effect of these processes determines the spatial scales over which a population is connected and is critically important for effective knowledge-based management and conservation. Questions regarding coral reef dynamics and management often relate to connectivity between reefs at regional scales in the order of tens to hundreds of kilometers. It is however empirically difficult to measure connectivity due to the small size, difficulty of sampling, complex biology and behaviour of larvae interacting with the dynamic nature of the oceanic environment (Paris et al., 2007).

Previous studies have employed genetic methods to infer levels of connectivity and gene flow among populations at regional and global scales. For example, Dorenbosch et al. (2006); Visram et al. (2010); Muths et al. (2015); Otwoma and Kochzius (2016) and Huyghe and Kochzius (2018) used genetic techniques to study reef fish while Macdonald et al. (2013); van der Ven et al. (2016) used the technique to study coral species. On the other hand, Lagrangian models have been employed on global ro regional scales (Cowen et al., 2006; Treml et al., 2008; Cowen and Sponaugle, 2009; Kool et al., 2013; Paris et al., 2007; Wood et al., 2014; Crochelet et al., 2016; Mayorga-Adame et al., 2017; van der Ven et al., 2016) for both coral reef, reef fish and mangrove propagule. The model study of Crochelet et al. (2016) used a low resolution (1/3°) altimetry data and aggregated the East African coast reef as a single contiguous reef. In their discussion, Crochelet et al. (2016) recommended use of high resolution biophysical model and splitting reefs of the East African every 50/100 km. While Mayorga-Adame et al. (2017) implemented a high resolution model, the domain was only along the East

African coast (Kenya - Tanzania). While the two methods have their limitations, they provide important information about the underlying mechanisms that contribute to the genetic structure of organisms such as corals.

Therefore, to complement these studies, this chapter applied a high resolution coupled biophysical model for broadcast corals over a broader western Indian Ocean region and splitting the reef habitat into 25 km cells to (1) determine the spatial and temporal structure of dispersal (2) quantify the role and importance of key circulation features in determining dispersal (3) identify subregions in the western Indian Ocean that act as source and sink for coral reef larvae and (4) investigate the potential of different pelagic duration for connectivity. Results from this work would be useful in developing hypotheses for understanding regional biogeography and provide the foundation for conservation planning.

4.2 Data and Methods

The modelling approach used in this study has three components: (1) a physical oceanographic component containing daily 3-D current velocities from hydrodynamic model, and (2) a Lagrangian module which takes the current fields from the hydrodynamic model to track the trajectory of individual larvae released in the domain and (3) a benthic module representing habitats for coral reefs.

4.2.1 Hydrodynamic model

The hydrodynamic model used here is the Regional Ocean Modelling System (ROMS; Shchepetkin and McWilliams, 2005) which is a split-explicit, free-surface ocean model discretized in coastline and terrain-following curvilinear coordinates. The ROMSTOOLS package (Penven et al. 2008) was used for the design of the model configuration built over the Indian Ocean as in chapter 3 and chapter 4 The high-resolution child domain was designed to resolve some of the mesoscale circulation features that might be important to the dispersal of larvae. Both the parent and child grids have 40 sigma levels that are stretched to increase resolution towards the surface. The model bathymetry was build using the Global Earth Bathymetric Chart of the Oceans (GEBCO1; Carpine-Lancre and Bv, 2003) and linearly interpolated onto the grid. Pressure gradient errors are reduced by smoothing the bathymetry such that the

smoothing parameter is less than a critical value of 0.2 (Haidvogel et al., 2008).

At the surface, the model is forced with monthly climatological heat and freshwater fluxes derived from Comprehensive Ocean-Atmosphere Data Set (COADS; da Silva et al., 1994). To improve model representation of the air-sea interaction, the COADS product is reinforced with the 9 km Pathfinder Advanced Very High-Resolution Radiometer (Casey and Cornillon, 1999) SST climatology as a restoring term of the boundary layer. The wind forcing is from QuikSCAT climatology at 0.5° resolution available from 2000 – 2007 Liu et al. (1998b). The model configuration has three open boundaries (North, East, and South) with initial and boundary conditions obtained from World Ocean Atlas 2009 (WOA; Conkright et al., 2002).

The model was run for 10 years and outputs stored daily with a statistical equilibrium reached after three years of spin-up (see Appendix 1). The hydrodynamic model outputs (currents, temperature, and salinity) were used to drive the Lagrangian model.

4.2.2 Larval dispersal simulation

Daily outputs of zonal and meridional velocities from ROMS were used to simulate passive larval dispersion using a Lagrangian model known as Ichthyop (Mullon et al., 2003; Lett et al., 2008). Ichthyop tracks the paths of individual particles in a three-dimensional flow incorporating spawning, movement, growth, mortality, and recruitment. The model was parameterized for broadcast spawners. The actual spawning period may vary across the distribution area of the coral reef. Therefore, to test the effect of a variation in the spawning season, one thousand model larvae were released from each of the centroids at surface every month over 7-year of the hydrodynamic output (in total 21 million model larvae released). The model larvae were tracked for different PLD (5 days, 15 days, 30 days and 60 days) based on various scenarios and accounts from authors in the region (Mangubhai et al., 2007; Mangubhai and Harrison, 2008, 2009). No attempt was made to replicate realistic scenario, but rather offer a representation of potential larval dispersal pathways to evaluate the connectivity between reefs in the region and also reduce on the computation cost and time.

The time-step of iteration was set to 10800 seconds (3 hrs.) lower than the ratio of cell size to maximum current velocity. This prevents the model larvae to cross more than one boundary o hydrodynamic cells in a single time step. Current velocities

were interpolated to each position of each model larvae and positions larvae recorded every 8 iterations (24 hrs.). Advection was simulated using a 4th order Runge-Kutta integration scheme which involves interpolating the velocity halfway between a particle and the 'destination' (the point it would have been advected to under a Forward Eulerian scheme) four times per time step. This produces more realistic outcomes, especially around complex coastlines (North et al., 2006). To account for the turbulent motion not captured at the resolution of the oceanographic data, a 'random walk' formulation was applied using a dissipation rate of 1 x 10^{-9} m^2/s^3 (Peliz et al., 2007).

In this study, model larvae were considered passive and confined to the surface layer after release without simulating active or vertical migration. The number of larvae released from each release location reaching recruitment zone was recorded for each PLD. Initial work by Crochelet et al. (2016) had the main East African reef (from Angoche, Northern Mozambique to Kiunga, Northern Kenya) as a single unit or node. Here, the individual reef nodes along the East African coast were used and grouped using country boundaries.

4.2.3 Reef habitat

Reef habitat for particle release and settlement was downloaded from UNEP-WCMC 2010 (http://data.unep-wcmc.org/datasets/1) and clipped over the study area. The clipped reef distribution polygon was then re-gridded onto a 1/4° cells using QGIS creating ∼170 habitat cells that define the release (centroids) and settlement (polygons) locations (Figure 4.1).

4.2.4 Analysis

Larval dispersal distance was calculated using the Haversine formulae (Robusto, 1957). The formulae determine the great-circle distance between two points on a sphere given their longitudes and latitudes. Botsford et al. (2001) and Kaplan et al. (2006) employed Euclidean distances rather than oceanographic distances to find the minimum distance between MPAs that allows for effective connectivity.

Larval density was calculated as histograms of particle location for each PLD using 25 km^2 bins and then converted to probability density functions (PDFs). Probability density functions were combined in space and time to create the probability maps for

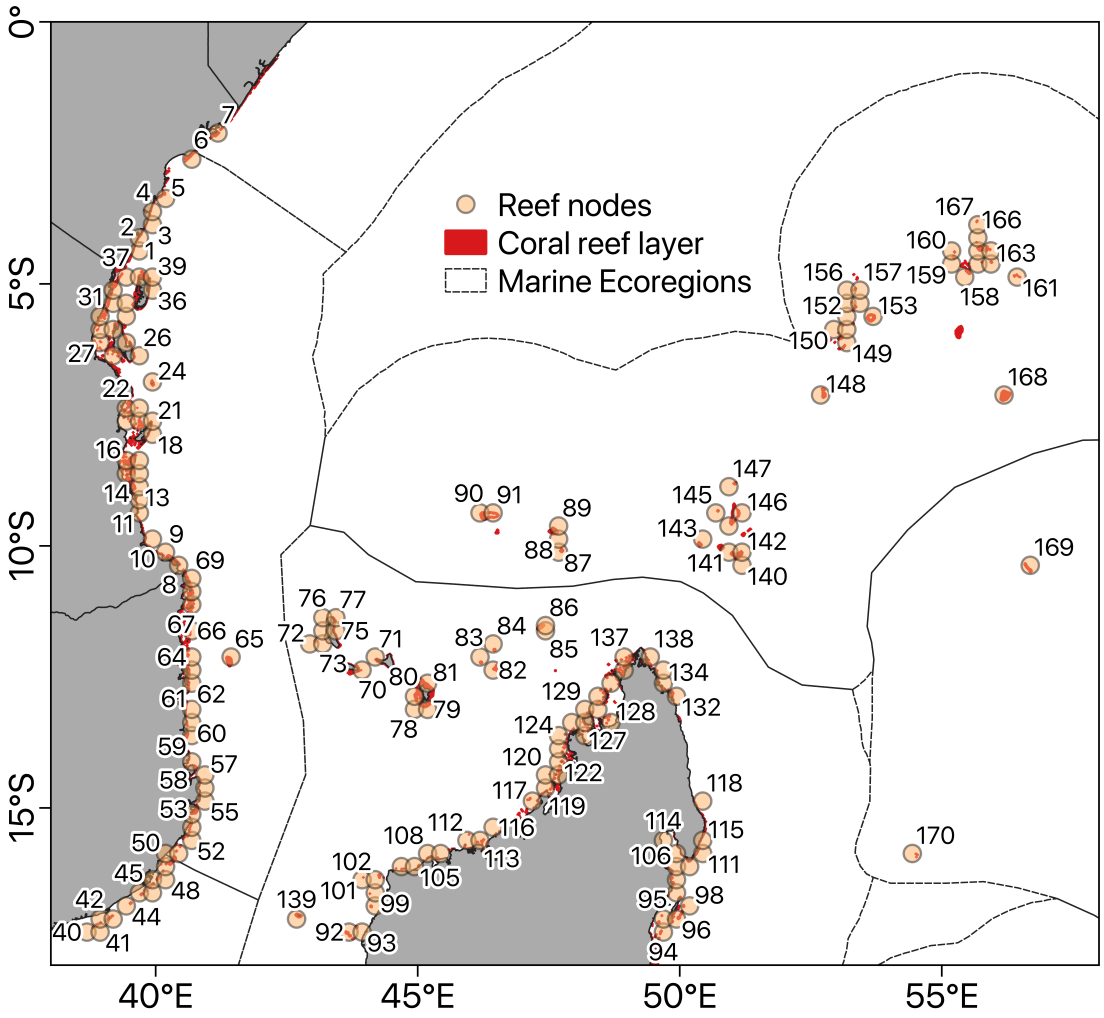

Fig. 4.1 Study area showing reef nodes created after re-gridding the original reef layer onto 1/4° grid cells. The numbers indicate assigned ID for each reef node/centroid. Overlaid is the Marine Ecoregions from Spalding et al. (2007)

the region.

The number of model larvae released from location i that ended up in the recruitment zone j was recorded and used to create a connectivity matrix. To examine the strength and direction of potential connections, the connectivity matrix was plotted showing the number of particles exchanged between each reef habitat. Self-recruitment defined as the fraction of larvae released from a reef habitat and settled back to that habitat plots along the diagonal of the plot. Connectivity is presented using a log_{10}

scale. Release and settling nodes are given on y-axis and x-axes, respectively.

Similar to other studies in the region (Crochelet et al., 2016) and elsewhere (Treml et al., 2008; Andrello et al., 2013; Holstein et al., 2014), network graph analysis was used to explore patterns of connectivity, identify reefs that act as stepping stones, and identify the connected upstream and downstream neighbours for each reef site. Reef centroids and larval trajectories defined nodes and edges of the graph, respectively. For the purpose of this work, several graph metrics were calculated (betweenness centrality, out-degree and, in-degree) corresponding to key ecological processes. Betweenness centrality quantifies the number of times a node acts as a bridge along the shortest path between two other nodes (Bode et al., 2006; Rozenfeld et al., 2008) and relates to the 'stepping stone' landscape ecology concept (Kininmonth et al., 2010). High betweenness centrality measure mean obligate "gateways" through which larvae have to pass in order to spread to other nodes. Following Crochelet et al. (2016) method, "occurrence" score for the reef was calculated to identify reefs with consistently high betweenness centrality independent of PLD. The number of PLDs for which each reef's betweenness centrality score was higher than the mean for that PLD was counted and referred as the "occurrence" score.

Node level metrics focus on local properties related to an individual reef's connectedness with its neighbours, its relative contribution of larvae to the local neighbourhood, and its role in connecting distant sites. A node's out-degree refers to the number of connections linking to downstream neighbours and the in-degree is the number of connections from upstream sources. Therefore, a set of connected nodes form a cluster a criterion known as the 'strong' connectivity criterion because connections are directional.

MATLAB software was used for all analyses and MatlabBGL toolbox used for network analysis.

4.3 Results

4.3.1 Dispersal distance

The distance travelled by larvae varied with PLD and release locations. The mean dispersal distance for all released larvae was 529±332 km while the maximum dispersal

distance was 1902 km (larvae release from south of Tanzania and drifted off-shore at the equator). The distance of larvae at the time of settlement was different between release locations. Larvae released along the East African coast dispersed an average of 405±181 km whereas the minimum distance was ∼15 km. In Seychelles archipelago, larvae dispersed an average of 101±63 km between Seychelles granite islands whereas in the Comoros Basin, the average distance was 115±73 km. Larvae released in northern Madagascar dispersed an average 326±194 km.

4.3.2 Larval dispersal paths

The general dispersal pattern following release highlight dominant pathways consistent with the general circulation, for example, the northward flowing EACC and mesoscale eddies in the Comoros Basin and Mozambique Channel (Figure 4.2 & Figure 4.3). At short PLD (5-days), the level of larval exchange is limited to reefs that are close to each other (Figure 4.2a) but as dispersal duration increases (Figure 4.2b, c, & d), the order of larval exchange between reefs across different sub-region increases. In all the PLDs tested, Agalega & Tromelin were completely disconnected from the connectivity network.

Because broadcast spawners release larvae in different months across the region, monthly (January to December) trajectories for maximum PLD (60 days) were examined in detail (Figure 4.3). The Seychelles granite islands are separated from the rest of the region from January to March, but the other 9 months show dispersal of larvae towards Comoros Basin and East African coast. The most persistent dispersal path in all months is along the East African coastal shelf in a predominantly northward direction (from southern Tanzania to northern Kenya). Off-shore advection of larvae particularly off the Kenya-Somali coast is evident from November to August (Figure 4.3k & l) where some larvae disperse towards Seychelles Archipelago from June to August. This corresponds to seasonal the strengthening of the EACC/Somali Current from June propagating north and turning offshore after crossing the equator, forming the Southern Gyre (Gamoyo et al., 2017).

The off-shore advection of larvae is absent in September and October (Figure 4.3i & j). The other noticeable drift patterns are the anticyclonic pathway as a result of the mesoscale eddies in the Comoros Basin all year round and cyclonic movement south of 15°S in the Mozambique Channel (January and February). The eddies routinely

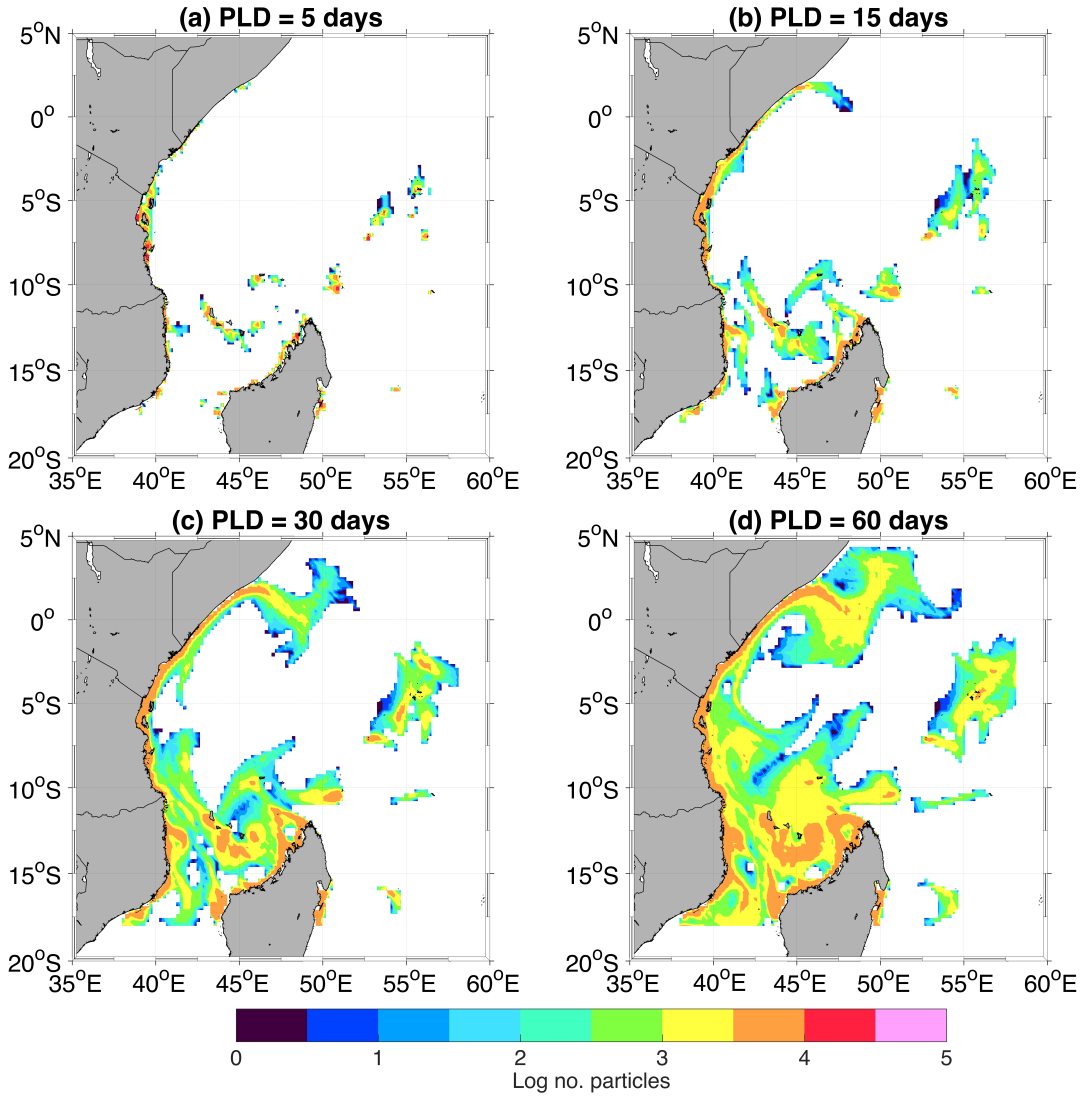

Fig. 4.2 Modelled potential density map simulated by the biophysical model for different PLDs (5 days, 15 days, 30 days & 60 days) excluding mortality. The larval densities are calculated as the number of particles passing through each grid cell.

transport larvae off-shore from the release point and loop back returning the larvae to their natal reefs mostly retaining the larvae into the eddies. Comoros archipelago is highly connected within itself and to East Africa and Madagascar coasts all year round, while East Africa is connected to Madagascar in a stepping stone fashion through Comoros. Along the Mozambique coast, the direction of exchange appears to take place from reefs within Cabo Delgado (Rongui, Vamizi, and Metundo) into the Comoros Basin, although the degree of influx happens in March, June, and July (Figure 4.3c, f, & g) possibly due to the Mozambique Channel eddies that propagate southward.

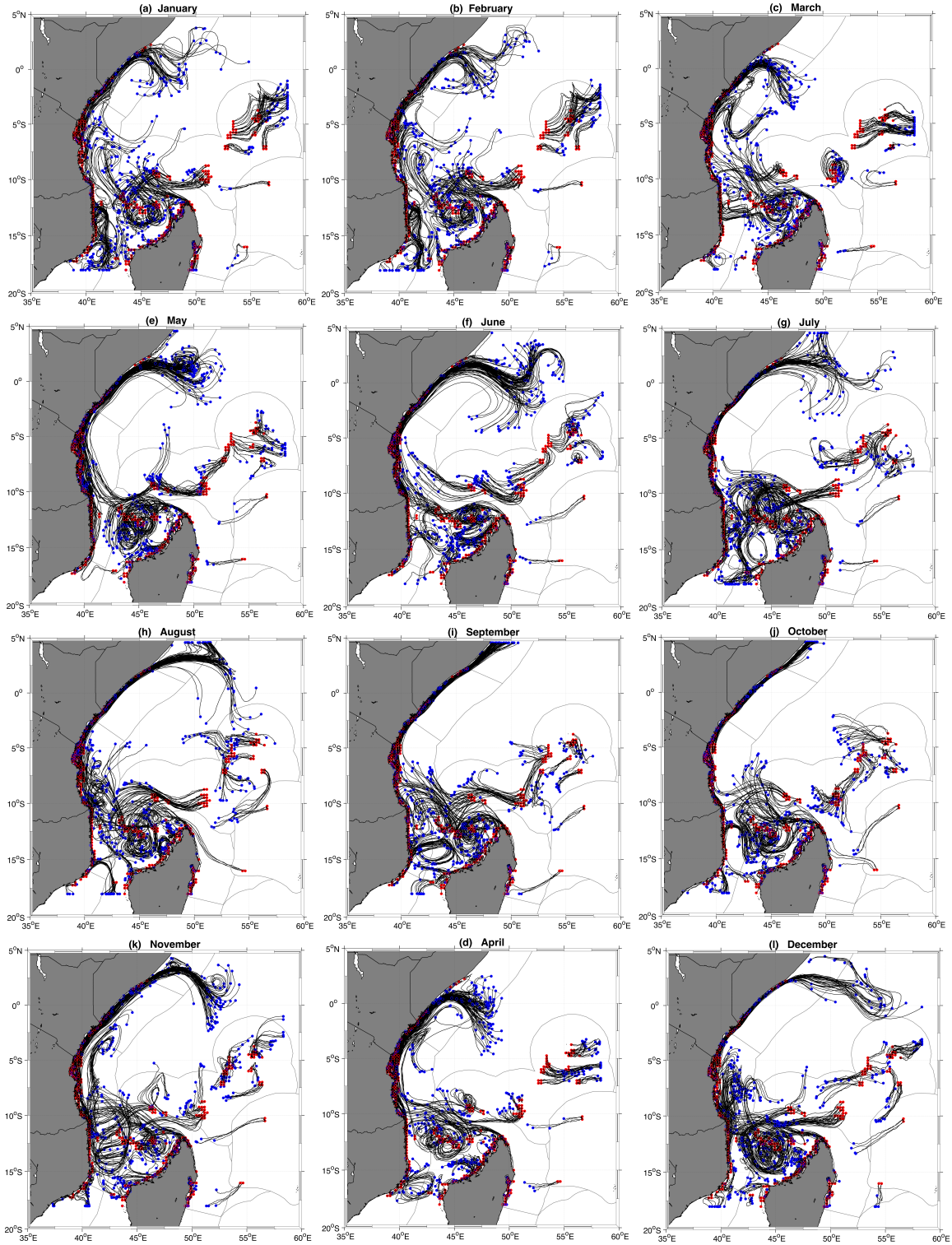

Fig. 4.3 Variability of modelled larval patterns simulated by the biophysical model released every 1^{st} day of the month. Because of large number of released particles, only a subset of the total number ar plotted to show clear trajectories.

4.3.3 Potential connectivity matrix

Although Figure 4.2 & Figure 4.3 highlight important pathways to connectivity, they don't provide information to show where larvae are coming from and where they settle. Therefore, connectivity matrices of exports and imports of coral larvae show the strength and direction of potential connections on a regional scale (Figure 4.4). Out of 28900 possible connections, 434, 549, 895 and 1503 connections were found for PLD of 5-days, 15-days, 30-days and 60-days respectively. At the broadest scale of comparison, there was considerable spatial variation in the exchange of larvae among sites and sub-regions, which interacted strongly with dispersal duration. At shorter PLD (5-days), reefs were disconnected over long distances, for example, Cosmoledo, Aldabra, Madagascar are completely disconnected from other sub-regions. In contrast, reefs along the East African coast (Tanzania - Kenya) are connected even at short PLD (Figure 4.4a); this is unsurprising due to the constant northward flowing EACC that results to larvae released in Tanzania settling in Kenya. Connectivity across different sub-regions is seen to increase with longer dispersal duration which increases dispersal distances. Eddies in the Comoros and North Mozambique Channel

4.3.4 Network analysis

Betweenness centrality values ranged between 0 to 675.3 (median 14, interquartile range 70) for PLD of 5-days, 0 to 4358.5 (median 89.9, interquartile range 350.5) for PLD of 15-days, 0 to 2679.3 (median 159.1, interquartile range 340.7) for 30-days PLD, and 0 to 6236.1 (median 193.3, interquartile range 449) for 60-days PLD. In the North Mozambique Channel, betweenness centrality was generally higher than in other regions due to its central position, the influence of the NEMC and eddies (Figure 4.5). In particular, six reef nodes had the maximum occurrence score of 4 (Table 4.1), thus emerged as the most important stepping stones for multi-generational connectivity while four reef nodes had occurrence score of 3 (Table 4.2), thus the second most important nodes as stepping stones. For all the PLDs tested, Tromelin (170) and Agalega (169) had betweenness centrality of zero thus emerged as less important to the overall connectedness of the network.

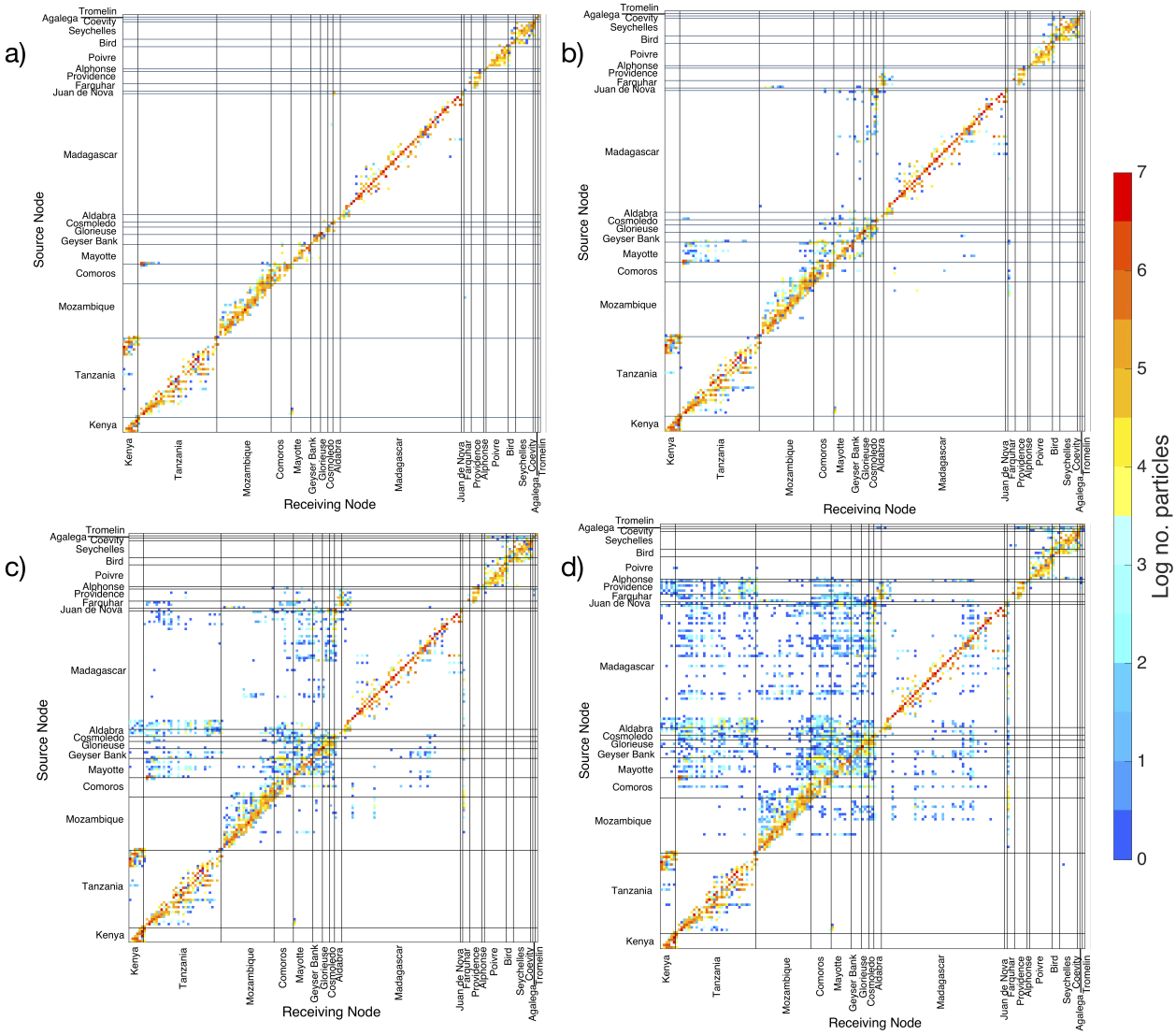

Fig. 4.4 Connectivity matrix indicating the probability for modelled coral larvae originating from a reef site i (vertical axis) to recruit at reef site j (horizontal axis) estimated from individual trajectories. The connectivity matrix is of 170 coral reef sites (nodes) representing all available coral reef locations in the region. Self-recruitment plot along the diagonal (i=j). a) is the connectivity matrix after 5 days pelagic duration, b) after 15 days PLD, c) after 30 days PLD and, d) after 60 days PLD.

The neighbourhood-level analysis focused on the connected upstream and downstream sites (Figure 4.6 & Figure 4.7) for every reef node within the WIO. Upstream and downstream neighbourhood characteristics of reef locations revealed there is an order of magnitude variation in both upstream and downstream reef area. Upstream reef locations provides an indication of potential larval supply. At the shortest PLD

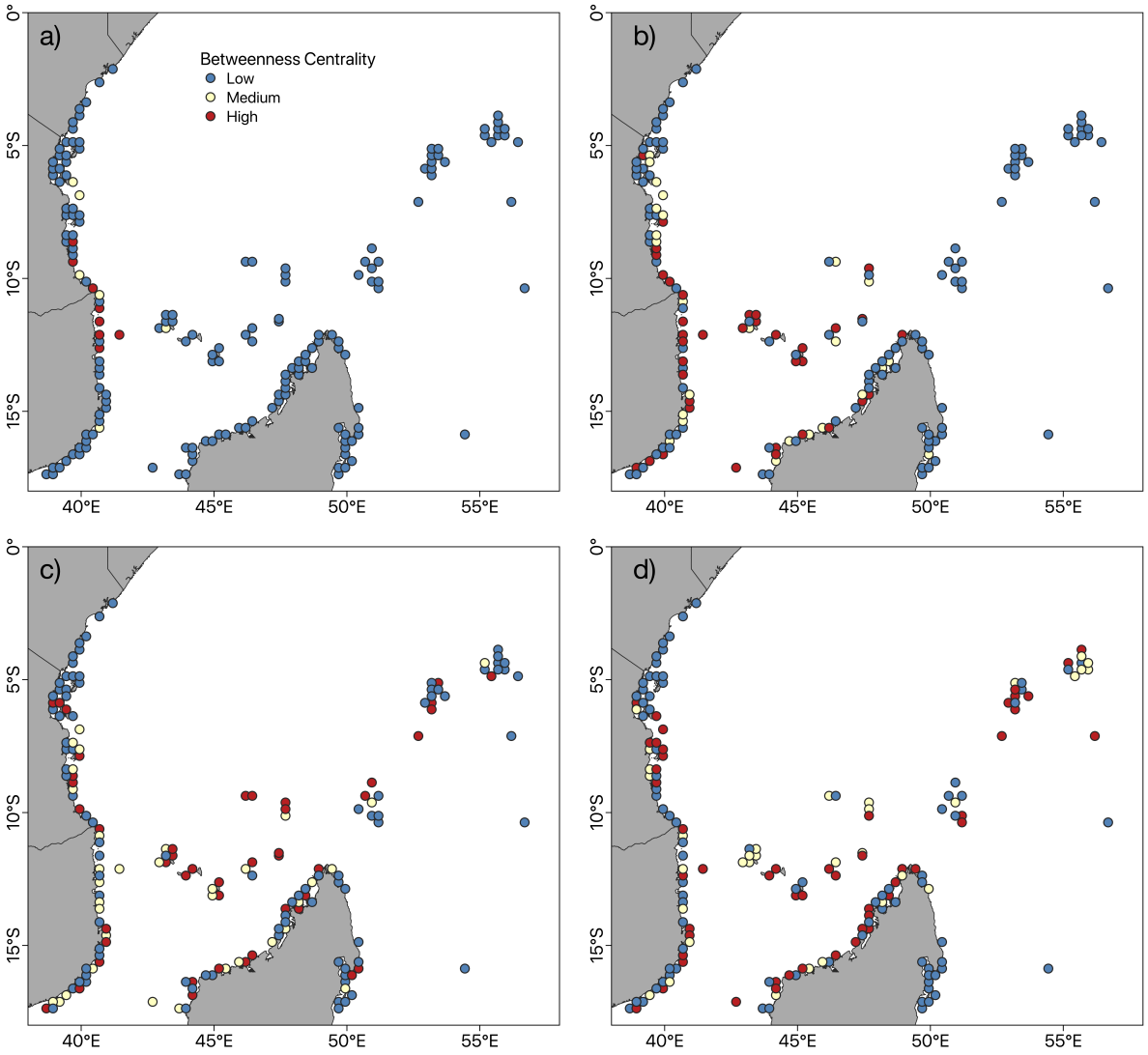

Fig. 4.5 Betweenness centrality of coral reef based on a) PLD = 5 days, (b) PLD = 15 days, c) PLD = 30 days, d) PLD = 60 days

(Figure 4.6a), the WIO is almost entirely dependent on local larval production to replenish populations. But as PLD increases (Figure 4.6b), the number of upstream reef locations increases meaning these reef locations receive larvae from different location to replenish populations. Downstream reef locations provides a measure of the likelihood of a larva spawned at a particular location finding a reef on which to settle. Figure 4.7 suggests that reef locations with high out-degree may be highly effective at supporting populations elsewhere. To identify reef nodes with consistently low or high upstream and downstream connection independent of PLD, the occurrence score was calculated. Twenty reef nodes (11.7%) had a high degree of upstream connections

Table 4.1 Reef nodes with occurrence score of 4, thus the most important nodes as stepping stones

			Betweenness centrality			
Id	**Country**	**Reef Node**	**pld5**	**pld15**	**pld30**	**pld60**
22	Tanzania	Mafia Latham-Island	79	769	508	788
49	Mozambique	Angoche-Nacala	173	395	457	486
60	Mozambique	Pemba-Mecufi	163	536	573	1578
71	Comoros	Anjouan	80	2740	573	807
77	Comoros	Ngazidja	70	2693	1389	2022
86	Glorieuses	Glorieuses	77	4359	303	2132

Table 4.2 Reef nodes with occurrence score of 3, thus the second most important nodes as stepping stones

			Betweenness centrality			
Id	**Country**	**Reef Node**	**pld5**	**pld15**	**pld30**	**pld60**
8	Tanzania	Mnazi Bay	675	472	1462	227*
37	Tanzania	Tanga-Shimoni	71	764	272*	807
91	Aldabra	Aldabra	0*	927	660	730
127	Madagascar	Nosy Be	130	646	403	1*

meaning many other nodes are linked to them while five (2.9%) of reefs had a high degree of downstream connections (occurrence score = 4). Sixteen reef nodes (9.4%) were pure sinks (upstream occurrence score = 0) and twenty reefs (11.7%) were pure sources (downstream occurrence score = 0). Neighbourhood scores were correlated using Spearman's rank correlation ($r = 0.43$, $p < 0.05$), meaning that reef nodes contributing larvae to many downstream neighbours are also receiving larvae by many upstream neighbours.

Coral reefs in the region were grouped into different clusters using a strong connectivity criterion (see methods). There were 73 strongly connected clusters and 11 weakly connected clusters for PLD of 5-days. Among the strongly connected clusters in this scenario, the largest one was formed by 19 reef nodes (11.18%). With increased pelagic duration, the number of strongly connected clusters decreased (Figure 4.8) for example

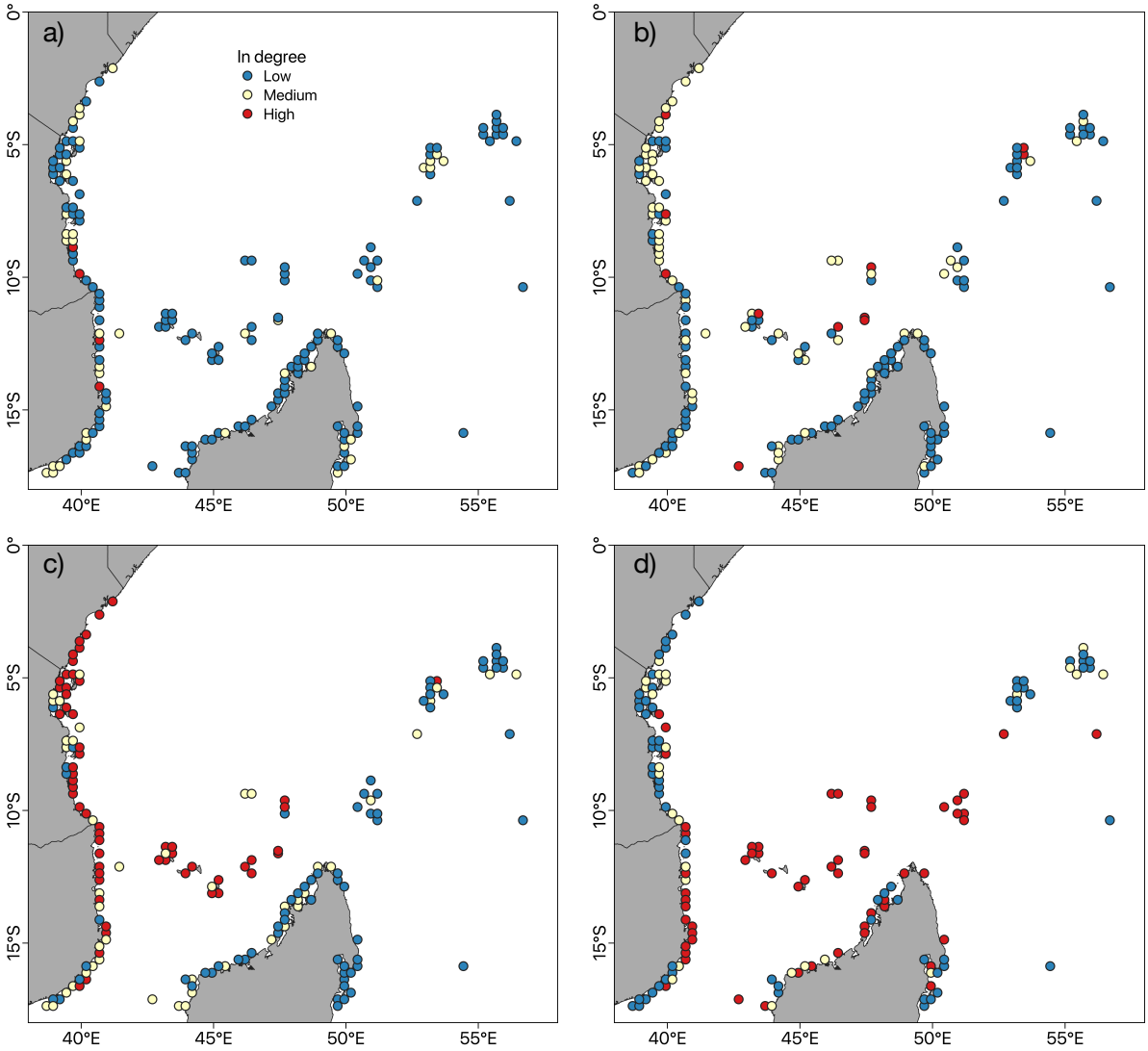

Fig. 4.6 Upstream dispersal neighbourhood based on a) PLD = 5 days, (b) PLD = 15 days, c) PLD = 30 days, d) PLD = 60 days.

at 60-days PLD, the number of strongly connected clusters was 20 and 3 for weakly connected components. The largest cluster was formed by 136 reef nodes (80%).

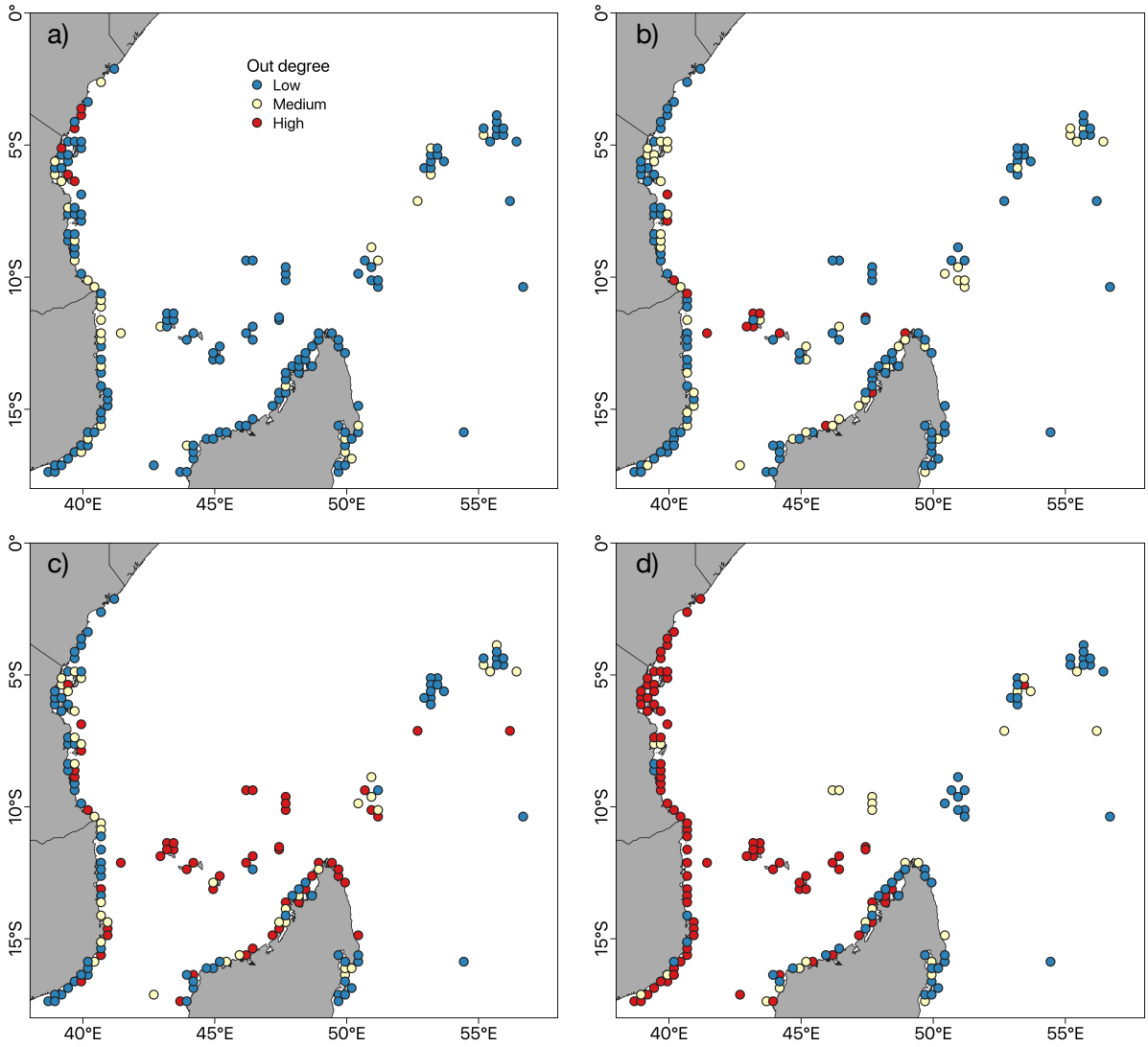

Fig. 4.7 Downstream dispersal neighbourhood based on a) PLD = 5 days, (b) PLD = 15 days, c) PLD = 30 days, d) PLD = 60 days.

4.4 Discussion

This study explored patterns of larval dispersal for broadcast spawners in the Western Indian Ocean region where reef-building fauna and biogeography is least known (Obura, 2012). The study also addressed the marine connectivity challenges identified by Crochelet et al. (2016) specifically, low-resolution altimetry data and the fact that reefs of the East African coast were aggregated together. With regional coverage and a high-resolution hydrodynamic model (∼9 km), the biophysical model and graph-theoretic

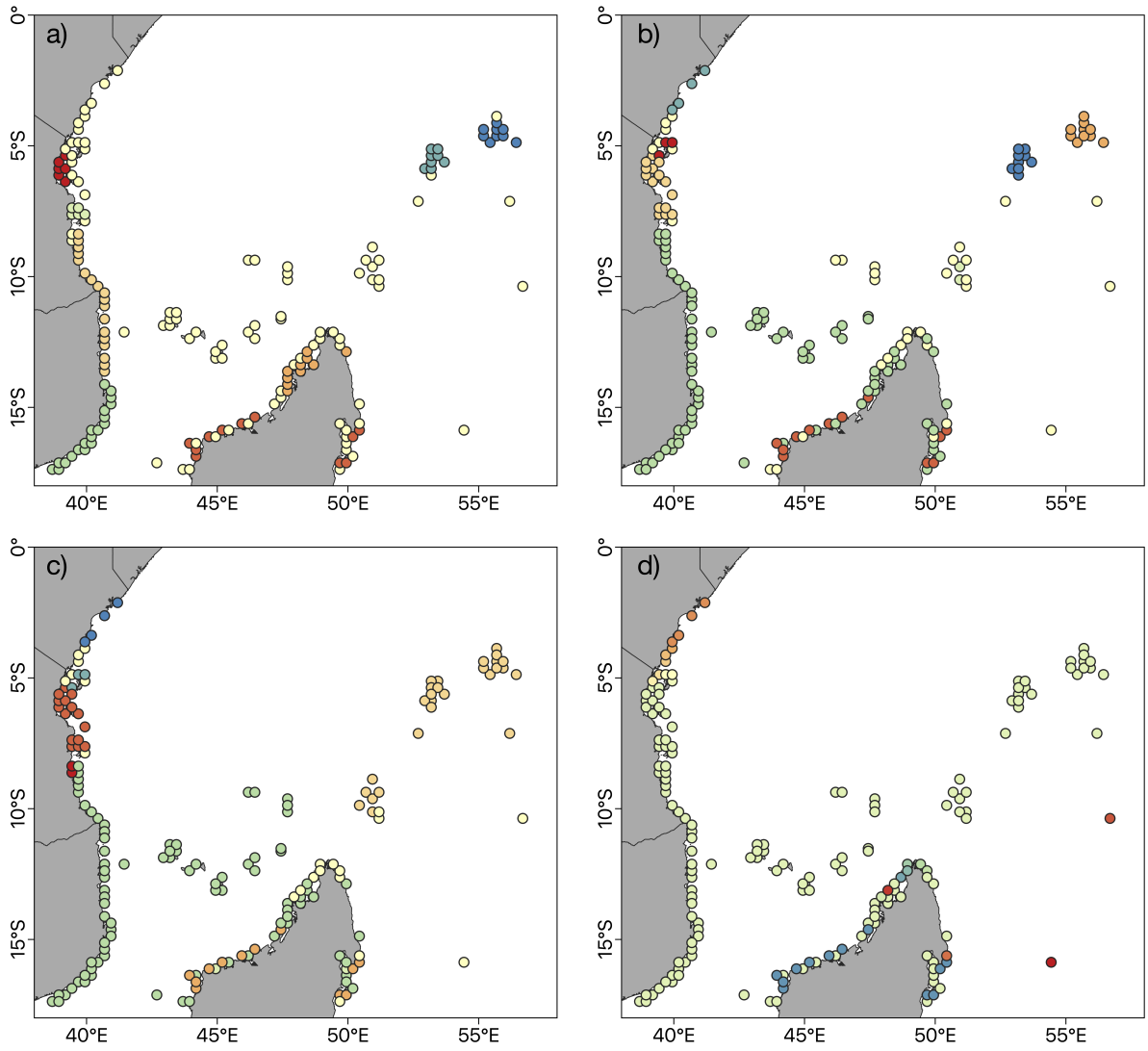

Fig. 4.8 Clusters identified using strong connectivity criterion based on a) PLD = 5 days, (b) PLD = 15 days, c) PLD = 30 days, d) PLD = 60 days. Clusters are differentiated by colour, separately for each figure.

approach presented a robust analytical framework for integration into conservation.

Larval density and trajectories (Figure 4.2 & Figure 4.3) highlighted the role ocean currents play in dispersing larvae. The spatial scale of larval dispersal is much smaller at shorter PLD with most larvae restricted close to the release nodes. Longer PLDs (> 15 days) demonstrated the potential for long-distance dispersal, thus, an increased level of connectance linking most reefs in a stepping stone fashion along the habitat corridors. Persistent patterns in coral dispersal were identified highlighting common

dispersal corridors, including their strength and direction. The scale of coral population connectivity across the study area was on the order of 50–500 km consistent with estimates from the Caribbean (Cowen et al., 2006) and for other marine taxa, for example, the case of an Aldabra giant land tortoise (*Dipsochelys dussumieri*) drifting across ∼730 km of ocean in an estimated time span of 3 weeks (Gerber et al., 2003) and the recovery of a mangrove (*Avicennia marina*) propagule that had travelled ∼700 km in 42 days (Steinke and Ward, 2003). Similar scales of connectivity are also supported by genetic studies, for example, high genetic structure was observed on local scales for species with a short pelagic duration (Ayre and Hughes, 2000; Gilmour et al., 2009), and wide genetic linkages associated with long-distance dispersal (Glynn and Ault, 2000; van Oppen et al., 2011; Figueiredo et al., 2013).

The dominant patterns of connectivity in the WIO region followed known patterns of regional ocean circulation (Schott et al., 2009; Ternon et al., 2014; Obura et al., 2019). The SEC flow from east to west isolating the Seychelles basin and gyre to other reef locations (Madagascar and the northern Mozambique Channel) from the main flow and from each other. On reaching the east of Madagascar, the SEC bifurcates into the NEMC and the SEMC at approximately the location of Saint Marie. The NEMC flows around the northern tip of Madagascar resulting into mostly westward dispersal (see Madagascar quadrant of the connectivity matrix, Figure 4.4c) and on reaching the East African coast, close to the border between Tanzania and Mozambique, the current bifurcates into the northward flowing EACC and southward into the Mozambique Channel and the formation of large cyclonic and anti-cyclonic eddies. This current regime has the potential to create barriers to larval flow between the northern region (Tanzania-Kenya) and the northern Mozambique coast (see the Mozambique quadrant of the connectivity matrix, Figure 4.4c & d). Along the Tanzania-Kenyan coastline, dispersal of larvae is always northwards with some southerly flow in the northern Kenya due to seasonal reversal of the Somali current. Eddies in the Mozambique Channel play an important role in larval dispersal as they transport water in all directions within the channel but with a net southward flow. These dynamics are capable of trapping particles for several months (Hancke et al., 2014). The movement of eddies and interactions at their boundaries can result in greater transport of larvae between Mozambique and Madagascar (see Figure 4.4c & d), as well as recirculation of some larvae entrained in the NEMC from the Comoros and Madagascar to Tanzania-Kenya.

A diversity of connectivity patterns have been reported from genetic studies in the WIO (Obura et al., 2019). The results presented here are congruent with studies that detected a barrier to gene flow between the north (Tanzania-Kenya) and south (Mozambique) mainland coast in reef fish (*Myripristis berndti* (Muths et al., 2011), *Epinephelus merra* (Muths et al., 2015)), the mangrove snail (*Cerithidea decollate* (Madeira et al., 2012)) and other taxa (Obura et al., 2019). Unrestricted gene flow between parts of Madagascar and the Northern Mozambique Channel/East African coast is also corroborated, for example, in blue sea star *Linckia laevigata* (Otwoma and Kochzius, 2016) and bluestripe snapper *Lutjanus kasmira* (Muths et al., 2012).

Connectivity between reefs was facilitated by several reef nodes acting as stepping stones for spreading individuals being transported through the network. 'Betweenness centrality' measures the importance of such nodal reefs for multi-generational larval dispersal and gene transfer. Reef locations in Tanzania (22, Mafia Latham-Island), Mozambique (49, Angoche-Nacala & 60, Pemba-Mucufi), Comoros (71, Anjouan & 77, Ngazidja), and Glorieuses (86), in particular, showed high betweenness centrality, meaning they are key stepping stones for the passage of larvae. Only three of the ten, Glorieuses, Angoche-Nacala and Mnazi bay are located in established MPAs. It is thus important to prioritise the other sites with high betweenness centrality for protection: northern Mafia Latham-Island in Tanzania, Pemba-Mecufi in Mozambique, Anjouan and Ngazidja in Comoros (Table 4.1 & Table 4.2), to ensure their health and function are maintained, to preserve their ability to act as stepping stones for larval and gene dispersal in the region. Loss of these key reef would impede the transfer of genetic information from one reef location ot the other, and result in fragmentation of the regional reef system, hindering recovery of downstream reefs after major coral mortality, such as from bleaching.

The neighbourhood analysis adds greater resolution to these general patterns and identifies the potential flow of larvae to and from all individual sites (Figure 4.6 & Figure 4.7). Upstream reef locations provides an indication of potential larval supply while downstream reef locations provides a measure of the likelihood of a larva spawned at a particular location finding a reef on which to settle. Therefore, these results suggest that downstream reef locations may be highly effective at supporting populations elsewhere. For marine reserves to interact effectively and maintain populations, they need to be located close enough together that they can obtain larvae from upstream reef

locations and deliver them to downstream reef locations. This site-specific resolution is needed to evaluate the degree to which individual reef sites should be regarded as open or closed systems with respect to local population dynamics and marine management (Cowen et al., 2000).

Beyond first-order connections, connectivity among coral reef locations was possible through obligate gateways, resulting in groups (clusters) of coral reef among which connectivity was assured in a strong or a weak sense. Reefs were grouped into strongly connected clusters and weakly connected clusters depending on their respective PLD. The large cluster between north of Mozambique and south of Tanzania was lost when PLD was greater than 5 days. Even if the number of clusters decreased as PLD and connectivity increased (compare the four panels of Figure 4.8), the system was never fully connected. Clusters of reefs based on strong connectivity criterion showed reef nodes that are able to reach every node of the cluster which is consistent with patterns of connectivity. Therefore, clusters formed by more than one reef node, show that all nodes in that cluster act as both sources and sinks. Rozenfeld et al. (2008) showed that source-sink dynamics is correctly accounted through the strong connectivity criterion, and can have important implications for population dynamics and genetic differentiation. Andrello et al. (2013) used this connectivity criterion to identify clusters of MPAs in the Mediterranean. He noted that each pure source and sink defined a single cluster. Therefore, preserving these corridors that regularly concentrate and nurture pelagic larvae during their ontogenetic journey is necessary

4.4.1 Caveats and future work

Several studies in the region and elsewhere have employed genetic methods (e.g., Ayre and Hughes, 2000; Gilmour et al., 2009; van Oppen et al., 2011; Muths et al., 2015; Otwoma and Kochzius, 2016; Huyghe and Kochzius, 2017, 2018) while others have used biophysical methods (e.g., Andrello et al., 2013; Wood et al., 2014; Andrello et al., 2015; Crochelet et al., 2016; Wood et al., 2016; Andrello et al., 2017; Mayorga-Adame et al., 2017) to infer patterns of connectivity and larval export. As suggested by Di Franco et al. (2015), combining genetic and biophysical modelling methods should be used together to overcome the weaknesses of each method. Although the hydrodynamic model used in this study had a horizontal grid size of $1/12^\circ$ ($\sim$ 9km), it does not resolve finer-scale turbulent motion affecting transport and could fail to capture near-shore processes that entrain larvae along coastlines (Werner et al., 2007; Andutta et al., 2012).

Though the inclusion of a random walk helps minimize this shortfall. Simplification of biological parameterization in the model (e.g. assumption that all larvae are passive drifters) can lead to an overestimation of dispersal distances (Cowen and Sponaugle, 2009; Treml et al., 2012; Wood et al., 2014). Therefore, further model exploration is necessary to quantify the implications of the biological simplifications, particularly sensitivity to species-specific parameterizations.

Despite these limitations, this work was an attempt to improve on Crochelet et al. (2016) work and gain insight into regional patterns of coral dispersal and identify important areas to protect, for example reef locations with high betweenness centrality (Mafia Latham-Island in Tanzania, Pemba-Mecufi in Mozambique, Anjouan and Ngazidja in Comoros). The connectivity and origin/destination results from this work would provide a basis for a working hypotheses for MPA network design. According to the Strategic Plan for Biodiversity adopted by the Convention on Biological Diversity, protected areas are targeted to cover 10% of the marine area by 2020 and must form well-connected networks. The density of MPAs in the western Indian Ocean region is still small compared to terrestrial protected areas, at about 2.5% of the area of countries' Exclusive Economic Zones (Obura et al., 2017). A higher density of MPAs implies shorter distances for larval dispersal which enhances the probability for connections, especially for species with shorter PLD.

4.5 Conclusion

This work demonstrated how a biophysical model and graph-theoretic framework aids in the understanding and identification of important connections between coral populations. Based on biophysical model outputs important coral reef linkages and nodes that act as gateways to dispersal can be used as a basis for improving coral reef management. Preserving these corridors that regularly concentrate and nurture pelagic larvae during their ontogenetic journey is necessary. The ultimate aim is to have a model framework able to assess how dispersal may influence shifts in coral distribution from annual to decadal scales, and in relation to climate change.

Having provided a preliminary outlook on dispersal and connectivity patterns in the region, the next chapter uses a suite of satellite data and Global Climate Models to understand the trend in thermal stress in the region as coral communities are

susceptible to thermal stress. Thermal stress results in bleaching which disrupts coral survival. Therefore, understanding thermal stress is important to determine the spatial extent of corals exposed to bleaching level thermal stress and how this will affect connectivity.

Chapter 5

Regional scale projections of coral bleaching thermal stress in the Western Indian Ocean

This result chapter is based on the work submitted for publication to PLOS ONE Journal as:

Gamoyo, M., David, O., & Reason, C.J.C. (2018). Connected we stand: Connectivity and varying thermal exposure provides hope for coral reefs in the Western Indian Ocean.

Abstract

Coral reefs and the services they provide are seriously threatened by climate change impacts in particular thermal stress that causes mass coral bleaching. The temperature threshold for coral bleaching depends on adaptation of corals to the local maximum. In 2016, positive sea surface temperature (SST) anomalies caused widespread bleaching in the western Indian Ocean. Sea surface temperature (SST) data from Advanced Very-High-Resolution Radiometer (AVHRR) for 1985–2016, global climate models (GCMs) for 2020–2100 and a biophysical connectivity model were used to investigate how projections of spatially variable thermal stress and connectivity between reefs may influence coral bleaching events in the future. About 56% of reef pixels showed positive SST trends, with greater warming trends months from June to September compared to January to May. This indicates greater warming during 'winter' months than 'summer' months - while this may be positive in relation to lesser warming during peak bleaching

months, the loss of winter cooling/recovery times may be significant. The frequency of bleaching-level thermal stress has increased over time from 1998 to 2016 and this trend is projected to continue upto the year 2100. Seventy percent of coral reel location are projected to experience thermal stress causing annual severe bleaching by 2050. Larval exchange between reefs of varying temperatures is likely in the Western Indian Ocean (WIO) and thus provide an opportunity to receive larvae that are more or less adapted to elevated temperatures that would be suggested by local conditions alone. Kenyan and northern Mozambique reefs receive larvae from cooler reef thus may suffer higher bleaching and mortality. Tanzania coast and NW Madagascar receives larvae from warmer reefs thus may survive future climate threats better. Results from this work provide new insights into coral reef future and possible adaptation which might conceivably increase the potential for these reefs to survive future climate threats.

5.1 Introduction

The Western Indian Ocean is ranked as the world's second richest marine biodiversity hotspot (Obura, 2012; Veron et al., 2015) with coral reefs, mangroves, pelagic and deep-sea habitats supporting economies and livelihoods. Coral reefs, in particular, are estimated to comprise US$ 18.1bn of the "ocean asset base" of the Western Indian Ocean region (Obura et al., 2017). Despite the economic value of coral reefs in the region, they are under increased pressure from human activities (e.g., pollution, over fishing and coral mining) and global climate change (Donner et al., 2005). Elevated SST is the most common factor affecting coral reefs where 1°C warmer than the maximum monthly mean (MMM) over a 12- week window can cause a syndrome known as coral bleaching (Hoegh-Guldberg and Pearse, 1995; Brown, 1997; Hoegh-Guldberg, 1999b; Donner et al., 2005). Coral bleaching in the region has been observed since 1982, with the frequency and severity of bleaching projected to increase under global warming, thus posing a serious threat to the future state of coral ecosystems (Hoegh-Guldberg, 1999b; Hughes et al., 2003; Donner et al., 2005). The recovery of coral reef is dependent on the severity of the bleaching and the time between individual bleaching events, and thus increased frequency in these events severely limits the capability of the reefs to recover (McCook, 1999).

The potential for coral bleaching in a particular region can be predicted using remotely sensed SST data from satellites. The National Oceanographic and Atmospheric

Administration (NOAA) Coral Reef Watch uses a reference threshold of MMM where if exceeded for a period of time, bleaching is likely to occur with potential mortality (Strong et al., 2004; Liu et al., 2006). The concept of Degree Heating Weeks was developed to measure thermal stress accumulation that coral reefs have experienced over the past 12 weeks (Liu et al., 2008). However, the satellite based hindcast and nowcast tools only provide information as to how bleaching thermal stress has evolved and the present likelihood of bleaching. With coral reefs being among the most sensitive ecosystems to climate change, anticipated increase in SST is likely to have negative impacts. The fate of coral reefs under global warming has been estimated in several previous studies (e.g., Hoegh-Guldberg, 1999b; Sheppard, 2003; Donner et al., 2005, 2007; Van Hooidonk et al., 2013, 2014, 2016). Donner et al. (2007), for example attributed the 2005 bleaching event in the Eastern Caribbean to anthropogenic forcing. These studies suggest that mass coral bleaching will be a frequent occurrence on most reefs worldwide, depending on assumptions about thermal adaptation.

The variable response of many coral reef species to temperature stress suggest some potential for corals and their endosymbionts to adapt or acclimate to global warming (Douglas, 2003; Hughes et al., 2003; Donner et al., 2005). The potential for corals to cope with change depends on both intrinsic factors (e.g., phenotypic plasticity, microevolution, or dispersal to new habitat) (Brown et al., 2002; Douglas, 2003; Hughes et al., 2003; Baker et al., 2004; Rowan, 2004; Kleypas et al., 2016) and extrinsic factors (e.g., rate, magnitude, and nature of climatic change) (Dawson et al., 2011). Previous studies have suggested that heat tolerance in *Acropora hyacinthus*, for example, is determined by acclimation and genetic inheritance Palumbi et al. (2014). Dixon et al. (2015) showed that when exposed to heat stress, larvae of *Acropora millepora* had a 10 times greater survival rate if the parents were from warmer waters. Thus, larvae coming from higher temperature regimes can provide important insight into the mechanisms underlying coral resistance to thermal stress. Mumby et al. (2011) illustrated the potential importance of larval connectivity across different temperature regimes in the Bahamas. Kleypas et al. (2016) used a biophysical model to quantify the potential for connectivity to bring immigrants from different temperature regimes to a particular reef to shift temperature tolerance in corals. Temperature tolerance of adult corals is tied to the temperature regime of the local environment. However, the influence of dispersal to introduce a mismatch between the temperature tolerance of dispersed larvae (based on

their parental reef) to conditions at their destination reef has not been widely researched.

Historical temperature variation and the cumulative effects of past disturbance events influence not only the condition of reefs but also the capacity of resident corals to respond to subsequent stress events (Maynard et al., 2015). Knowledge of thermal history, future projections and the capacity of dispersal to deliver individuals adapted to different temperature regimes are vital to investigate how differences in thermal stress among reefs, and dispersal of larvae between them, may influence the ability of corals to resist future stress. The purpose of this chapter is to assess and understand thermal stress for coral reefs in the Western Indian Ocean and evaluate the role of anthropogenic climate forcing in the 2016 WIO bleaching event and the probability of events like 2016 occurring in the future.

The likelihood of severe coral bleaching over the coming decades due to warming is estimated by coupled models developed for the IPCC AR5. The analysis is conducted for two different suites of representative concentration pathways (RCPs) including (i) RCP4.5 the stabilization of atmospheric greenhouse gas concentrations before the end of the century and (ii) RCP8.5 business as usual which leads to high greenhouse gas concentration levels. Comparison of the two scenarios would identify the range in thermal stress that coral reefs in the region may face under climate change. These scenarios would also help in detecting coral reef locations that may be susceptible to severe annual bleaching thermal stress earlier (climate losers) versus later (climate winners).

As global warming continues, reef-building corals could avoid decline through exchange of heat-tolerant genotypes (thermal tolerant symbionts or reefs that are acclimatized across a range of temperature). Therefore, the potential for exchange of temperature-tolerant immigrants, would be quantified.

5.2 Materials and methods

Coral reef locations based on geomorphology were obtained from the Global Distribution of Coral Reefs compiled by UNEP World Conservation Monitoring Centre (UNEP-WCMC; http://www.unep-wcmc.org) which merges data from the Millennium Coral Reef Mapping Project (IMaRS-USF, 2005) and the World Atlas of Coral Reefs

(Spalding et al., 2001). The downloaded layer of coral reefs for the Western Indian Ocean was re-gridded to 9-km grid cell to match the remapped coupled model and reduced the approximately 3000 coral reef cells into about 636 reef pixels, thereby reducing the computational cost.

To assess warming trends and previous bleaching stress at gridded reef pixels, the SST dataset from AVHRR (1985-2016) was used. For future scenarios, monthly SST data for the Relative Concentration Pathway experiments (RCP 4.5 and RCP8.5) conducted for the fifth phase of the Coupled Model Inter-comparison Project (CMIP5 Moss et al., 2010; Taylor et al., 2012) was used. The CMIP5 data are archived and are made freely available by the Program for Climate Model Diagnosis and Inter-comparison (PCMDI) at http://pcmdi3.llnl.gov/esgcet/home.htm. In this study, the gridded CMIP5 datasets were retrieved from the Asia-Pacific Data Research Centre. Compared to the previous generation of climate models (CMIP3), the new generation CMIP5 models are parameterized by a new set of atmospheric composition forcing. The ten models Table 5.1 were chosen because they reproduce the seasonal cycle of SST in the study region without adjusting towards observed climatology. Multi-model ensembles were then calculated to reduce the uncertainty in the results. This method is a standard one typically used in climate model analyses (Reifen and Toumi, 2009). The multi-model ensemble means from the coupled models were re-mapped and interpolated onto a higher resolution grid ($\sim$9 km) using statistical tools and masked for reef containing pixels using climate data operators (CDO) so as to evaluate the general conditions at reef locations.

A range of different thermal metrics were calculated and arranged into three themes: 1) SST trend provides the long-term (31-year) historical trajectory of annual-mean temperature as the slope of a linear generalized least squares model. 2) Intra-annual temperature variations on reefs was described by long-term monthly averages. The warmest of these, the Maximum of the Monthly Means (MMM, °C), is used by NOAA Coral Reef Watch (CRW) as the stress threshold for monitoring conditions conducive to bleaching (Liu et al., 2014). The climatologically warmest month indicates the period when bleaching-level thermal stress is most likely. 3) Bleaching-level thermal stress was calculated using Degree Heating Months (DHM), which combines magnitude and duration of temperature exceeding the MMM. DHMs were calculated for each year by summing the positive anomalies equal to the maximum four-month SST above the

maximum monthly mean. Using the DHM metric, Donner et al. (2005) concluded that bleaching typically begins at a DHM = 1 °C-month and mass coral bleaching with associated coral mortality starts at a DHM $\geq$ 2 °C-month.

Table 5.1 Individual models from CMIP5 used in this study.

Model name	**Modelling centre**	**Ocean grid points**
ACCESS1.0	Centre for Australian Weather and Climate Research	360 * 300
ACCESS1.3	Centre for Australian Weather and Climate Research	360 * 300
CESM1-BGC	Climate and Global Dynamics Laboratory (CGD)	288 * 192
EC-EARTH	European Network for Earth System Modelling	360 * 1800
GFDL-ESM2G	NOAA Geophysical Fluid Dynamics Laboratory	360 * 210
GFDL-ESM2M	NOAA Geophysical Fluid Dynamics Laboratory	360 * 200
HadGEM2-CC	Met Office Hadley Centre	360 * 216
HadGEM2-ES	Met Office Hadley Centre	360 * 216
MPI-ESM-MR	Max Planck Institute for Meteorology	360 * 180
NorESM1-M	Norwegian Climate Centre	320 * 384

To quantify the potential for connectivity to bring immigrants from different temperature regimes to a particular reef, an offline Lagrangian particle tracking model ICHTHYOP (Lett et al., 2008). coupled with Regional Ocean Modelling System (ROMS) was used to track the physical particles at the surface layer for three dispersal periods (10, 30 and 60 days). One hundred particles were released from each gridded reef cell for each calendar month and tracked for their respective dispersal duration over the seven years of simulation. The time step of iteration was set to 3,600 s (1 h), which is sufficiently short for larvae not to cross more than one boundary of hydrodynamic cells in a single time step and the output is saved every 24 hrs. Advection was simulated using a Runge-Kutta fourth order numerical scheme. Potential connectivity which is the probability of dispersal from a release site that settle at site was calculated at the end of the dispersal period (e.g., the locations of all particles at day 10, 30 and 60). The mean potential connectivity was then calculated over the 7-year period that includes seasonal variability.

Thermal stress threshold (TST) was used as a metric for thermal tolerance because it accounts for the climatological maximum temperature as well as its variability at each site (Kleypas et al., 2016). The MMM at each gridded reef cell was calculated from the ROMS SST and the local temperature stress threshold (TST) calculated as the MMM +1 °C, the standard metric of the NOAA heat-stress calculation. Another approach in calculating TST, is using MMM $+2.5\sigma$ (where σ = the standard deviation of the MMM). TST based on potential connectivity (TST_{pc}) was calculated for each reef cell as:

$$TST_{pc,i} = \frac{\sum_j a_{i,j} f TST_j}{\sum_j a_{i,j} f} \tag{5.1}$$

Where $a_{i,j}$ is the potential connectivity between reef i and j, while f is the fecundity and TST_j is the TST at reef j. Fecundity was assumed to be constant at all reef site, thus, while it cancels out of this equation, f would be relevant if one were to consider differences in fecundity from site to site.

5.3 Results

Annual cycle in sea surface temperature

The annual cycle in SST averaged over the study area for the various CMIP5 models compared to SST from AVHRR satellite data exhibits maximum SST in April during the inter-monsoon season and a minimum value in August because of latent heat loss caused by strong southwesterly monsoon winds (Figure 5.1). The CMIP5 SST shows a similar annual cycle to the satellite data; however, all the models (except ACCESS1.3) are cooler than the observations during the summer months (January to May). The multi-model ensemble SST means improves the annual cycle but with a cooler bias during the summer months. The observed bias in the coupled models is linked to a weaker southwest monsoon than observed (Levine et al., 2013; Li and Xie, 2014).

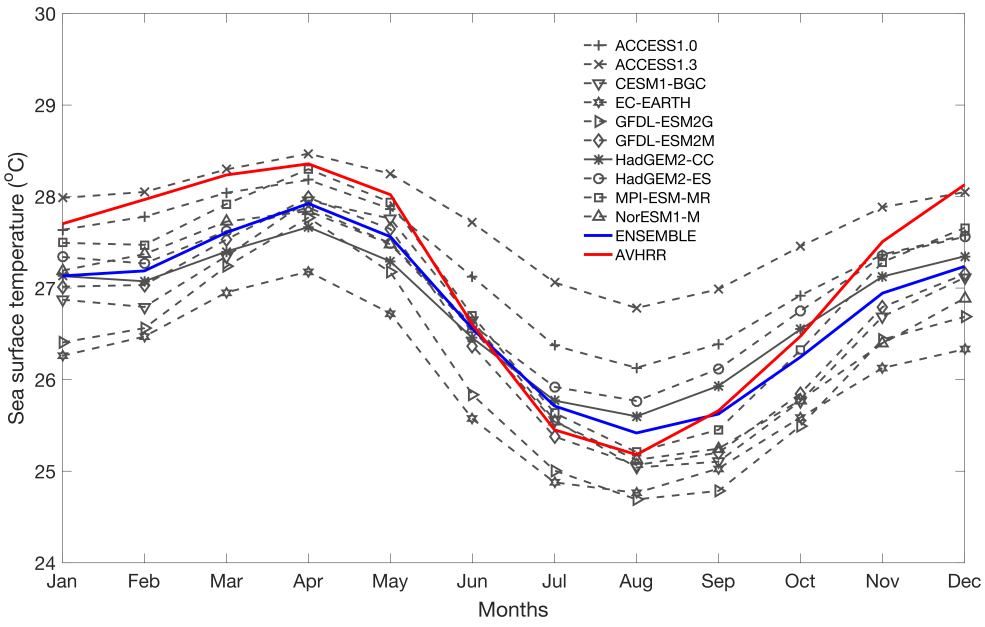

Fig. 5.1 Annual cycle in sea surface temperature spatially averaged over the study region (35°E - 60°E and 5°N to 20°S) over the study region based on CMIP5 models. Individual coupled models (dashed lines), ensemble mean (blue line) and satellite data (red line)

Sea surface temperature trend

Over the summer months (January to May), positive trends have been observed at 57% of the reefs in the region (mainly in Kenya, Aldabra, Farquhar, Seychelles and in Nosy Ankomba and St. Marie) (Figure 5.2a). There is a mixture of positive and negative trends for reefs in Tanzania, Mozambique, Comoros and northwestern Madagascar while reefs south of 15°S (west of Madagascar) show negative trends in SST. In winter months (June to October) (Figure 5.2b), about 88% of the reefs experienced positive trends with about 11% of the reefs (Nosy Ankomba, St. Marie) having negative trends.

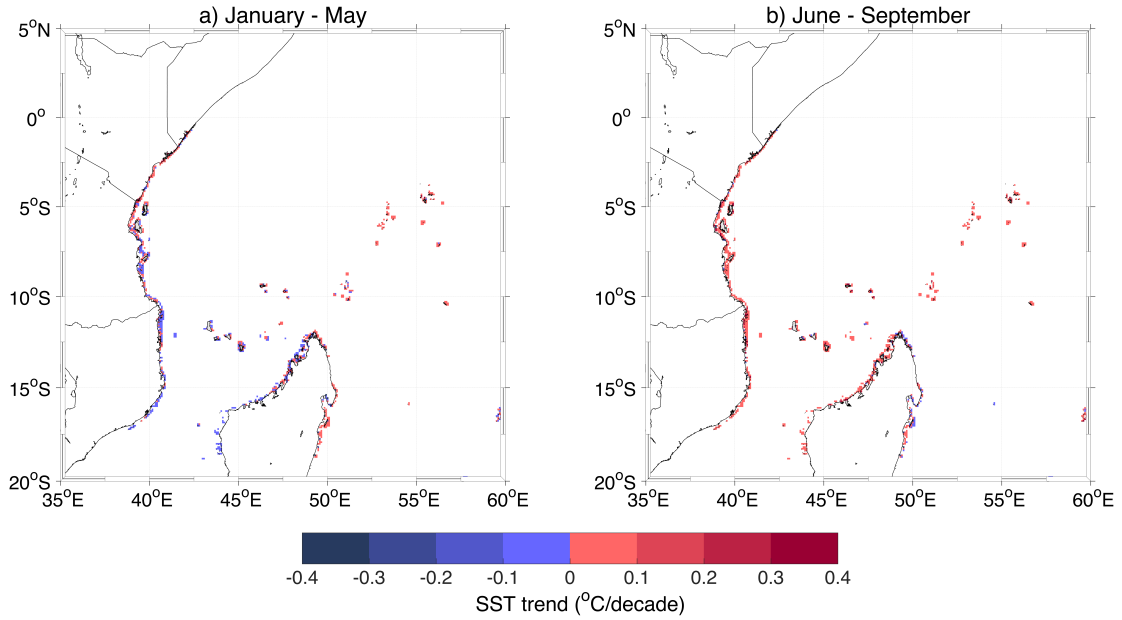

Fig. 5.2 Trend in sea surface temperature from 1985 to 2016 (°C/decade). (a) During warm season from January to May and (b) during cool season from June to October

Averaging across all reefs in the region, annual SSTs have increased on average by 0.36±0.1°C/decade from 1985-2016 (Figure 5.3a). Over winter months (June to October), the rate of warming is about 0.4±0.24°C/decade whereas, in summer (January to May), the rate of warming is 0.1±0.14°C/decade. 5% of reef locations experience their hottest temperature in January and May, while this is 50% for March (Figure 5.3b). Over the 31-year period, most reefs in the region were exposed to bleaching thermal threshold of DHM $\geq$ 1°C-month, with the greatest number of reefs exposed occurring in 1998 (80%), 2005 (36%), 2010 (50%) and 2016 (68%) (Figure 5.3c). These years all correspond to bleaching events and the mature phase of El Niño events. The years 1998 and 2016 were the two highest ranked years for all reefs in the region.

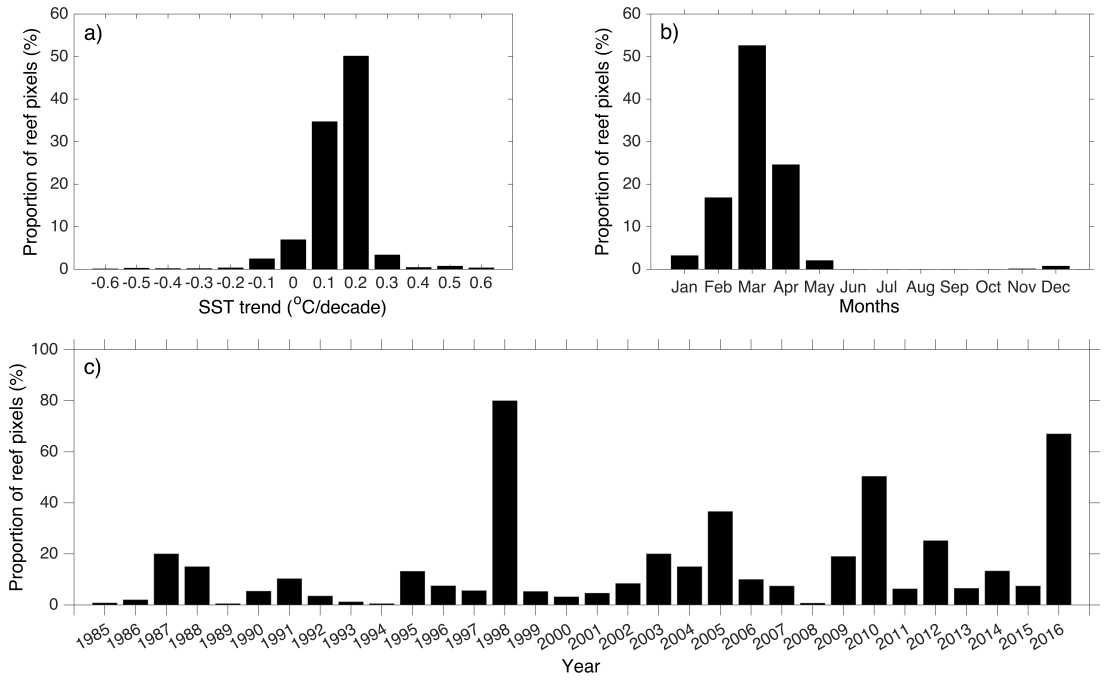

Fig. 5.3 Histograms of thermal metrics for reefs in the Western Indian Ocean region. (a) Annual trend in SST (b) warmest month (c) bleaching level thermal stress events from 1985-2016

Severity of the 1998 and 2016 bleaching events

Mass bleaching of corals in the region varied between 1998 and 2016 bleaching years with the cumulative footprint of the two bleaching events affecting reefs almost over the entire region. The difference in severity and extensive nature of thermal stress during these two events can be explained by their differences in the spatial distribution of SST anomalies (Figure 5.4) and accumulation of heat stress (DHMs) (Figure 5.5). During the bleaching months (January to May) of 1998, the SST anomaly averaged over the whole study region was 0.58±0.27°C whereas in 2016 it was greater, at 0.81±0.22°C but the spatial pattern of the anomalies varied between the two years with 1998 showing high anomalies (> 0.8°C) in Kenya, NW Madagascar and the southern Seychelles islands. In contrast, 2016 had anomalies above 0.8°C in the Mozambique Channel and the southern Seychelles islands (Figure 5.4a & b). Even though 2016 anomalies were on average higher than 1998, the anomalies in 1998 were much higher in some areas (Kenya, S Seychelles, NW Madag) so higher bleaching. The anomaly pattern was more even in 2016, and with adaptation of reefs over the previous two decades might have

resulted in less bleaching.

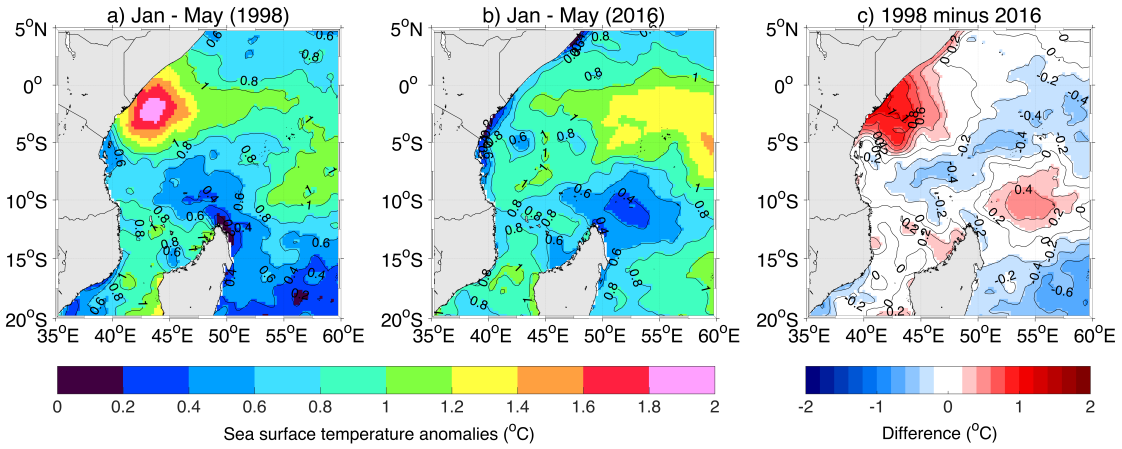

Fig. 5.4 Plots of SST anomalies during January to May (summer months) of (a) 1998 (b) 2016 and (c) difference between the two years with positive anomalies showing higher anomaly in 1998 than 2016

547 (86%) reef locations of the 636 reef pixels were exposed to some degree of thermal stress that caused bleaching and mortality during the two bleaching years. The calculated metric for sustained thermal stress in 1998 exceeded the 2°C-month for 40% of the reef locations while 20% of reefs experienced the 1°C-month. By contrast, about 30% of reefs experienced the 1°C-month whereas 25% of the reefs the $\geq$ 2°C-month thermal stress threshold affecting reefs in Mayotte, Glorieuses, Aldabra and St. Marie (Madagascar) (Figure 5.5a & b and Figure 5.6).

The sustained thermal stress between the two bleaching years was not similar, as a result, the proportion of coral reefs experienced moderate to severe bleaching in 1998 was 85% of the 373 surveyed reefs compared to 52% of the 313 surveyed corals reefs in 2016 (Figure 5.7).

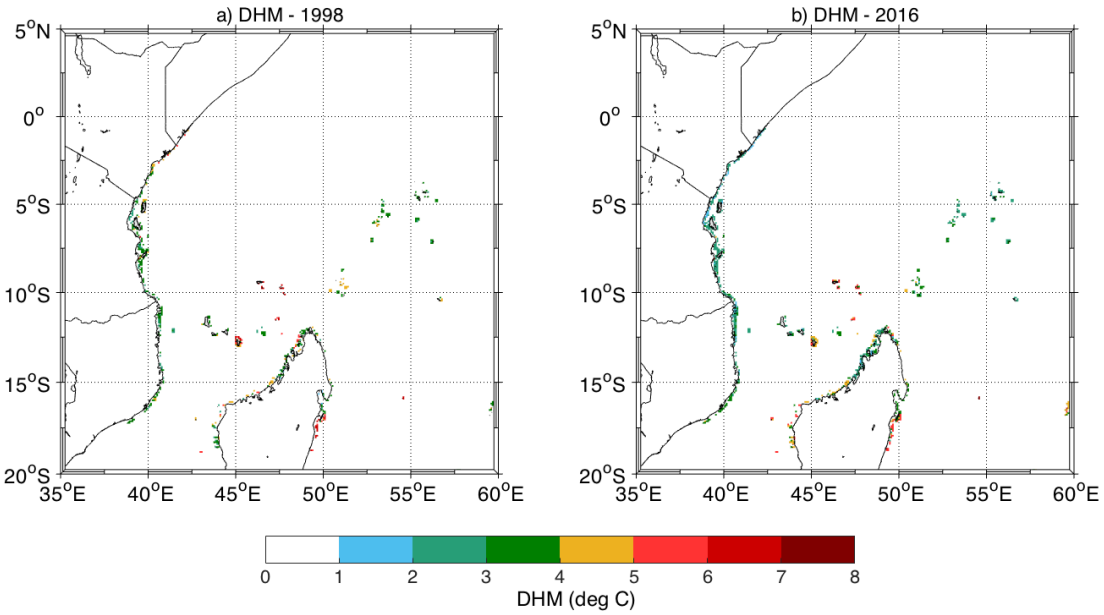

Fig. 5.5 Frequency of bleaching level thermal stress in 1998 and 2016. Bleaching level stress is defined as DHM $\geq$ 1°C-month. (a) Bleaching thermal stress threshold during 1998 event and (b) during 2016 bleaching event

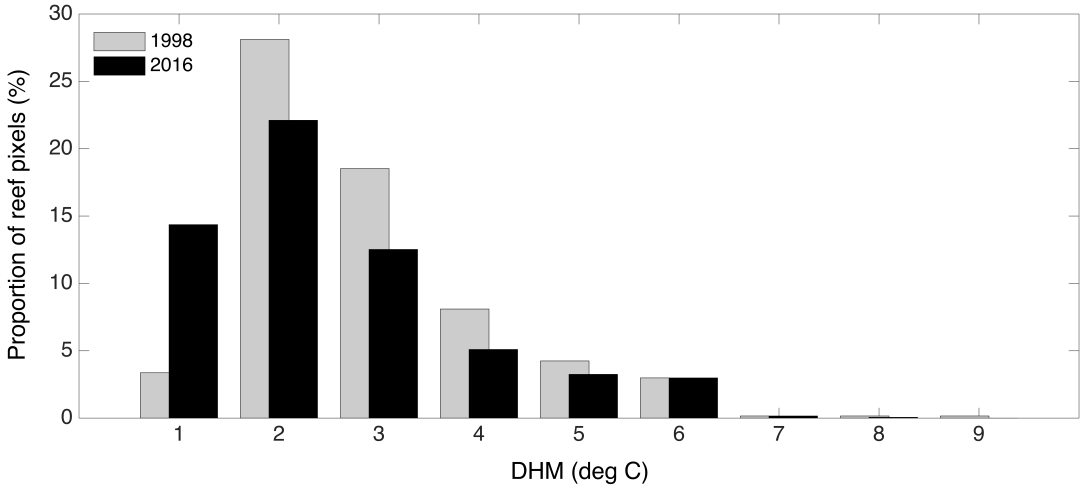

Fig. 5.6 Frequency distribution in the bleaching level thermal stress for reefs in the region during 1998 and 2016 bleaching events.

5.3.0.1 Attributing the 2016 bleaching event

As discussed in the previous section, the summer months (January to May) of 2016 saw anomalously warm SST which caused coral bleaching across the region. The ensemble

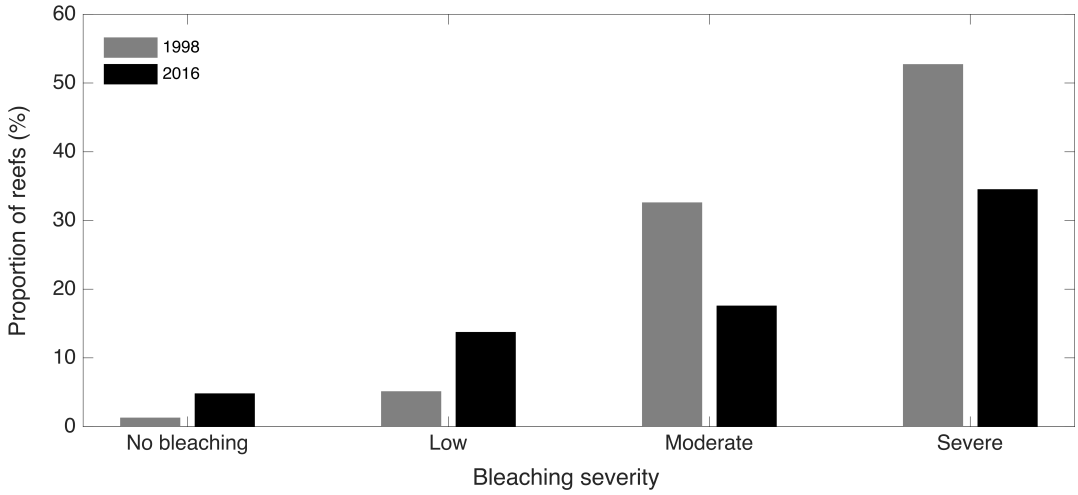

Fig. 5.7 Frequency distribution of bleaching scores for reefs surveyed. Grey bars for 1998 bleaching event represents the new high resolution mass coral bleaching database from Donner et al. (2017) while the black bars represents 2016 bleaching reports from CORDIO East Africa

CMIP5 data from the ten global climate models listed in Table 5.1 under RCP4.5 and RCP8.5 emission pathways were used to consider the contribution of natural climate variability and anthropogenic forcing to the thermal stress that caused the 2016 bleaching event. The spread of different individual model simulations (the red and blue shading) arises both from differences between the models in their responses to the different specified climate forcing agents (natural and anthropogenic) and from internal (unforced) climate variability. The CMIP5 all-Forcing simulations (include both anthropogenic and natural forcing) indicates a continuing positive SST trend in the region throughout the period (Figure 5.8a) whereas the natural forcing only simulations implies no warming trend after about 1980 (Figure 5.8b). This implies that the observed warming and specifically anomalous warming in 2016 is unlikely to be due to natural climate variability alone.

The accumulated thermal stress from CMIP5 models under RCP4.5 shows higher level thermal stress (DHM ≥ 2°C-month) across coral reefs in the Comoros archipelago, west of Madagascar, St. Marie and Seychelles archipelago (Figure 5.9a). Coral reefs along the East African coast were projected to experience lower thermal stress (DHM = 1°C-month). The pattern of bleaching level thermal stress is also replicated under RCP8.5 with more reef locations along the East African coast projected to experience

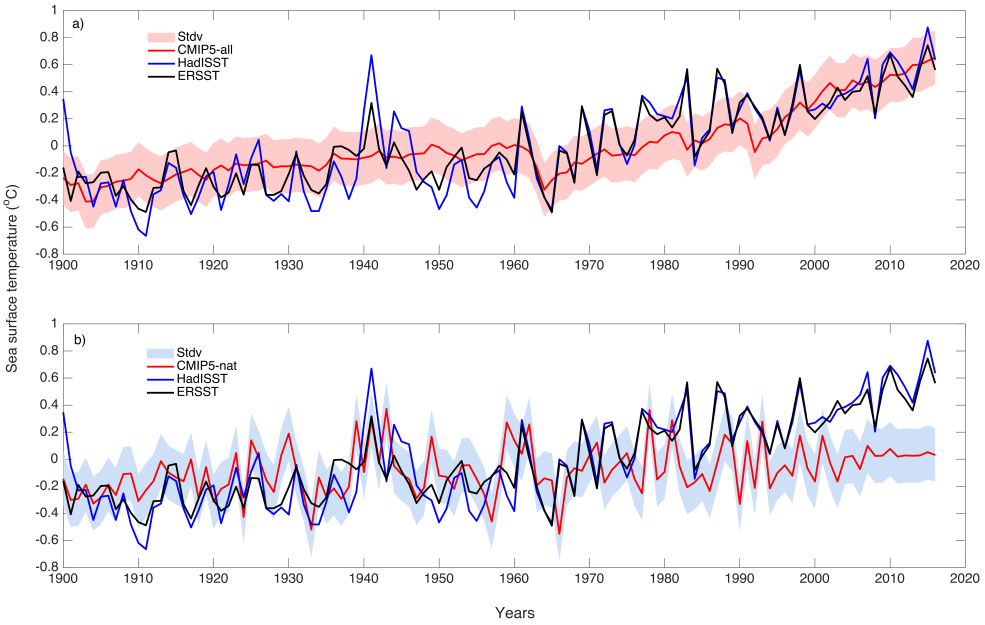

Fig. 5.8 Comparison of observed mean SST anomalies from two observational datasets to CMIP5 climate model historical experiments. Using (a) CMIP5 experiments perturbed by both anthropogenic and natural forcing and (b) perturbed by natural forcing only. The red and blue shading depict the ±2 standard deviation of annual anomalies across all 10 individual models

thermal stress. Averaging across all coral reefs for 2016, the accumulated thermal stress under RCP4.5 was 2.91±0.12°C-month compared to 3.03±0.16°C-month under RCP8.5, and 3.41±0.16°C-month from observed AVHRR satellite data. Although the calculated DHM values under the two scenarios is lower by about 0.5°C, it highlights the likelihood of anthropogenic influence during the 2016 bleaching event.

Projecting future bleaching events

The percentage of reefs exposed to thermal stress are projected to increase between 2020 and 2100 (Figure 5.10). Under RCP4.5, the proportion of reefs projected to experience moderate thermal stress at a DHM of 1°C-month is 39% compared to 42% under RCP8.5. Severe thermal stress (DHM $\geq$ 2°C-month) is projected for 45% of coral reefs under RCP4.5 compared to 38% of the reefs RCP8.5. About 8% of coral reefs in the region are projected to escape bleaching thermal stress under RCP4.5 and

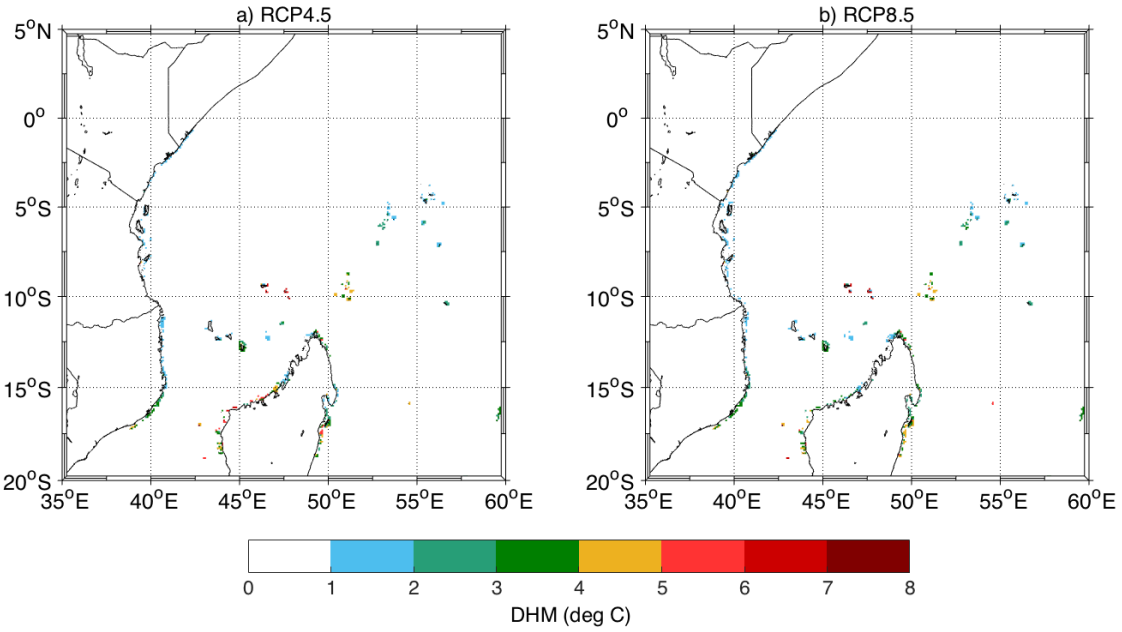

Fig. 5.9 Thermal stress calculated as DHM for the 2016 bleaching event using ensemble CMIP5 models under (a) RCP4.5 and (b) RCP8.5 scenarios

6% under RCP8.5.

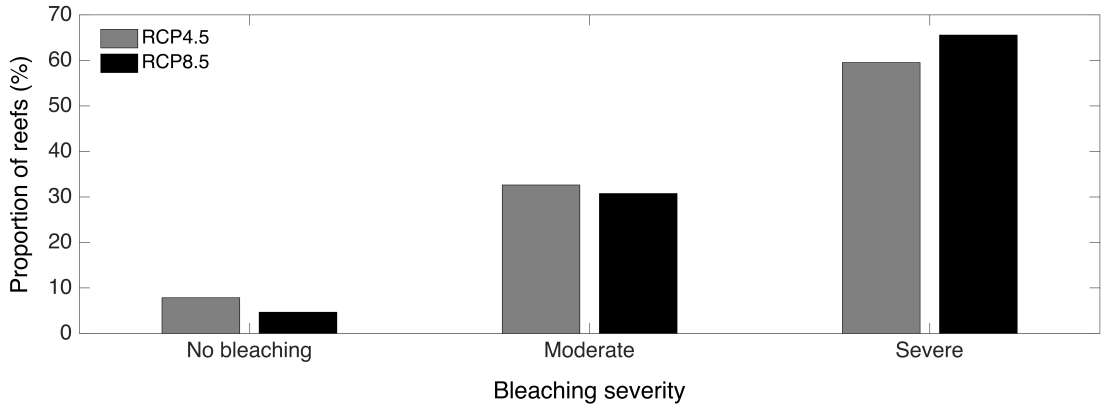

Fig. 5.10 Projected bleaching severity under RCP4.5 and RCP8.5 scenarios averaged over coral reefs in the study region.

Spatial projections of DHMs highlight the difference between thermal stress under RCP4.5 and RCP8.5 from 2020 to 2100 (Figure 5.11). Under RCP4.5, coral reefs in the region are projected to experience severe thermal stress (DHM ≥ 2°C-month)

between 2050 and 2070 with very few (less than 5%) projected to experience these conditions after 2080. Coral reefs south of 15°S in Mozambique (Angoche, Pebane), West of Madagascar (Juah de Nova, Maintirano, Masoarivo), East of Madagascar (St. Marie), Farquhar, Cosmoledo and Seychelles are projected to experience these conditions earliest (around 2050s) while coral reefs along the East African coast and northwest tip of Madagascar are projected to experience these conditions latest (around 2080). Although the projected thermal stress at DHM > 2°C threshold is evident under RCP4.5, the spatial extent is smaller relative to RCP8.5 from 2050 to 2100. By 2100, some reefs along the East African coast, north of Mozambique and northwest of Madagascar are projected to experience moderate bleaching stress. Severe thermal stress over the same period is projected for other reefs in the region.

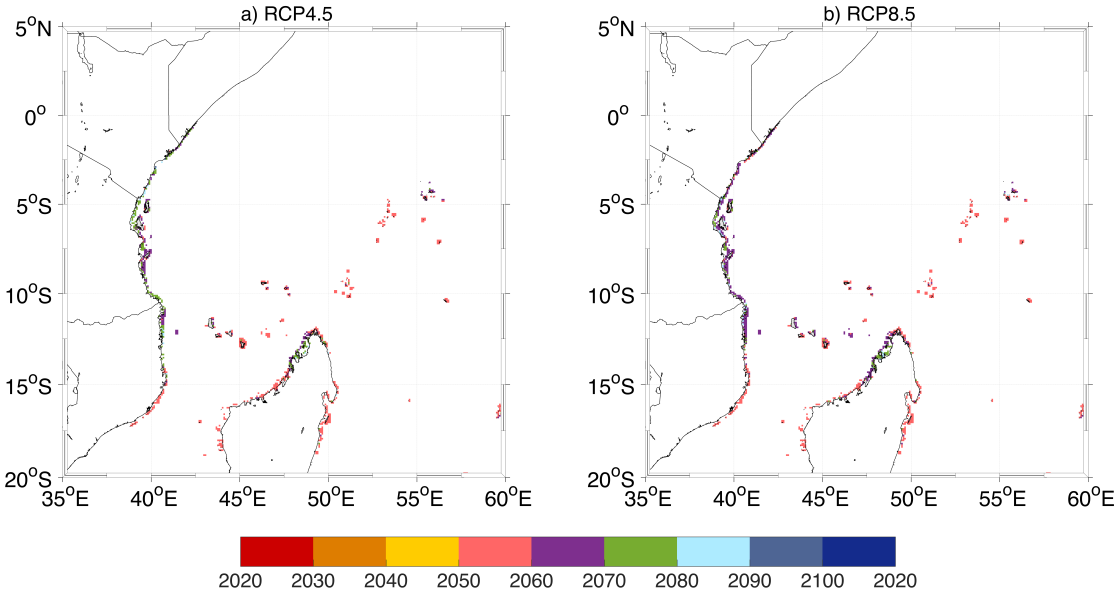

Fig. 5.11 Projected timing of bleaching level thermal stress for coral reefs in the region under RCP4.5 and RCP8.5 scenarios

Capacity of dispersal to deliver individuals adapted to different temperature regimes

The TST for reefs across the study domain varied greatly at local levels, with the majority being between 29 - 31°C (Figure 5.12a). The highest values of up to 33 - 34°C occurred in northern Seychelles islands, off west Madagascar and near Mafia island

(Tanzania). The lowest TST values were found north of 4°S on the Kenya coast at the southen extent of the cool Somali current, and in central Tanzania (Mafia, Songosongo and Unguja islands) and Madagascar (St. Marie). The transport of larvae results in individuals from one reef being transported to destination reefs with higher or lower TSTs than the natal reef. Figure 5.12b – d show reefs where recruited larvae come from warmer (blue) or cooler (red) source reefs, with the expectation that larvae from warmer reefs (blue) may survive future climate threats better, while larvae from cooler reefs (red) may suffer higher bleaching and mortality. For PLD of 10 days, except for the Kenya coast, most of the study domain reefs are a patchwork, receiving larvae from warmer and cooler source reefs. Kenyan reefs receive larvae from cooler reefs. For PLDs of 30 and 60 days the pattern is broadly the same for the Kenya coast, as well as northern Mozambique, receiving larvae from cooler locations. The Tanzania coast receives larvae from warmer reefs, while islands in the northern Mozambique Channel and NW Madagascar are a patchwork. For example in the Comoros, in Grande Comore, TST of source reefs is warmer by around 1.5°C compared to the local reefs, while in Anjouan and Moheli source reefs are cooler by 1°C and in Mayotte, TST of source reefs are cooler by around 1.3°C. The Amirantes in the Seychelles show high variation for different PLDs: for PLD of 30 days most reefs receive larvae from warmer locations, while at 60 days all the Amirants receive larvae from cooler locations.

5.4 Discussion

The trend in tropical SST computed over the past decades indicates warming superimposed on considerable spatial, interannual and seasonal variability with the western Indian Ocean significantly warmer than it was in the 1950s (Munday et al., 2009; Roxy et al., 2014). Most reefs in the region show positive trends during the warm season (January to May) except reefs in central Tanzania, Mozambique, and western Madagascar showing a negative trend in SST (Figure 5.2a). During the cool season (June to September), warming of coral reefs waters was distinctively positive over most of the reefs except for a few reefs in St. Marie and the northeastern tip of Madagascar (Figure 5.2b). The warming trend observed during the cool season might be due to shifting in the atmospheric circulation with the ascending cell over the eastern Pacific and subsidence over the Maritime continent resulting in low level easterlies over the western Indian Ocean (Roxy et al., 2014). The consequence of increased

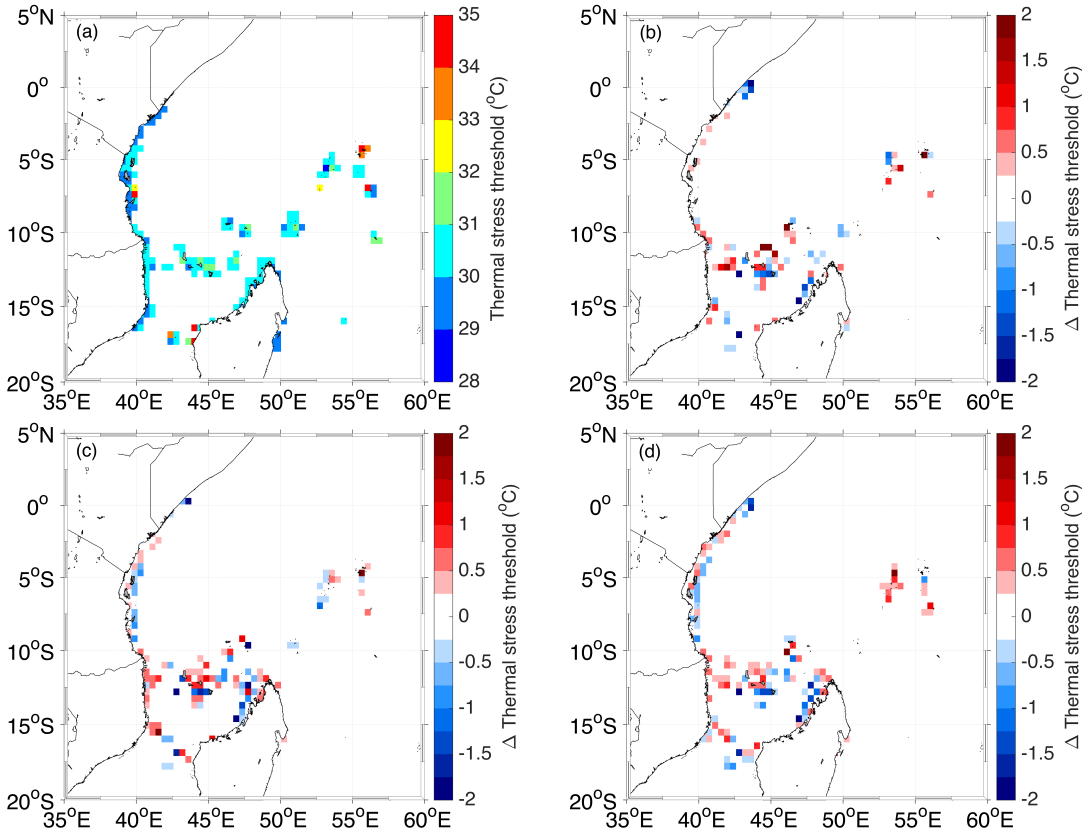

Fig. 5.12 (a) Thermal stress threshold (TST) for each reef location determined by the MMM+1°C. The difference between the TST of the destination reef and the TST larvae dispersing into and the local TST: for PLDs of (b) 10-days, (c) 30-days and (d) 60-days. Positive TSTs (red) show reef locations where immigrants come from cooler regimes (lower tolerance to heat stress) while negative TSTs (blue) show reef locations receiving larvae from warmer regions (higher tolerance).

warming during the cool season is prolonged bleaching episodes and less time to recover. With increased warming, the level of coral diseases might increase Maynard et al. (2015).

Interannual variability in bleaching level thermal stress shows that reefs in the region have been exposed to bleaching thermal stress with 1998 and 2016 being the most severe (Figure 5.3c). Both these years were associated with very strong El-Niño events but the timing and intensity of the bleaching events were different. Although 2016 was the warmest year, fewer corals were exposed to severe bleaching stress. In 1998, the proportion of reefs that were severely bleached was more than 50% and very few ($< 5\%$) escaped without bleaching. According to the Global Coral Reefs Monitoring Network, coral reefs in Seychelles and Kenya suffered the most in 1998 but

have since shown good recovery. Other countries like Tanzania, Comoros, Madagascar, and Mozambique have shown a decline in reef cover after the 1998 bleaching event. The strong El-Niño and the positive Indian Ocean Dipole of 1998 might have resulted in the extensive and much more severe bleaching compared to what was observed in 2016.

The projected occurrence of thermal stress leading to the 2016 bleaching event was assessed under RCP4.5 and RCP8.5 scenarios. The proportion of reefs that were exposed to severe thermal stress (DHM $\geq$ 2°C-month) was above 60% under the two RCP scenarios. This suggests that the severe bleaching thermal stress experienced across most reefs in 2016 could be attributed to anthropogenic influences due to committed warming from past greenhouse gas emissions. Under either scenario, the ensemble CMIP5 models project that severe thermal stress will exceed the current level, thus increasing the frequency of occurrences of severe coral bleaching and mortality in the future. With a 30-year range in the projected severe bleaching thermal stress, there is a time frame between 2020 to 2050 in which moderate bleaching will be experienced. Coral reefs projected to experience severe thermal stress earlier are potentially climate losers while those projected to experience these conditions much later (around 2080) are potentially climate winners and potentially act as temporary refugia. By 2060, DHM values over much of the regions coral reefs are projected to exceed four under RCP4.5 and a decade earlier under RCP8.5.

Coral reefs may recover from bleaching events, however, the recovery time enabling reefs to remain healthy will depend on coral communities which drive adaptation. Previous studies have suggested the potential of coral reefs adapting to thermal stress through changing symbionts in their tissues to more temperature-tolerant (Loya et al., 2001; Baker et al., 2004; Berkelmans and Van Oppen, 2006). However, a recent study by Kleypas et al. (2016) illustrated the potential importance of larval dispersal to thermal stress adaptation across different temperature regimes in the Coral Triangle. Using the same method as Kleypas et al. (2016), the results illustrate and expand on the concept originally proposed by Mumby et al. (2011) for the WIO region. The transport of larvae results in individuals from one reef being transported to destination reefs with higher or lower TSTs than the natal reef. Recruited larvae from warmer (blue) are expected to survive future climate threats better compared to recruited larvae from cooler (red) source reefs (Figure 5.12b – d), expected to suffer higher

bleaching and mortality. As long as exogenous larvae originate from reefs with temperatures that differ from the sink reef, they can potentially alter the overall temperature tolerance of a species by increasing the diversity of individuals (or alleles) with respect to temperature tolerance. With longer dispersal periods, the potential for connectivity to regions of significantly warmer or cooler temperatures increases. Therefore, this analysis represents the physical limits of how much larval exchange from cooler/hotter source could contribute to temperature threshold.

An important and logical assumption of the TST based on connectivity is that coral thermal tolerance is strongly influenced by the type of symbionts and acclimation capacity of corals. Distribution of many *Symbiodinium* types span temperature ranges as great as 15 °C (LaJeunesse et al., 2004; Goulet et al., 2008; Wicks et al., 2010; Cooper et al., 2011) but *Symbiodinium* types often persist as genetically isolated populations at the scale of individual reefs (Santos and Coffroth, 2003; Howells et al., 2009). Previous work of Bellantuono et al. (2012) showed that *Acropora millepora* acquired bleaching resistance with no detectable changes in the *Symbiodinium*. Altogether, these pieces of evidence suggest that both genetic clades of symbionts and thermal pre-stress has a role in heat tolerance in corals. Therefore, larvae originating from reefs with temperatures that differ from the sink reef can potentially alter the overall temperature tolerance of species by increasing the diversity of individuals with respect to temperature tolerance. Reefs that are connected to other reefs within a population are more likely to have greater genetic diversity than isolated locations (Liggins et al., 2014).

Management implications

Coral reef managers are increasingly aware of the threat posed to coral reefs by global warming. However, a better understanding of future projections for the region coral reefs may improve efforts by managers and policymakers to implement locally to regional scale actions that can support the natural resilience of reefs (Hughes et al., 2010). The results here help in identifying coral reefs that can act as temporary refugia (climate winners) in a warming world. Coral reef regions that will experience severe bleaching stress last are potential thermal refugia and include reefs along the East African coast and northwest tip of Madagascar under the RCP4.5 scenario. McClanahan and Muthiga (2017) identified reefs in northern Mozambique as being potential climate refugia due to their location at the edge of a coral reef diversity center with limited potential to expand. Maina et al. (2008) also identified reefs along the

east of Madagascar with the lowest susceptibility to thermal stress. This study also found several reefs in these regions that experienced low thermal stress during 1998 and 2016 bleaching events (Figure 5.3) and also projected to be exposed to low thermal stress in the coming decades (Figure 5.11).

5.5 Conclusion

The findings in this chapter contribute to the understanding of global climate change impacts in the western Indian Ocean region. In the case of 2016, there is a clear distinction between the CMIP5 model ensemble for experiments run with only natural forcing and those when anthropogenic forcing is included. This distinction suggests that at least part of the observed warming in the region during 2016 may be attributed to anthropogenic forcing. Under both optimistic and business as usual scenarios, global warming over the next 50 years could increase the magnitude and frequency of bleaching and accelerate the reported decline of coral reefs in the region. A comparison of the results from the two RCP scenarios presents an overview of possible climate futures for the coral reefs in this region, presuming that the models realistically represent the response of the climate system to external forcing.

Chapter 6

Conclusion and Future work

This thesis was designed to achieve the following key objectives as presented in chapter 1.

1. To develop a high-resolution model using the Regional Ocean Modelling System (ROMS) for the Western Indian Ocean region to study the mean circulation pattern chapter 3

2. To configure a particle tracking individual-based model in Ichthyop coupled with the high-resolution ocean model outputs from ROMS to investigate how spatial and temporal variability influences dispersal of broadcast coral larvae, infer connectivity networks and reef nodes that act as gateways which larvae have to pass in order to spread to other nodes chapter 4

3. To assess and understand thermal history trends and patterns for reefs and project annual severe bleaching from an ensemble of Coupled Model Intercomparison Project phase 5 models approximate scale of reefs (∼9 km). Also, to infer on the potential for connectivity to bring immigrants from different temperature regimes and the degree to which connectivity can shift temperature tolerance in corals chapter 5

A model-based configuration for the Western Indian Ocean was designed to simulate oceanic circulation and drive the Lagrangian model. The performance of the configuration was extensively assessed through comparisons with in situ and satellite observations. The simulated water mass properties are shown to be consistent with those present in the satellite and WOA09 climatology. However, the model is limited in its ability to accurately simulate the distribution of these water properties especially sea surface salinity. This could be due to initial and boundary conditions used to

force the ocean model. simulated mean SSH compares well with AVISO absolute dynamic topography, implying the basin-scale circulation in the configuration is well approximated. Using an eddy detection and tracking scheme, based on a hybrid-criteria that combines the use of the Okubo-Weiss parameter and closed SSH loops, the properties of the Southern Gyre were investigated. The statistical census revealed that the Southern Gyre had a mean lifespan of 98-days with a rotational speed of 0.6 m/s. Energy conversion terms showed that the dominant eddy forcing mechanism for the Southern gyre is due to barotropic instabilities and remote forcing from Rossby waves.

The high-resolution ocean model output was used to drive the Lagrangian tracking tool Ichthyop. Coupling Lagrangian models with high-resolution ocean model give better estimations of the importance of ocean dynamics on larval dispersal. A total of 170 reef cells were used to investigate dispersal pathways, level of connectivity and reef nodes that act as important gateways to dispersal. Results from the biophysical model highlighted the dominant pathways and barriers to dispersal, for example, the south to the north dispersal of coral larvae along the East African coast due to the constantly northward flowing EACC. SEC acted as a barrier to dispersal for broadcast corals in the Seychelles archipelago and those found in Madagascar. A barrier to dispersal was also evident between coral reef in the Mozambique channel and those north along the East African coast. Relative connectivity matrices were developed to identify the level of connectivity among reefs. The estimates of connectivity varied with respect to PLD. Areas of high connectivity (e.g. NE of Madagascar, the Islands in Comoros Basin; and along the East African coast), as well as areas of limited larval exchange (e.g. Tromelin and Seychelles archipelago), were identified. The neighbourhood analysis added a greater resolution to the general pattern of connectivity and identified the potential flow of larvae to and from all individual sites. The configuration and persistence of the neighborhoods are dependent on the PLD, the strength of and variability in ocean currents, and the local topology.

The connectivity component of this work has implications for marine conservation planning at multiple scales. Perhaps most importantly, the spatial and temporal variability in dispersal across the western Indian Ocean requires the conservation approach be tailored toward the connectivity characteristics of the site and region of interest. These patterns in connectivity should help in the design and implementa-

tion of regional management by linking the ecological dynamics with marine governance.

As global warming is expected to affect coral reefs worldwide through severe coral bleaching and possible mortality, chapter 5 assessed sea surface temperature history and future projections at the approximate of reefs. Across reef regions the western Indian Ocean, thermal stress history showed warming for most reefs with the proportion of reefs exposed to annual bleaching threshold increased in recent decades. Even though 2016 was the warmest (0.81 °C) compared to 1998 (0.58 °C) over the region, the spatial pattern of SST anomalies responsible for bleaching in 1998 impacted more reefs compared to 2016. Anomalously warm SST in 2016 was attributable in large part to anthropogenic forcing. Spatial projections of DHM values highlighted the disparity between thermal stress under the RCP4.5 and RCP8.5 scenarios. Under the RCP8.5 scenario, most reefs are projected to experience annual severe bleaching (DHM $\geq$ 2 °C) by 2050. The spatial extent of coral reef areas exceeding this threshold is projected to increase by 2060. Although the projected thermal stress for severe bleaching is still evident under the RCP4.5 scenario, its spatial extent is widely reduced relative to the RCP8.5. With expected rising temperatures associated with global warming, survival of most marine organisms especially coral reef would depend on the ability to cope via changes in physiology and phenology. Connectivity through larval dispersal thus plays a role in determining the genetic make-up of temperature tolerant corals across the population. Considering future increases in surface temperatures, if selection favours larvae from warmer regions, then larvae sourced from warmer water reefs should be more successful than those from cooler reefs. Using a prospective approach such as in this study is advantageous when anticipating shifts in predicted disturbance regimes.

Future work

While the ROMS configuration satisfactorily simulates the western Indian Ocean system, producing and expanding upon a set of results that are consistent with other studies, there is substantial scope for improvement. The northern boundary of the ROMS configuration was set at 5°N, therefore, the interaction between the Southern Gyre and the Great Whirl was not established. It would be necessary to extend the domain further north into the Arabian Sea to investigate the possibility of the two cells merging as postulated from other studies (e.g., Beal and Donohue, 2013; Vic et al., 2014; Akuetevi and Wirth, 2015). It is also paramount to perform longer inter-annual

simulations to investigate to what extent ENSO and IOD have on the Southern Gyre.

Coral larvae in the coupled biophysical model were considered passive, and no mortality was applied. These assumptions have critical consequences on dispersal distance and patterns of connectivity. Therefore, it would be important to incorporate biological factors related to larval abilities (e.g. swimming, orientation and active settling) and physical parameters such as temperature to account for mortality. Global warming will have an impact on larval dispersal, therefore, it would be interesting to incorporate future climate projections to investigate implications for coral connectivity.

Bibliography

Akuetevi, C. Q. C. and Wirth, A. (2015). Dynamics of turbulent western-boundary currents at low latitude in a shallow-water model. *Ocean Science*, 11(3):471–481.

Almany, G., Connolly, S., Heath, D., Hogan, J., Jones, G., McCook, L., Mills, M., Pressey, R., and Williamson, D. (2009). Connectivity, biodiversity conservation and the design of marine reserve networks for coral reefs. *Coral Reefs*, 28(2):339–351. 10.1007/s00338-009-0484-x.

Almany, G. R., Berumen, M. L., Thorrold, S. R., Planes, S., and Jones, G. P. (2007). Local replenishment of coral reef fish populations in a marine reserve. *Science*, 316(5825):742–744.

Andrello, M., Guilhaumon, F., Albouy, C., Parravicini, V., Scholtens, J., Verley, P., Barange, M., Sumaila, U. R., Manel, S., and Mouillot, D. (2017). Global mismatch between fishing dependency and larval supply from marine reserves. *Nature Communications*, 8:16039.

Andrello, M., Mouillot, D., Beuvier, J., Albouy, C., Thuiller, W., and Manel, S. (2013). Low connectivity between mediterranean marine protected areas: a biophysical modeling approach for the dusky grouper epinephelus marginatus. *PLoS One*, 8(7):e68564.

Andrello, M., Mouillot, D., Somot, S., Thuiller, W., and Manel, S. (2015). Additive effects of climate change on connectivity between marine protected areas and larval supply to fished areas. *Diversity and Distributions*, 21(2):139–150. https://doi.org/10.1111/ddi.12250.

Andutta, F. P., Kingsford, M. J., and Wolanski, E. (2012). 'sticky water'enables the retention of larvae in a reef mosaic. *Estuarine, Coastal and Shelf Science*, 101:54–63. 10.1016/j.ecss.2012.02.013.

Atwood, D. K., Hendee, J. C., and Mendez, A. (1992). An assessment of global warming stress on caribbean coral reef ecosystems. *Bull mar Sci*, 51(1):118–130.

Ayre, D. J. and Hughes, T. P. (2000). Genotypic diversity and gene flow in brooding and spawning corals along the great barrier reef, australia. *Evolution*, 54(5):1590–1605.

Babcock, R., Bull, G., Harrison, P. L., Heyward, A., Oliver, J., Wallace, C., and Willis, B. (1986). Synchronous spawnings of 105 scleractinian coral species on the great barrier reef. *Marine Biology*, 90(3):379–394.

Backeberg, B. and Reason, C. (2010). A connection between the south equatorial current north of madagascar and mozambique channel eddies. *Geophysical Research Letters*, 37(4):L04604.

Baker, A. C. (2003). Flexibility and specificity in coral-algal symbiosis: diversity, ecology, and biogeography of symbiodinium. *Annual Review of Ecology, Evolution, and Systematics*, 34(1):661–689.

Baker, A. C., Glynn, P. W., and Riegl, B. (2008). Climate change and coral reef bleaching: An ecological assessment of long-term impacts, recovery trends and future outlook. *Estuarine, Coastal and Shelf Science*, 80(4):435–471. 10.1016/j.ecss.2008.09.003.

Baker, A. C., Starger, C. J., McClanahan, T. R., and Glynn, P. W. (2004). Coral reefs: corals' adaptive response to climate change. *Nature*, 430(7001):741.

Barnes, R. D. (1989). Diversity of organisms: how much do we know? *American Zoologist*, 29(3):1075–1084. https://doi.org/10.1093/icb/29.3.1075.

Barnes, R. D. et al. (1987). *Invertebrate zoology.* Number Ed. 5 in Saunders series in organismic biology. Fort Worth, TX: Harcourt Brace Jovanovich College Publishers.

Barnes, R. S. K. and Hughes, R. N. (1999). *An Introduction to Marine Ecology.* Blackwell Publishing Ltd, Oxford, UK. doi:10.1002/9781444313284.

Beal, L. and Donohue, K. (2013). The great whirl: Observations of its seasonal development and interannual variability. *Journal of Geophysical Research: Oceans*, 118(1):1–13.

Beal, L. M. and Chereskin, T. K. (2003). The volume transport of the somali current during the 1995 southwest monsoon. *Deep Sea Research Part II: Topical Studies in Oceanography*, 50(12-13):2077–2089.

Bellantuono, A. J., Granados-Cifuentes, C., Miller, D. J., Hoegh-Guldberg, O., and Rodriguez-Lanetty, M. (2012). Coral thermal tolerance: tuning gene expression to resist thermal stress. *PLoS One*, 7(11):e50685.

Berkelmans, R. and Van Oppen, M. J. (2006). The role of zooxanthellae in the thermal tolerance of corals: a 'nugget of hope'for coral reefs in an era of climate change. *Proceedings of the Royal Society of London B: Biological Sciences*, 273(1599):2305–2312. 10.1098/rspb.2006.3567.

Bleck, R. (2002). An oceanic general circulation model framed in hybrid isopycnic-cartesian coordinates. *Ocean modelling*, 4(1):55–88. 10.1016/S1463-5003(01)00012-9.

Bode, M., Bode, L., and Armsworth, P. R. (2006). Larval dispersal reveals regional sources and sinks in the great barrier reef. *Marine Ecology Progress Series*, 308:17–25.

Borsa, P., Durand, J.-D., Chen, W.-J., Hubert, N., Muths, D., Mou-Tham, G., and Kulbicki, M. (2016). Comparative phylogeography of the western indian ocean reef fauna. *Acta oecologica*, 72:72–86.

Botsford, L., White, J. W., Coffroth, M.-A., Paris, C. B., Planes, S., Shearer, T., Thorrold, S. R., and Jones, G. P. (2009). Connectivity and resilience of coral reef metapopulations in marine protected areas: matching empirical efforts to predictive needs. *Coral reefs*, 28(2):327–337. doi:10.1007/s00338-009-0466-z.

Botsford, L. W., Hastings, A., and Gaines, S. D. (2001). Dependence of sustainability on the configuration of marine reserves and larval dispersal distance. *Ecology Letters*, 4(2):144–150.

Bouwmeester, J., Gatins, R., Giles, E. C., Sinclair-Taylor, T. H., and Berumen, M. L. (2016). Spawning of coral reef invertebrates and a second spawning season for scleractinian corals in the central red sea. *Invertebrate Biology*, 135(3):273–284.

Boylan, P. and Kleypas, J. (2008). New insights into the exposure and sensitivity of coralreefs to ocean warming. In *11th International Coral Reef Symposium*, volume 2, pages 854–858.

Brandt, P., Stramma, L., Schott, F., Fischer, J., Dengler, M., and Quadfasel, D. (2002). Annual rossby waves in the arabian sea from topex/poseidon altimeter and in situ data. *Deep Sea Research Part II: Topical Studies in Oceanography*, 49(7):1197–1210.

Brochier, T., Lett, C., Tam, J., Fréon, P., Colas, F., and Ayón, P. (2008). An individual-based model study of anchovy early life history in the northern humboldt current system. *Progress in Oceanography*, 79(2-4):313–325.

Brown, B., Dunne, R., Goodson, M., and Douglas, A. (2002). Experience shapes the susceptibility of a reef coral to bleaching. *Coral Reefs*, 21(2):119–126.

Brown, B. E. (1997). Coral bleaching: causes and consequences. *Coral reefs*, 16(1):S129–S138.

Brown, C., Jackson, G., Holt, S., and Holt, G. (2005). Spatial and temporal patterns in modeled particle transport to estuarine habitat with comparisons to larval fish settlement patterns. *Estuarine, Coastal and Shelf Science*, 64(1):33–46.

Bruce, J. G. (1979). Eddies off the somali coast during the southwest monsoon. *Journal of Geophysical Research: Oceans (1978–2012)*, 84(C12):7742–7748.

Carlos, A. A., Baillie, B. K., Kawachi, M., and Maruyama, T. (1999). Phylogenetic position of symbiodinium (dinophyceae) isolates from tridacnids (bivalvia), cardiids (bivalvia), a sponge (porifera), a soft coral (anthozoa), and a free-living strain. *Journal of Phycology*, 35(5):1054–1062.

Carpine-Lancre, J. and Bv, G. (2003). A history of GEBCO: The 100 year story of the General Bathymetric Chart of the Oceans 1903-2003. ISBN:9080620548.

Carroll, A., Harrison, P., and Adjeroud, M. (2006). Sexual reproduction of acropora reef corals at moorea, french polynesia. *Coral reefs*, 25(1):93–97.

Casey, K. S. and Cornillon, P. (1999). A comparison of satellite and in situ–based sea surface temperature climatologies. *Journal of Climate*, 12(6):1848–1863. https://doi.org/10.1175/1520-0442(1999)012<1848:ACOSAI>2.0.CO;2.

Chapman, G. (1983). An Introduction to Marine Ecology. *New Scientist*, 98(1357):392–393.

Chelton, D., Schlax, M., Lyman, J., and Johnson, G. (2003). Equatorially trapped rossby waves in the presence of meridionally sheared baroclinic flow in the pacific ocean. *Progress in Oceanography*, 56(2):323–380.

Chelton, D. B., Deszoeke, R. A., Schlax, M. G., El Naggar, K., and Siwertz, N. (1998). Geographical variability of the first baroclinic rossby radius of deformation. *Journal of Physical Oceanography*, 28(3):433–460.

Collins, C., Hermes, J., and Reason, C. (2014). Mesoscale activity in the comoros basin from satellite altimetry and a high-resolution ocean circulation model. *Journal of Geophysical Research: Oceans*, 119(8):4745–4760.

Collins, C., Reason, C., and Hermes, J. (2012). Scatterometer and reanalysis wind products over the western tropical indian ocean. *Journal of Geophysical Research: Oceans*, 117(C3):C03045. DOI:10.1029/2011JC007531.

Conkright, M. E., Locarnini, R. a., Garcia, H. E., O'Brien, T. D., Boyer, T. P., Stepens, C., and Antonov, J. I. (2002). World Ocean Atlas 2001: Objective analyses, data statistics, and figures CD-ROM documentation. *National Oceanographic Data Center Internal Report (NOAA Atlas NESDIS)*, 17(September):17.

Connell, J. H., Hughes, T. P., and Wallace, C. C. (1997). A 30-year study of coral abundance, recruitment, and disturbance at several scales in space and time. *Ecological Monographs*, 67(4):461–488.

Connolly, S. R. and Baird, A. H. (2010). Estimating dispersal potential for marine larvae: dynamic models applied to scleractinian corals. *Ecology*, 91(12):3572–3583. doi 10.1890/10-0143.1.

Cooper, T. F., Berkelmans, R., Ulstrup, K. E., Weeks, S., Radford, B., Jones, A. M., Doyle, J., Canto, M., O'Leary, R. A., and van Oppen, M. J. (2011). Environmental factors controlling the distribution of symbiodinium harboured by the coral acropora millepora on the great barrier reef. *PLoS One*, 6(10):e25536.

Cowen, R. K., Lwiza, K. M., Sponaugle, S., Paris, C. B., and Olson, D. B. (2000). Connectivity of marine populations: open or closed? *Science*, 287(5454):857–859.

Cowen, R. K., Paris, C. B., and Srinivasan, A. (2006). Scaling of connectivity in marine populations. *Science*, 311(5760):522–527.

Cowen, R. K. and Sponaugle, S. (2009). Larval Dispersal and Marine Population Connectivity. *Annual Review of Marine Science*, 1:443–466. 10.1146/annurev.marine.010908.163757.

Cox, M. D. (1979). A numerical study of somali current eddies. *Journal of Physical Oceanography*, 9(2):311–326.

Crochelet, E., Roberts, J., Lagabrielle, E., Obura, D., Petit, M., and Chabanet, P. (2016). A model-based assessment of reef larvae dispersal in the western indian ocean reveals regional connectivity patterns—potential implications for conservation policies. *Regional Studies in Marine Science*, 7:159–167.

da Silva, A., Young, C., and Levitus, S. (1994). Atlas of surface marine data 1994, Vol. 4: Anomalies of fresh water fluxes. *NOAA Atlas, NESDIS*. http://rda.ucar.edu/datasets/ds541.1/docs/doc/atlas/Vol4.ps.Z.

Dawson, T. P., Jackson, S. T., House, J. I., Prentice, I. C., and Mace, G. M. (2011). Beyond predictions: biodiversity conservation in a changing climate. *science*, 332(6025):53–58.

de Ruijter, W. P., Ridderinkhof, H., Lutjeharms, J. R., Schouten, M. W., and Veth, C. (2002). Observations of the flow in the mozambique channel. *Geophysical Research Letters*, 29(10):140–1. doi:10.1029/2001GL013714.

Debreu, L., Marchesiello, P., Penven, P., and Cambon, G. (2012). Two-way nesting in split-explicit ocean models: algorithms, implementation and validation. *Ocean Modelling*, 49:1–21.

Debreu, L., Vouland, C., and Blayo, E. (2008). Agrif: Adaptive grid refinement in fortran. *Computers & Geosciences*, 34(1):8–13.

Di Franco, A., Calò, A., Pennetta, A., De Benedetto, G., Planes, S., and Guidetti, P. (2015). Dispersal of larval and juvenile seabream: Implications for mediterranean marine protected areas. *Biological Conservation*, 192:361–368.

Dixon, G. B., Davies, S. W., Aglyamova, G. V., Meyer, E., Bay, L. K., and Matz, M. V. (2015). Genomic determinants of coral heat tolerance across latitudes. *Science*, 348(6242):1460–1462.

Done, T. T., Ogden, J. J., Wiebe, W., Rosen, B., et al. (1996). Biodiversity and ecosystem function of coral reefs. In *Global biodiversity assessment-pages: 393-429*. John Wiley & Sons.

Donner, S. D. (2011). An evaluation of the effect of recent temperature variability on the prediction of coral bleaching events. *Ecological Applications*, 21(5):1718–1730. 10.1890/10-0107.1.

Donner, S. D., Knutson, T. R., and Oppenheimer, M. (2007). Model-based assessment of the role of human-induced climate change in the 2005 caribbean coral bleaching event. *Proceedings of the National Academy of Sciences*, 104(13):5483–5488.

Donner, S. D., Rickbeil, G. J., and Heron, S. F. (2017). A new, high-resolution global mass coral bleaching database. *PloS one*, 12(4):e0175490.

Donner, S. D., Skirving, W. J., Little, C. M., Oppenheimer, M., and Hoegh-Guldberg, O. (2005). Global assessment of coral bleaching and required rates of adaptation under climate change. *Global Change Biology*, 11(12):2251–2265.

Donohue, K. A. and Toole, J. M. (2003). A near-synoptic survey of the southwest indian ocean. *Deep Sea Research Part II: Topical Studies in Oceanography*, 50(12):1893–1931.

Dorenbosch, M., Pollux, B., Pustjens, A., Rajagopal, S., Nagelkerken, I., van der Velde, G., and Moon-van der Staay, S. (2006). Population structure of the dory snapper, lutjanus fulviflamma, in the western indian ocean revealed by means of aflp fingerprinting. *Hydrobiologia*, 568(1):43–53.

Douglas, A. (2003). Coral bleaching—-how and why? *Marine pollution bulletin*, 46(4):385–392.

Ducet, N., Le Traon, P.-Y., and Reverdin, G. (2000). Global high-resolution mapping of ocean circulation from topex/poseidon and ers-1 and-2. *Journal of Geophysical Research-Oceans*, 105(C8):19477–19498.

Duda, A. M. and Sherman, K. (2002). A new imperative for improving management of large marine ecosystems. *Ocean & Coastal Management*, 45(11-12):797–833. doi:10.1016/S0964-5691(02)00107-2.

Düing, W. and Schott, F. (1978). Measurements in the source region of the somali current during the monsoon reversal. *Journal of Physical Oceanography*, 8(2):278–289.

Evans, R. H. and Brown, O. B. (1981). Propagation of thermal fronts in the somali current system. *Deep Sea Research Part A. Oceanographic Research Papers*, 28(5):521–527.

Ffield, A. and Gordon, A. L. (1992). Vertical mixing in the indonesian thermocline. *Journal of Physical Oceanography*, 22(2):184–195.

Figueiredo, J., Baird, A. H., and Connolly, S. R. (2013). Synthesizing larval competence dynamics and reef-scale retention reveals a high potential for self-recruitment in corals. *Ecology*, 94(3):650–659.

Findlater, J. (1969a). Interhemispheric transport of air in the lower troposphere over the western indian ocean. *Quarterly Journal of the Royal Meteorological Society*, 95(404):400–403. doi 10.1002/qj.49709540412.

Findlater, J. (1969b). A major low-level air current near the indian ocean during the northern summer. *Quarterly Journal of the Royal Meteorological Society*, 95(404):362–380.

Findlater, J. (1978). Observational aspects of the low-level cross-equatorial jet stream of the western indian ocean. In *Monsoon Dynamics*, pages 1251–1262. Springer. doi 10.1007/978-3-0348-5759-8.

Fischer, J., Schott, F., and Stramma, L. (1996). Currents and transports of the great whirl-socotra gyre system during the summer monsoon, august 1993. *Journal of Geophysical Research: Oceans*, 101(C2):3573–3587.

Gabriela Mayorga-Adame, C., Ted Strub, P., Batchelder, H. P., and Spitz, Y. H. (2016). Characterizing the circulation off the k enyan-t anzanian coast using an ocean model. *Journal of Geophysical Research: Oceans*, 121(2):1377–1399. doi 10.1002/2015JC010860.

Gaines, S. and Roughgarden, J. (1985). Larval settlement rate: a leading determinant of structure in an ecological community of the marine intertidal zone. *Proceedings of the National Academy of Sciences*, 82(11):3707–3711.

Gamoyo, M., Reason, C., and Obura, D. (2015). Rainfall variability over the east african coast. *Theoretical and Applied Climatology*, 120(1-2):311–322. doi 10.1007/s00704-014-1171-6.

Gamoyo, M., Reason, C. J., and Collins, C. (2017). A numerical investigation of the southern gyre using roms. *Journal of Marine Systems*, 169:11–24. https://doi.org/10.1016/j.jmarsys.2017.01.002.

Gaylord, B. and Gaines, S. D. (2000). Temperature or transport? range limits in marine species mediated solely by flow. *The American Naturalist*, 155(6):769–789.

Gerber, L. R., Botsford, L. W., Hastings, A., Possingham, H. P., Gaines, S. D., Palumbi, S. R., and Andelman, S. (2003). Population models for marine reserve design: a retrospective and prospective synthesis. *Ecological Applications*, 13(sp1):47–64. https://doi.org/10.1890/1051-0761(2003)013[0047:PMFMRD]2.0.CO;2.

Gilmour, J. P., Smith, L. D., and Brinkman, R. M. (2009). Biannual spawning, rapid larval development and evidence of self-seeding for scleractinian corals at an isolated system of reefs. *Marine Biology*, 156(6):1297–1309.

Glynn, P. W. (1993). Coral reef bleaching: ecological perspectives. *Coral Reefs*, 12(1):1–17. 10.1007/BF00303779.

Glynn, P. W. and Ault, J. (2000). A biogeographic analysis and review of the far eastern pacific coral reef region. *Coral reefs*, 19(1):1–23.

Glynn, P. W. and D'Croz, L. (1990). Experimental evidence for high temperature stress as the cause of El Niño-coincident coral mortality. *Coral Reefs*, 8(4):181–191. 10.1007/BF00265009.

Glynn, P. W., Gassman, N., Eakin, C., Cortes, J., Smith, D., and Guzman, H. (1991). Reef coral reproduction in the eastern pacific: Costa rica, panama, and galapagos islands (ecuador). *Marine Biology*, 109(3):355–368.

Gordon, A., Sprintall, J., Van Aken, H., Susanto, D., Wijffels, S., Molcard, R., Ffield, A., Pranowo, W., and Wirasantosa, S. (2010). The indonesian throughflow during 2004–2006 as observed by the instant program. *Dynamics of Atmospheres and Oceans*, 50(2):115–128.

Gordon, A. L. (2001). Interocean exchange. *International Geophysics series*, 77:303–316.

Gordon, A. L. (2005). The indonesian seas. *Oceanography*, 18(4):14.

Goulet, T. L., Simmons, C., and Goulet, D. (2008). Worldwide biogeography of symbiodinium in tropical octocorals. *Marine Ecology Progress Series*, 355:45–58.

Graham, N. A. J. and Nash, K. L. (2013). The importance of structural complexity in coral reef ecosystems. *Coral Reefs*, 32(2):315–326. doi 10.1007/s00338-012-0984-y.

Grimm, V., Berger, U., Bastiansen, F., Eliassen, S., Ginot, V., Giske, J., Goss-Custard, J., Grand, T., Heinz, S. K., Huse, G., et al. (2006). A standard protocol for describing individual-based and agent-based models. *Ecological modelling*, 198(1-2):115–126.

Grimsditch, G., Mwaura, J., Kilonzo, J., Amiyo, N., and Obura, D. (2008). High zooxanthellae densities and turnover correlate with low bleaching tolerance in kenyan corals. *Coastal oceans research and development in the Indian Ocean status report*, pages 235–236.

Gruber, N., Frenzel, H., Doney, S. C., Marchesiello, P., McWilliams, J. C., Moisan, J. R., Oram, J. J., Plattner, G.-K., and Stolzenbach, K. D. (2006). Eddy-resolving simulation of plankton ecosystem dynamics in the california current system. *Deep Sea Research Part I: Oceanographic Research Papers*, 53(9):1483–1516.

Haidvogel, D. B., Arango, H., Budgell, W. P., Cornuelle, B. D., Curchitser, E., Di Lorenzo, E., Fennel, K., Geyer, W. R., Hermann, A. J., Lanerolle, L., et al. (2008). Ocean forecasting in terrain-following coordinates: Formulation and skill assessment of the regional ocean modeling system. *Journal of Computational Physics*, 227(7):3595–3624. 10.1016/j.jcp.2007.06.016.

Haidvogel, D. B. and Beckmann, A. (1999). Numerical ocean circulation modeling. *Series On Environmental Science And Management; Vol. 2*. ISBN:978-1-86094-114-6.

Halo, I., Backeberg, B., Penven, P., Ansorge, I., Reason, C., and Ullgren, J. (2014a). Eddy properties in the mozambique channel: A comparison between observations and two numerical ocean circulation models. *Deep Sea Research Part II: Topical Studies in Oceanography*, 100:38–53.

Halo, I., Backeberg, B., Penven, P., Ansorge, I., Reason, C., and Ullgren, J. (2014b). Eddy properties in the mozambique channel: A comparison between observations and two numerical ocean circulation models. *Deep Sea Research Part II: Topical Studies in Oceanography*, 100:38–53.

Halo, I., Penven, P., Backeberg, B., Ansorge, I., Shillington, F., and Roman, R. (2014c). Mesoscale eddy variability in the southern extension of the east madagascar current: Seasonal cycle, energy conversion terms, and eddy mean properties. *Journal of Geophysical Research: Oceans*, 119(10):7324–7356.

Han, W., McCreary Jr, J. P., Anderson, D., and Mariano, A. J. (1999). Dynamics of the eastern surface jets in the equatorial indian ocean*. *Journal of Physical Oceanography*, 29(9):2191–2209.

Hancke, L., Roberts, M., and Ternon, J.-F. (2014). Surface drifter trajectories highlight flow pathways in the mozambique channel. *Deep Sea Research Part II: Topical Studies in Oceanography*, 100:27–37.

Harrison, P. L., Babcock, R. C., Bull, G. D., Oliver, J. K., Wallace, C. C., and Willis, B. L. (1984). Mass spawning in tropical reef corals. *Science*, 223(4641):1186–1189.

Harrison, P. L. and Booth, D. J. (2007). Coral reefs: naturally dynamic and increasingly disturbed ecosystems. *Marine ecology*, pages 316–377.

Harrison, P. L. and Wallace, C. C. (1990). Reproduction, dispersal and recruitment of scleractinian corals. *Coral Reefs. Ecosyst. World*, 25:133–207.

Hastenrath, S. and Greischar, L. (1991). The monsoonal current regimes of the tropical indian ocean: Observed surface flow fields and their geostrophic and wind-driven components. *Journal of Geophysical Research: Oceans*, 96(C7):12619–12633.

Hedgecock, D., Barber, P. H., and Edmands, S. (2007). Genetic approaches to measuring connectivity. *Oceanography*, 20(3):70–79.

Hellberg, M. (2007). Footprints on water: the genetic wake of dispersal among reefs. *Coral Reefs*, 26(3):463–473.

Hermes, J. and Reason, C. (2008). Annual cycle of the south indian ocean (seychelles-chagos) thermocline ridge in a regional ocean model. *Journal of Geophysical Research: Oceans*, 113(C4):C04035.

Hermes, J. C. and Reason, C. J. (2009). The sensitivity of the seychelles–chagos thermocline ridge to large-scale wind anomalies. *ICES Journal of Marine Science*, 66(7):1455–1466.

Hinrichsen, H.-H., Möllmann, C., Voss, R., Köster, F., and Kornilovs, G. (2002). Biophysical modeling of larval baltic cod (gadus morhua) growth and survival. *Canadian Journal of Fisheries and Aquatic Sciences*, 59(12):1858–1873.

Hoareau, T. B., Boissin, E., Paulay, G., and Bruggemann, J. H. (2013). The south-western indian ocean as a potential marine evolutionary hotspot: perspectives from comparative phylogeography of reef brittle-stars. *Journal of Biogeography*, 40(11):2167–2179.

Hoegh-Guldberg, O. (1999a). Climate change, coral bleaching and the future of the world's coral reefs. *Marine and Freshwater Research*, 50(8):839. doi:10.1071/MF99078.

Hoegh-Guldberg, O. (1999b). Global warming and coral reef ecosystems: ecological consequences of increased tropical sea tempertures. *Journal of Marine and Freshwater Research*, 50(8):867–878. doi:10.1071/MF99121.

Hoegh-Guldberg, O. and Bruno, J. F. (2010). The impact of climate change on the world's marine ecosystems. *Science*, 328(5985):1523–1528.

Hoegh-Guldberg, O., Mumby, P., Hooten, A., Steneck, R., Greenfield, P., Gomez, E., Harvell, D., Sale, P., Edwards, A., Caldeira, K., et al. (2008). Coral adaptation in the face of climate change: Response. *Science*, 320(5874):315–316. https://doi.org/10.1126/science.320.5874.315.

Hoegh-Guldberg, O. and Pearse, J. S. (1995). Temperature, food availability, and the development of marine invertebrate larvae. *American Zoologist*, 35(4):415–425.

Holstein, D. M., Paris, C. B., and Mumby, P. J. (2014). Consistency and inconsistency in multispecies population network dynamics of coral reef ecosystems. *Marine Ecology Progress Series*, 499:1–18.

Howells, E., Van Oppen, M., and Willis, B. (2009). High genetic differentiation and cross-shelf patterns of genetic diversity among great barrier reef populations of symbiodinium. *Coral Reefs*, 28(1):215–225.

Huggett, J., Fréon, P., Mullon, C., and Penven, P. (2003). Modelling the transport success of anchovy engraulis encrasicolus eggs and larvae in the southern benguela: the effect of spatio-temporal spawning patterns. *Marine Ecology Progress Series*, 250:247–262.

Hughes, T. (1999). Off-reef transport of coral fragments at lizard island, australia. *Marine Geology*, 157(1-2):1–6. doi 10.1016/S0025-3227(98)00187-X.

Hughes, T., Baird, A., Dinsdale, E., Harriott, V., Moltschaniwskyj, N., Pratchett, M., Tanner, J., and Willis, B. (2002). Detecting regional variation using meta-analysis and large-scale sampling: Latitudinal patterns in recruitment. *Ecology*, 83(2):436–451.

Hughes, T. P., Baird, A. H., Bellwood, D. R., Card, M., Connolly, S. R., Folke, C., Grosberg, R., Hoegh-Guldberg, O., Jackson, J. B., Kleypas, J., et al. (2003). Climate change, human impacts, and the resilience of coral reefs. *science*, 301(5635):929–933. 10.1126/science.1085046.

Hughes, T. P., Graham, N. A. J., Jackson, J. B. C., Mumby, P. J., and Steneck, R. S. (2010). Rising to the challenge of sustaining coral reef resilience. *Trends in Ecology & Evolution*, 25(11):633–642. doi 10.1016/j.tree.2010.07.011.

Huyghe, F. and Kochzius, M. (2017). Highly restricted gene flow between disjunct populations of the skunk clownfish (amphiprion akallopisos) in the indian ocean. *Marine Ecology*, 38(1):e12357.

Huyghe, F. and Kochzius, M. (2018). Sea surface currents and geographic isolation shape the genetic population structure of a coral reef fish in the indian ocean. *PloS one*, 13(3):e0193825.

IMaRS-USF, I. (2005). Millennium coral reef mapping project. *Validated maps. UNEP World Conservation Monitoring Centre, Cambridge, UK.*

International Hydrographic Organization, I. and Sieger, R. (2012). Limits of oceans and seas in digitized, machine readable form. doi:10.1594/PANGAEA.777975.

James, M. K., Armsworth, P. R., Mason, L. B., and Bode, L. (2002). The structure of reef fish metapopulations: modelling larval dispersal and retention patterns. *Proceedings of the Royal Society of London B: Biological Sciences*, 269(1505):2079–2086.

Jensen, T. G. (1991). Modeling the seasonal undercurrents in the somali current system. *Journal of Geophysical Research: Oceans*, 96(C12):22151–22167.

Jones, A. and Berkelmans, R. (2010). Potential costs of acclimatization to a warmer climate: growth of a reef coral with heat tolerant vs. sensitive symbiont types. *PloS one*, 5(5):e10437.

Jones, A. M., Berkelmans, R., van Oppen, M. J., Mieog, J. C., and Sinclair, W. (2008). A community change in the algal endosymbionts of a scleractinian coral following a natural bleaching event: field evidence of acclimatization. *Proceedings of the Royal Society of London B: Biological Sciences*, 275(1641):1359–1365.

Jones, G., Almany, G., Russ, G., Sale, P., Steneck, R., Van Oppen, M., and Willis, B. (2009). Larval retention and connectivity among populations of corals and reef fishes: history, advances and challenges. *Coral reefs*, 28(2):307–325. 10.1007/s00338-009-0469-9.

Jones, G., Milicich, M., Emslie, M., and Lunow, C. (1999). Self-recruitment in a coral reef fish population. *Nature*, 402(6763):802–804.

Jones, R., Ricardo, G., and Negri, A. (2015). Effects of sediments on the reproductive cycle of corals. *Marine Pollution Bulletin*, 100(1):13–33.

Kaplan, D. M., Botsford, L. W., and Jorgensen, S. (2006). Dispersal per recruit: an efficient method for assessing sustainability in marine reserve networks. *Ecological Applications*, 16(6):2248–2263.

Kijazi, A. L. and Reason, C. (2012). Intra-seasonal variability over the northeastern highlands of tanzania. *International Journal of Climatology*, 32(6):874–887.

Kingsford, M. J., Leis, J. M., Shanks, A., Lindeman, K. C., Morgan, S. G., and Pineda, J. (2002). Sensory environments, larval abilities and local self-recruitment. *Bulletin of Marine Science*, 70(1):309–340.

Kininmonth, S. J., De'ath, G., and Possingham, H. P. (2010). Graph theoretic topology of the great but small barrier reef world. *Theoretical Ecology*, 3(2):75–88.

Kinlan, B. P., Gaines, S. D., and Lester, S. E. (2005). Propagule dispersal and the scales of marine community process. *Diversity and Distributions*, 11(2):139–148.

Kleypas, J. A., Thompson, D. M., Castruccio, F. S., Curchitser, E. N., Pinsky, M., and Watson, J. R. (2016). Larval connectivity across temperature gradients and its potential effect on heat tolerance in coral populations. *Global change biology*, 22(11):3539–3549.

Knox, R. (1976). On a long series of measurements of indian ocean equatorial currents near addu atoll. *Deep Sea Research and Oceanographic Abstracts*, 23(3):211 – IN1. doi:10.1016/0011-7471(76)91325-5.

Koch-Larrouy, A., Madec, G., Bouruet-Aubertot, P., Gerkema, T., Bessières, L., and Molcard, R. (2007). On the transformation of pacific water into indonesian throughflow water by internal tidal mixing. *Geophysical Research Letters*, 34(4):L04604.

Kool, J. T., Moilanen, A., and Treml, E. A. (2013). Population connectivity: recent advances and new perspectives. *Landscape Ecology*, 28(2):165–185.

LaJeunesse, T. and Trench, R. (2000). Biogeography of two species of symbiodinium (freudenthal) inhabiting the intertidal sea anemone anthopleura elegantissima (brandt). *The Biological Bulletin*, 199(2):126–134.

LaJeunesse, T. C. (2001). Investigating the biodiversity, ecology, and phylogeny of endosymbiotic dinoflagellates in the genus symbiodinium using the its region: in search of a "species" level marker. *Journal of Phycology*, 37(5):866–880.

LaJeunesse, T. C., Smith, R., Walther, M., Pinzón, J., Pettay, D. T., McGinley, M., Aschaffenburg, M., Medina-Rosas, P., Cupul-Magaña, A. L., Pérez, A. L., et al. (2010). Host–symbiont recombination versus natural selection in the response of coral–dinoflagellate symbioses to environmental disturbance. *Proceedings of the Royal Society of London B: Biological Sciences*, 277(1696):2925–2934.

LaJeunesse, T. C., Thornhill, D. J., Cox, E. F., Stanton, F. G., Fitt, W. K., and Schmidt, G. W. (2004). High diversity and host specificity observed among symbiotic dinoflagellates in reef coral communities from hawaii. *Coral reefs*, 23(4):596–603.

Lalli, C. and Parsons, T. (1995). *Biological Oceanography: An Introduction*. Butterworth-Heinemann Ltd., Oxford, UK.

Large, W. G., McWilliams, J. C., Doney, S. C., et al. (1994). Oceanic vertical mixing: A review and a model with a nonlocal boundary layer parameterization. *Reviews of Geophysics*, 32(4):363–404.

Lazure, P. and Dumas, F. (2008). An external–internal mode coupling for a 3d hydrodynamical model for applications at regional scale (mars). *Advances in water resources*, 31(2):233–250.

Leetmaa, A., Quadfasel, D., and Wilson, D. (1982). Development of the flow field during the onset of the somali current, 1979. *Journal of Physical Oceanography*, 12(12):1325–1342.

Lester, S. E., Ruttenberg, B. I., Gaines, S. D., and Kinlan, B. P. (2007). The relationship between dispersal ability and geographic range size. *Ecology Letters*, 10(8):745–758.

Lett, C., Penven, P., Ayón, P., and Fréon, P. (2007). Enrichment, concentration and retention processes in relation to anchovy (engraulis ringens) eggs and larvae distributions in the northern humboldt upwelling ecosystem. *Journal of Marine Systems*, 64(1-4):189–200.

Lett, C., Roy, C., Levasseur, A., Van Der Lingen, C. D., and Mullon, C. (2006). Simulation and quantification of enrichment and retention processes in the southern benguela upwelling ecosystem. *Fisheries Oceanography*, 15(5):363–372.

Lett, C., Verley, P., Mullon, C., Parada, C., Brochier, T., Penven, P., and Blanke, B. (2008). A lagrangian tool for modelling ichthyoplankton dynamics. *Environmental Modelling & Software*, 23(9):1210–1214. 10.1016/j.envsoft.2008.02.005.

Levine, R. C., Turner, A. G., Marathayil, D., and Martin, G. M. (2013). The role of northern arabian sea surface temperature biases in cmip5 model simulations and future projections of indian summer monsoon rainfall. *Climate dynamics*, 41(1):155–172.

Levinton, J. S. and Levinton, J. S. (1995). *Marine Biology: Function, Biodiversity, Ecology.*, volume 420. Oxford University Press New York.

Li, G. and Xie, S.-P. (2014). Tropical biases in cmip5 multimodel ensemble: The excessive equatorial pacific cold tongue and double itcz problems. *Journal of Climate*, 27(4):1765–1780.

Liggins, L., Gleeson, L., and Riginos, C. (2014). Evaluating edge-of-range genetic patterns for tropical echinoderms, acanthaster planci and tripneustes gratilla, of the kermadec islands, southwest pacific. *Bulletin of Marine Science*, 90(1):379–397.

Liu, G., Heron, S. F., Eakin, C. M., Muller-Karger, F. E., Vega-Rodriguez, M., Guild, L. S., De La Cour, J. L., Geiger, E. F., Skirving, W. J., Burgess, T. F., et al. (2014). Reef-scale thermal stress monitoring of coral ecosystems: new 5-km global products from noaa coral reef watch. *Remote Sensing*, 6(11):11579–11606.

Liu, G., Matrosova, L., Penland, C., Gledhill, D., Eakin, C., Webb, R., Christensen, T., Heron, S., Morgan, J., Skirving, W., et al. (2008). Noaa coral reef watch coral bleaching outlook system. In *Proceedings of the 11th international coral reef symposium*, pages 956–960.

Liu, G., Strong, A. E., Skirving, W. J., and Arzayus, L. F. (2006). Overview of NOAA Coral Reef Watch Program's near-real-time satellite global coral bleaching monitoring activities. *Proceedings of the 10th International Coral Reef Symposium*, 1793(August 2016):1783–1793.

Liu, W. T., Tang, W., and Polito, P. S. (1998a). Nasa scatterometer provides global ocean-surface wind fields with more structures than numerical weather prediction. *Geophysical Research Letters*, 25(6):761–764.

Liu, W. T., Tang, W. Q., and Polito, P. S. (1998b). NASA scatterometer provides global ocean-surface wind fields with more structures than numerical weather prediction. *Geophysical Research Letters*, 25(6):761–764. doi 10.1029/98gl00544.

Loya, Y., Sakai, K., Yamazato, K., Nakano, Y., Sambali, H., and van Woesik, R. (2001). Coral bleaching: the winners and the losers. *Ecology letters*, 4(2):122–131. https://doi.org/10.1046/j.1461-0248.2001.00203.x.

Luther, M. E. and O'Brien, J. J. (1989). Modelling the variability in the somali current. *Elsevier oceanography series*, 50:373–386.

Lutjeharms, J. R. (2006). The agulhas current retroflection. *The Agulhas Current*, pages 151–207.

Macdonald, A., Lamb, J., and Schleyer, M. (2013). Panmixia in east african populations of platygyra daedalea (scleractinia: Faviidae). *Western Indian Ocean Journal of Marine Science*, 11:179–191.

Macdonald, A. H., Sampayo, E. M., Ridgway, T., and Schleyer, M. H. (2008). Latitudinal symbiont zonation in stylophora pistillata from southeast africa. *Marine Biology*, 154(2):209–217.

Mackinson, S., Daskalov, G., Heymans, J. J., Neira, S., Arancibia, H., Zetina-Rejón, M., Jiang, H., Cheng, H. Q., Coll, M., Arreguin-Sanchez, F., Keeble, K., and Shannon, L. (2009). Which forcing factors fit? Using ecosystem models to investigate the relative influence of fishing and changes in primary productivity on the dynamics of marine ecosystems. *Ecological Modelling*, 220(21):2972–2987. 10.1016/j.ecolmodel.2008.10.021.

Madeira, C., Alves, M. J., Mesquita, N., Silva, S. E., and Paula, J. (2012). Tracing geographical patterns of population differentiation in a widespread mangrove gastropod: genetic and geometric morphometrics surveys along the eastern african coast. *Biological Journal of the Linnean Society*, 107(3):647–663.

Mafimbo, A. J. and Reason, C. (2010). Air-sea interaction over the upwelling region of the somali coast. *Journal of Geophysical Research: Oceans*, 115(C1):C01001.

Maina, J., Venus, V., McClanahan, T. R., and Ateweberhan, M. (2008). Modelling susceptibility of coral reefs to environmental stress using remote sensing data and gis models. *Ecological modelling*, 212(3-4):180–199.

Mangubhai, S., Harris, A., and Graham, N. A. (2007). Synchronous daytime spawning of the solitary coral fungia danai (fungiidae) in the chagos archipelago, central indian ocean. *Coral Reefs*, 26(1):15–15. https://doi.org/10.1007/s00338-006-0173-y.

Mangubhai, S. and Harrison, P. L. (2008). Gametogenesis, spawning and fecundity of Platygyra daedalea (Scleractinia) on equatorial reefs in Kenya. *Coral Reefs*, 27(1):117–122. 10.1007/s00338-007-0297-8.

Mangubhai, S. and Harrison, P. L. (2009). Extended breeding seasons and asynchronous spawning among equatorial reef corals in Kenya. *Marine Ecology Progress Series*, 374:305–310. doi:10.3354/meps07910.

Manyilizu, M., Dufois, F., Penven, P., and Reason, C. (2014). Interannual variability of sea surface temperature and circulation in the tropical western indian ocean. *African Journal of Marine Science*, 36(2):233–252.

Manyilizu, M., Penven, P., and Reason, C. (2016). Annual cycle of the upper-ocean circulation and properties in the tropical western indian ocean. *African Journal of Marine Science*, 38(1):81–99.

Marchesiello, P., Debreu, L., and Couvelard, X. (2009). Spurious diapycnal mixing in terrain-following coordinate models: The problem and a solution. *Ocean Modelling*, 26(3):156–169.

Mason, E., Molemaker, J., Shchepetkin, A. F., Colas, F., McWilliams, J. C., and Sangrà, P. (2010). Procedures for offline grid nesting in regional ocean models. *Ocean modelling*, 35(1):1–15.

May, R. M. (2001). *Stability and complexity in model ecosystems*, volume 6. Princeton university press. 10.1109/TSMC.1978.4309856.

Maynard, J., Van Hooidonk, R., Eakin, C. M., Puotinen, M., Garren, M., Williams, G., Heron, S. F., Lamb, J., Weil, E., Willis, B., et al. (2015). Projections of climate conditions that increase coral disease susceptibility and pathogen abundance and virulence. *Nature Climate Change*, 5(7):688.

Mayorga-Adame, C. G., Batchelder, H. P., Spitz, Y., et al. (2017). Modeling larval connectivity of coral reef organisms in the kenya-tanzania region. *Frontiers in Marine Science*, 4:92.

McClanahan, T. R. (2000). Bleaching damage and recovery potential of Maldivian coral reefs. *Marine Pollution Bulletin*, 40(7):587–597. 10.1016/S0025-326X(00)00064-3.

McClanahan, T. R., Ateweberhan, M., Muhando, C. A., Maina, J., and Mohammed, M. S. (2007). Effects of climate and seawater temperature variation on coral bleaching and mortality. *Ecological Monographs*, 77(4):503–525.

McClanahan, T. R. and Muthiga, N. A. (2017). Environmental variability indicates a climate-adaptive center under threat in northern mozambique coral reefs. *Ecosphere*, 8(5):e01812.

McCook, L. J. (1999). Macroalgae, nutrients and phase shifts on coral reefs: scientific issues and management consequences for the great barrier reef. *Coral Reefs*, 18(4):357–367. 10.1007/s003380050213.

McCreary, J. P. and Kundu, P. K. (1988). A numerical investigation of the somali current during the southwest monsoon. *Journal of Marine Research*, 46(1):25–58.

McCreary, J. P., Kundu, P. K., and Molinari, R. L. (1993). A numerical investigation of dynamics, thermodynamics and mixed-layer processes in the indian ocean. *Progress in Oceanography*, 31(3):181–244.

McCreary, J. P., Miyama, T., Furue, R., Jensen, T., Kang, H.-W., Bang, B., and Qu, T. (2007). Interactions between the indonesian throughflow and circulations in the indian and pacific oceans. *Progress in Oceanography*, 75(1):70–114.

McField, M., Bood, N., Fonseca, A., ARRIvILLAGA, A., Franquesa Rinos, A., and Loreto Viruel, R. M. (2005). Status of the mesoamerican reef after the 2005 coral bleaching event. *Status of Caribbean coral reefs after bleaching and hurricanes in*, pages 45–60.

McKenna, S. S., Allen, G. G., et al. (2005). *A rapid marine biodiversity assessment of northwest Madagascar. Bulletin of the Rapid Assessment Program 31*. Center for Applied Biodiversity Science, Conservation International.

McPhaden, M. (1982). Variability in the central equatorial indian ocean,. 2. oceanic heat and turbulent energy balances. *Journal of Marine Research*, 40(2):403–419.

McPhaden, M. J., Meyers, G., Ando, K., Masumoto, Y., Murty, V., Ravichandran, M., Syamsudin, F., Vialard, J., Yu, L., and Yu, W. (2009). Rama: the research moored array for african–asian–australian monsoon analysis and prediction. *Bulletin of the American Meteorological Society*, 90(4):459–480.

Meyer, C. P., Geller, J. B., and Paulay, G. (2005). Fine scale endemism on coral reefs: archipelagic differentiation in turbinid gastropods. *Evolution*, 59(1):113–125.

Miller, C. B., Lynch, D. R., Carlotti, F., Gentleman, W., and Lewis, C. V. (1998). Coupling of an individual-based population dynamic model of calanus finmarchicus to a circulation model for the georges bank region. *Fisheries Oceanography*, 7(3-4):219–234.

Miller, K. and Mundy, C. (2003). Rapid settlement in broadcast spawning corals: implications for larval dispersal. *Coral reefs*, 22(2):99–106.

Moberg, F. and Folke, C. (1999). Ecological goods and services of coral reef ecosystems. *Ecological economics*, 29(2):215–233.

Mohammed, M. S., Muhando, C., and Machano, H. (2002). Coral Reef Degradation in Tanzania: Results of Monitoring 1999–2002. *Coral Reef Degradation in the Indian Ocean Status Report 2002*, 1:21–30.

Moss, R. H., Edmonds, J. A., Hibbard, K. A., Manning, M. R., Rose, S. K., Van Vuuren, D. P., Carter, T. R., Emori, S., Kainuma, M., Kram, T., et al. (2010). The next generation of scenarios for climate change research and assessment. *Nature*, 463(7282):747.

Muller-Parker, G., D'elia, C. F., and Cook, C. B. (2015). Interactions between corals and their symbiotic algae. In *Coral Reefs in the anthropocene*, pages 99–116. Springer. https://doi.org/10.1007/978-94-017-7249-5.

Mullon, C., Cury, P., and Penven, P. (2002). Evolutionary individual-based model for the recruitment of anchovy (engraulis capensis) in the southern benguela. *Canadian Journal of Fisheries and Aquatic Sciences*, 59(5):910–922.

Mullon, C., Fréon, P., Parada, C., Van Der Lingen, C., and Huggett, J. (2003). From particles to individuals: modelling the early stages of anchovy (engraulis capensis/encrasicolus) in the southern benguela. *Fisheries Oceanography*, 12(4-5):396–406.

Mumby, P. J., Elliott, I. A., Eakin, C. M., Skirving, W., Paris, C. B., Edwards, H. J., Enríquez, S., Iglesias-Prieto, R., Cherubin, L. M., and Stevens, J. R. (2011). Reserve design for uncertain responses of coral reefs to climate change. *Ecology letters*, 14(2):132–140.

Munday, P., Leis, J., Lough, J., Paris, C., Kingsford, M., Berumen, M., and Lambrechts, J. (2009). Climate change and coral reef connectivity. *Coral Reefs*, 28(2):379–395.

Muths, D., Gouws, G., Mwale, M., Tessier, E., and Bourjea, J. (2012). Genetic connectivity of the reef fish lutjanus kasmira at the scale of the western indian ocean. *Canadian Journal of Fisheries and Aquatic Sciences*, 69:842–853.

Muths, D., Tessier, E., and Bourjea, J. (2015). Genetic structure of the reef grouper e pinephelus merra in the w est i ndian o cean appears congruent with biogeographic and oceanographic boundaries. *Marine Ecology*, 36(3):447–461.

Muths, D., Tessier, E., Gouws, G., Craig, M., Mwale, M., Mwaluma, J., Mwandya, A., and Bourjea, J. (2011). Restricted dispersal of the reef fish myripristis berndti at the scale of the sw indian ocean. *Marine Ecology Progress Series*, 443:167–180.

New, A., Alderson, S., Smeed, D., and Stansfield, K. (2007). On the circulation of water masses across the mascarene plateau in the south indian ocean. *Deep Sea Research Part I: Oceanographic Research Papers*, 54(1):42–74. doi:10.1016/j.dsr.2006.08.016.

Newell, B. S. (1957). *A preliminary survey of the hydrography of the British East African coastal waters*. HM Stationery Office.

Ngoile, M. A. and Linden, O. (1997). Lessons learned from eastern africa: the development of policy on iczm at national and regional levels. *Ocean & Coastal Management*, 37(3):295–318. https://doi.org/10.1016/S0964-5691(98)80009-4.

North, E., Hood, R., Chao, S.-Y., and Sanford, L. (2006). Using a random displacement model to simulate turbulent particle motion in a baroclinic frontal zone: A new implementation scheme and model performance tests. *Journal of Marine Systems*, 60(3-4):365–380.

Obura, D. (2012). The diversity and biogeography of western indian ocean reef-building corals. *PloS one*, 7(9):e45013. https://doi.org/10.1371/journal.pone.0045013.

Obura, D., Bandeira, S., Bodin, N., Burgener, V., Braulik, G., Chassot, E., Gullström, M., Kochzius, M., Nicoll, M., Osuka, K., et al. (2019). The northern mozambique channel. In *World Seas: an Environmental Evaluation*, pages 75–99. Elsevier. doi: https://doi.org/10.1016/B978-0-08-100853-9.00003-8.

Obura, D., Causey, B., and Church, J. (2006). Management response to a bleaching event. *Coral Reefs and Climate Change. Science and Management.*, pages 181–206. doi:10.1029/61CE11.

Obura, D., Smits, M., Chaudhry, T., McPhillips, J., Beal, D., and Astier, C. (2017). Reviving the western indian ocean economy: actions for a sustainable future. *World Wide Fund for Nature (Formerly World Wildlife Fund), Gland, Switzerland Google Scholar*.

Obura, D. O. (2005). Resilience and climate change: lessons from coral reefs and bleaching in the Western Indian Ocean. *Estuarine, Coastal and Shelf Science*, 63(3):353–372. 10.1016/j.ecss.2004.11.010.

Obura, D. O. (2009). Reef corals bleach to resist stress. *Marine Pollution Bulletin*, 58(2):206–212. 10.1016/j.marpolbul.2008.10.002.

Ogallo, L. (1988). Relationships between seasonal rainfall in east africa and the southern oscillation. *International Journal of Climatology*, 8(1):31–43.

Okubo, A. (1970). Horizontal dispersion of floatable particles in the vicinity of velocity singularities such as convergences. In *Deep sea research and oceanographic abstracts*, volume 17, pages 445–454. Elsevier.

Olive, P. (1995). Annual breeding cycles in marine invertebrates and environmental temperature: probing the proximate and ultimate causes of reproductive synchrony. *Journal of thermal biology*, 20(1-2):79–90.

Oliver, J. K., Babcock, R. C., Harrison, P. L., and Willis, B. L. (1988). Geographic extent of mass coral spawning: Clues to ultimate causal factors. *Sixth International Coral Reef Symposium*.

Otwoma, L. M. and Kochzius, M. (2016). Genetic population structure of the coral reef sea star linckia laevigata in the western indian ocean and indo-west pacific. *PloS one*, 11(10):e0165552. https://doi.org/10.1371/journal.pone.0165552.

Padilla-Gamiño, J. L., Pochon, X., Bird, C., Concepcion, G. T., and Gates, R. D. (2012). From parent to gamete: vertical transmission of symbiodinium (dinophyceae) its2 sequence assemblages in the reef building coral montipora capitata. *PLoS One*, 7(6):e38440.

Palumbi, S. R. (2003). Population genetics, demographic connectivity, and the design of marine reserves. *Ecological applications*, 13(sp1):146–158. https://doi.org/10.1890/1051-0761(2003)013[0146:PGDCAT]2.0.CO;2.

Palumbi, S. R., Barshis, D. J., Traylor-Knowles, N., and Bay, R. A. (2014). Mechanisms of reef coral resistance to future climate change. *Science*, 344(6186):895–898.

Palumbi, S. R., Gaines, S. D., Leslie, H., and Warner, R. R. (2003). New wave: high-tech tools to help marine reserve research. *Frontiers in Ecology and the Environment*, 1(2):73–79. doi:10.2307/3868033.

Paris, C. B., Chérubin, L. M., and Cowen, R. K. (2007). Surfing, spinning, or diving from reef to reef: Effects on population connectivity. *Marine Ecology Progress Series*, 347:285–300. 10.3354/meps06985.

Paris, C. B., Cowen, R. K., Claro, R., and Lindeman, K. C. (2005). Larval transport pathways from cuban snapper (lutjanidae) spawning aggregations based on biophysical modeling. *Marine Ecology Progress Series*, 296:93–106.

Parravicini, V., Kulbicki, M., Bellwood, D., Friedlander, A., Arias-Gonzalez, J., Chabanet, P., Floeter, S., Myers, R., Vigliola, L., D'Agata, S., et al. (2013). Global patterns and predictors of tropical reef fish species richness. *Ecography*, 36(12):1254–1262.

Peliz, A., Marchesiello, P., Dubert, J., Marta-Almeida, M., Roy, C., and Queiroga, H. (2007). A study of crab larvae dispersal on the western iberian shelf: Physical processes. *Journal of Marine Systems*, 68(1-2):215–236.

Penven, P., Echevin, V., Pasapera, J., Colas, F., and Tam, J. (2005). Average circulation, seasonal cycle, and mesoscale dynamics of the peru current system: A modeling approach. *Journal of Geophysical Research: Oceans*, 110(C10):C10021.

Penven, P., Lutjeharms, J., and Florenchie, P. (2006). Madagascar: A pacemaker for the agulhas current system? *Geophysical Research Letters*, 33(17):57–61.

Penven, P., Marchesiello, P., Debreu, L., and Lefevre, J. (2008). Software tools for pre-and post-processing of oceanic regional simulations. *Environmental Modelling & Software*, 23(5):660–662.

Planes, S., Doherty, P., and Bernardi, G. (2001). Strong genetic divergence among populations of a marine fish with limited dispersal, acanthochromis polyacanthus, within the great barrier reef and the coral sea. *Evolution*, 55(11):2263–2273.

Planes, S., Jones, G. P., and Thorrold, S. R. (2009). Larval dispersal connects fish populations in a network of marine protected areas. *Proceedings of the National Academy of Sciences*, pages pnas–0808007106. 10.1073/pnas.0808007106.

Pochon, X. and Gates, R. D. (2010). A new symbiodinium clade (dinophyceae) from soritid foraminifera in hawai'i. *Molecular phylogenetics and evolution*, 56(1):492–497.

Pochon, X., LaJeunesse, T., and Pawlowski, J. (2004). Biogeographic partitioning and host specialization among foraminiferan dinoflagellate symbionts (symbiodinium; dinophyta). *Marine Biology*, 146(1):17–27.

Quadfasel, D., Frische, A., and Cresswell, G. (1996). The circulation in the source area of the South Equatorial Current in the eastern Indian Ocean. *Journal of Geophysical Research: Oceans*, 101(C5):12483–12488. 10.1029/96JC00437.

Quod, J.-P. and Bigot, L. (2000). Coral bleaching in the indian ocean islands: Ecological consequences and recovery in madagascar, comoros, mayotte and reunion. *Coral reef degradation in the Indian Ocean*, pages 108–113.

Railsback, S. F. (2001). Concepts from complex adaptive systems as a framework for individual-based modelling. *Ecological modelling*, 139(1):47–62.

Rao, S. A., Behera, S. K., Masumoto, Y., and Yamagata, T. (2002). Interannual subsurface variability in the tropical indian ocean with a special emphasis on the indian ocean dipole. *Deep Sea Research Part II: Topical Studies in Oceanography*, 49(7):1549–1572.

Reason, C., Allan, R., Lindesay, J., and Ansell, T. (2000). Enso and climatic signals across the indian ocean basin in the global context: Part i, interannual composite patterns. *International Journal of Climatology*, 20(11):1285–1327.

Reifen, C. and Toumi, R. (2009). Climate projections: Past performance no guarantee of future skill? *Geophysical Research Letters*, 36(13):L13704.

Rhines, P. B. and Holland, W. R. (1979). A theoretical discussion of eddy-driven mean flows. *Dynamics of Atmospheres and Oceans*, 3(2):289–325.

Rhines, P. B. and Young, W. R. (1982). Homogenization of potential vorticity in planetary gyres. *Journal of Fluid Mechanics*, 122:347–367.

Richmond, R. H. and Hunter, C. L. (1990). Reproduction and recruitment of corals: comparisons among the caribbean, the tropical pacific, and the red sea. *Marine Ecology Progress Series*, pages 185–203.

Ridderinkhof, H. and De Ruijter, W. (2003). Moored current observations in the mozambique channel. *Deep Sea Research Part II: Topical Studies in Oceanography*, 50(12-13):1933–1955. doi:10.1016/S0967-0645(03)00041-9.

Ridderinkhof, H., Van der Werf, P., Ullgren, J., Van Aken, H., Van Leeuwen, P., and De Ruijter, W. (2010). Seasonal and interannual variability in the mozambique channel from moored current observations. *Journal of Geophysical Research: Oceans*, 115(C6):C06010–1.

Risien, C. M. and Chelton, D. B. (2008). A global climatology of surface wind and wind stress fields from eight years of quikscat scatterometer data. *Journal of Physical Oceanography*, 38(11):2379–2413.

Robusto, C. C. (1957). The cosine-haversine formula. *The American Mathematical Monthly*, 64(1):38–40.

Rochford, D. (1964). Hydrology of the indian ocean. iii. water masses of the upper 500 metres of the south-east indian ocean. *Marine and Freshwater Research*, 15(1):25–55.

Roughgarden, J., Gaines, S., and Possingham, H. (1988). Recruitment dynamics in complex life cycles. *Science*, 241(4872):1460–1466.

Rowan, R. (1998). Diversity and ecology of zooxanthellae on coral reefs. *Journal of Phycology*, 34(3):407–417.

Rowan, R. (2004). Coral bleaching: thermal adaptation in reef coral symbionts. *Nature*, 430(7001):742.

Rowan, R., Knowlton, N., Baker, A., and Jara, J. (1997). Landscape ecology of algal symbionts creates variation in episodes of coral bleaching. *Nature*, 388(6639):265.

Rowan, R. and Powers, D. A. (1991). A molecular genetic classification of zooxanthellae and the evolution of animal-algal symbioses. *Science*, 251(4999):1348–1351.

Roxy, M. K., Ritika, K., Terray, P., and Masson, S. (2014). The curious case of indian ocean warming. *Journal of Climate*, 27(22):8501–8509.

Rozenfeld, A. F., Arnaud-Haond, S., Hernández-García, E., Eguíluz, V. M., Serrão, E. A., and Duarte, C. M. (2008). Network analysis identifies weak and strong links in a metapopulation system. *Proceedings of the National Academy of Sciences*, 105(48):18824–18829.

Saji, N., Goswami, B., Vinayachandran, P., and Yamagata, T. (1999). A dipole mode in the tropical indian ocean. *Nature*, 401(6751):360–363.

Santos, S. R. and Coffroth, M. A. (2003). Molecular genetic evidence that dinoflagellates belonging to the genus symbiodinium freudenthal are haploid. *The Biological Bulletin*, 204(1):10–20.

Scheltema, R. S. (1986). Long-distance dispersal by planktonic larvae of shoal-water benthic invertebrates among central pacific islands. *Bulletin of Marine Science*, 39(2):241–256.

Schleyer, M., Kruger, A., and Benayahu, Y. (1997). Reproductive strategies of south african corals. In *Proc 6th int Conf Coelenterate Biol. Nationaal Natuurhistorisch Museum, Leiden, The Netherlands*, pages 429–435.

Schott, F. (1983). Monsoon response of the somali current and associated upwelling. *Progress in Oceanography*, 12(3):357–381.

Schott, F., Fieux, M., Kindle, J., Swallow, J., and Zantopp, R. (1988). The boundary currents east and north of madagascar: 2. direct measurements and model comparisons. *Journal of Geophysical Research: Oceans*, 93(C5):4963–4974. doi:10.1029/JC093iC05p04963.

Schott, F., Swallow, J. C., and Fieux, M. (1990). The somali current at the equator: annual cycle of currents and transports in the upper 1000 m and connection to neighbouring latitudes. *Deep Sea Research Part A. Oceanographic Research Papers*, 37(12):1825–1848.

Schott, F. A. and McCreary Jr, J. P. (2001). The monsoon circulation of the indian ocean. *Progress in Oceanography*, 51(1):1–123.

Schott, F. A., Xie, S.-P., and McCreary, J. P. (2009). Indian ocean circulation and climate variability. *Reviews of Geophysics*, 47(1). 10.1029/2007RG000245.

Schouten, M. W., de Ruijter, W. P., Van Leeuwen, P. J., and Ridderinkhof, H. (2003). Eddies and variability in the mozambique channel. *Deep Sea Research Part II: Topical Studies in Oceanography*, 50(12-13):1987–2003. doi:10.1016/S0967-0645(03)00042-0.

Sebastián, C. R., Sink, K. J., McClanahan, T. R., and Cowan, D. A. (2009). Bleaching response of corals and their symbiodinium communities in southern africa. *Marine Biology*, 156(10):2049–2062.

Selkoe, K. and Toonen, R. J. (2011). Marine connectivity: a new look at pelagic larval duration and genetic metrics of dispersal. *Marine Ecology Progress Series*, 436:291–305.

Shanks, A. L., Grantham, B. A., and Carr, M. H. (2003). Propagule dispersal distance and the size and spacing of marine reserves. *Ecological applications*, pages S159–S169.

Shchepetkin, A. F. and McWilliams, J. C. (2003). A method for computing horizontal pressure-gradient force in an oceanic model with a nonaligned vertical coordinate. *Journal of Geophysical Research: Oceans (1978–2012)*, 108(C3):3090.

Shchepetkin, A. F. and McWilliams, J. C. (2005). The regional oceanic modeling system (roms): a split-explicit, free-surface, topography-following-coordinate oceanic model. *Ocean Modelling*, 9(4):347–404.

Sheppard, C. R. (2003). Predicted recurrences of mass coral mortality in the indian ocean. *Nature*, 425(6955):294.

Sherman, K. (2006). The large marine ecosystem network approach to wssd targets. *Ocean & coastal management*, 49(9-10):640–648. doi 10.1016/j.ocecoaman.2006.06.012.

Shetye, S., Gouveia, A., and Shenoi, S. (1994). Circulation and water masses of the arabian sea. *Proceedings of the Indian Academy of Sciences-Earth and Planetary Sciences*, 103(2):107–123.

Shetye, S. R. and Gouveia, A. D. (1998). Coastal circulation in the north indian ocean: Coastal segment (14, sw). *Journal of Geophysical Research: Oceans (1978–2012)*, 11:523–556.

Shlesinger, Y., Goulet, T., and Loya, Y. (1998). Reproductive patterns of scleractinian corals in the northern red sea. *Marine Biology*, 132(4):691–701.

Spalding, M. D., Fox, H. E., Allen, G. R., Davidson, N., Ferdana, Z. A., Finlayson, M., Halpern, B. S., Jorge, M. A., Lombana, A., Lourie, S. A., et al. (2007). Marine ecoregions of the world: a bioregionalization of coastal and shelf areas. *BioScience*, 57(7):573–583.

Spalding, M. D., Ravilious, C., and Green, E. P. (2001). World atlas of coral reefs. prepared at the unep world conservation monitoring centre. *University of California, Berkeley, EEUU.[Links]*, page 424 p. :.

Steinke, T. and Ward, C. (2003). Use of plastic drift cards as indicators of possible dispersal of propagules of the mangrove avicennia marina by ocean currents. *African Journal of Marine Science*, 25:169–176.

Stramma, L. and Lutjeharms, J. R. (1997). The flow field of the subtropical gyre of the south indian ocean. *Journal of Geophysical Research: Oceans (1978–2012)*, 102(C3):5513–5530.

Straub, D. N. (1994). Dispersive effects of zonally varying topography on quasi-geostrophic rossby waves. *Geophysical & Astrophysical Fluid Dynamics*, 75(2-4):107–130.

Strong, A. E., Liu, G., Meyer, J., Hendee, J. C., and Sasko, D. (2004). Coral reef watch 2002. *Bulletin of Marine Science*, 75(2):259–268.

Subrahmanyam, B., Robinson, I., Blundell, J., and Challenor, P. (2001). Indian ocean rossby waves observed in topex/poseidon altimeter data and in model simulations. *International Journal of Remote Sensing*, 22(1):141–167.

Sumich, J. L. (1996). *An Introduction to the Biology of Marine Life*. Wm. C. Brown Publishers. https://books.google.co.ke/books?id=P2Eu1h0eVgEC.

Swallow, J. (1984). Some aspects of the physical oceanography of the indian ocean. *Deep Sea Research Part A. Oceanographic Research Papers*, 31(6-8):639–650.

Swallow, J., Fieux, M., and Schott, F. (1988). The boundary currents east and north of madagascar: 1. geostrophic currents and transports. *Journal of Geophysical Research: Oceans (1978–2012)*, 93(C5):4951–4962.

Swallow, J. C., Molinari, R. L., Bruce, J. G., Brown, O. B., and Evans, R. H. (1983). Development of near-surface flow pattern and water mass distribution in the somali basin in response to the southwest monsoon of 1979. *Journal of Physical Oceanography*, 13(8):1398–1415.

Swallow, J. C., Schott, F., and Fieux, M. (1991). Structure and transport of the east african coastal current. *Journal of Geophysical Research: Oceans*, 96(C12):22245–22257.

Swearer, S. E., Caselle, J. E., Lea, D. W., and Warner, R. R. (1999). Larval retention and recruitment in an island population of a coral-reef fish. *Nature*, 402(6763):799–802.

Taylor, K. E., Stouffer, R. J., and Meehl, G. A. (2012). An overview of cmip5 and the experiment design. *Bulletin of the American Meteorological Society*, 93(4):485–498.

Taylor, M. S. and Hellberg, M. E. (2003). Genetic evidence for local retention of pelagic larvae in a caribbean reef fish. *Science*, 299(5603):107–109.

Ternon, J., Bach, P., Barlow, R., Huggett, J., Jaquemet, S., Marsac, F., Ménard, F., Penven, P., Potier, M., and Roberts, M. (2014). The mozambique channel: From physics to upper trophic levels. *Deep Sea Research Part II: Topical Studies in Oceanography*, 100:1–9.

Thornhill, D. J., Fitt, W. K., and Schmidt, G. W. (2006). Highly stable symbioses among western atlantic brooding corals. *Coral Reefs*, 25(4):515–519.

Thorrold, S. R., Zacherl, D. C., and Levin, L. A. (2007). Population connectivity and larval dispersal: using geochemical signatures in calcified structures. *Oceanography*, 20(3):80–89.

Tilburg, C. E., Reager, J. T., and Whitney, M. M. (2005). The physics of blue crab larval recruitment in delaware bay: a model study. *Journal of Marine Research*, 63(2):471–495.

Tomczak, M. and Godfrey, J. S. (1994). *Regional oceanography : an introduction*. Pergamon. ISBN:0080410219.

Tomczak, M. and Godfrey, J. S. (2003). *Regional oceanography : an introduction*. Daya Publ. House. https://www.mt-oceanography.info/regoc/pdfversion.html.

Tomczak, M. and Godfrey, J. S. (2013). *Regional oceanography: an introduction*. Elsevier.

Trakhtenbrot, A., Nathan, R., Perry, G., and Richardson, D. M. (2005). The importance of long-distance dispersal in biodiversity conservation. *Diversity and Distributions*, 11(2):173–181.

Treml, E., Roberts, J., Chao, Y., Halpin, P., Possingham, H., and Riginos, C. (2012). Reproductive output and duration of the pelagic larval stage determine seascape-wide connectivity of marine populations. *Integrative and comparative biology*, 52(4):525.

Treml, E. A., Halpin, P. N., Urban, D. L., and Pratson, L. F. (2008). Modeling population connectivity by ocean currents, a graph-theoretic approach for marine conservation. *Landscape Ecology*, 23(1):19–36.

Trench, R. K. (1988). Specificity in dinomastigote-marine invertebrate symbioses: an evaluation of hypotheses of mechanisms involved in producing specificity. In *Cell to Cell Signals in Plant, Animal and Microbial Symbiosis*, pages 325–346. Springer.

Ullgren, J., van Aken, H., Ridderinkhof, H., and de Ruijter, W. (2012). The hydrography of the mozambique channel from six years of continuous temperature, salinity, and velocity observations. *Deep Sea Research Part I: Oceanographic Research Papers*, 69:36–50.

van der Ven, R. M., Triest, L., De Ryck, D. J., Mwaura, J. M., Mohammed, M. S., and Kochzius, M. (2016). Population genetic structure of the stony coral acropora tenuis shows high but variable connectivity in east africa. *Journal of biogeography*, 43(3):510–519.

Van Hooidonk, R., Maynard, J., and Planes, S. (2013). Temporary refugia for coral reefs in a warming world. *Nature Climate Change*, 3(5):508.

Van Hooidonk, R., Maynard, J., Tamelander, J., Gove, J., Ahmadia, G., Raymundo, L., Williams, G., Heron, S. F., and Planes, S. (2016). Local-scale projections of coral reef futures and implications of the paris agreement. *Scientific reports*, 6:39666.

Van Hooidonk, R., Maynard, J. A., Manzello, D., and Planes, S. (2014). Opposite latitudinal gradients in projected ocean acidification and bleaching impacts on coral reefs. *Global Change Biology*, 20(1):103–112.

van Oppen, M. J., Peplow, L. M., Kininmonth, S., and Berkelmans, R. (2011). Historical and contemporary factors shape the population genetic structure of the broadcast spawning coral, acropora millepora, on the great barrier reef. *Molecular Ecology*, 20(23):4899–4914.

Veron, J. (1995). *Corals in space and time: the biogeography and evolution of the Scleractinia*. Cornell University Press.

Veron, J., Stafford-Smith, M., DeVantier, L., and Turak, E. (2015). Overview of distribution patterns of zooxanthellate scleractinia. *Frontiers in Marine Science*, 1:81.

Veron, J. E. N., Hoegh-Guldberg, O., Lenton, T. M., Lough, J. M., Obura, D. O., Pearce-Kelly, P., Sheppard, C. R. C., Spalding, M., Stafford-Smith, M. G., and Rogers, A. D. (2009). The coral reef crisis: The critical importance of <350 ppm CO2. *Marine Pollution Bulletin*, 58(10):1428–1436. 10.1016/j.marpolbul.2009.09.009.

Vic, C., Roullet, G., Carton, X., and Capet, X. (2014). Mesoscale dynamics in the arabian sea and a focus on the great whirl life cycle: A numerical investigation using roms. *Journal of Geophysical Research: Oceans*, 119(9):6422–6443.

Visram, S., Yang, M.-C., Pillay, R. M., Said, S., Henriksson, O., Grahn, M., and Chen, C. A. (2010). Genetic connectivity and historical demography of the blue barred parrotfish (scarus ghobban) in the western indian ocean. *Marine Biology*, 157(7):1475–1487.

Vousden, D., Scott, L. E. P., Sauer, W., Bornman, T., Ngoile, M., Stapley, J., and Lutjeharms, J. (2008). Establishing a basis for ecosystem management in the western indian ocean. *South African Journal of Science*, 104(11-12):417–420. ISSN:0038-2353.

Wakeford, M., Done, T., and Johnson, C. (2008). Decadal trends in a coral community and evidence of changed disturbance regime. *Coral Reefs*, 27(1):1–13. doi:10.1007/s00338-007-0284-0.

Wang, L., Koblinsky, C. J., and Howden, S. (2001). Annual rossby wave in the southern indian ocean: Why does it "appear" to break down in the middle ocean? *Journal of physical oceanography*, 31(1):54–74.

Warner, R. R., Swearer, S. E., Caselle, J. E., Sheehy, M., and Paradis, G. (2005). Natal trace-elemental signatures in the otoliths of an open-coast fish. *Limnology and Oceanography*, 50(5):1529–1542.

Warren, B., Stommel, H., and Swallow, J. (1976). Water masses and patterns of flow in the somali basin during the southwest monsoon of 1964. In *Deep Sea Research and Oceanographic Abstracts*, volume 13, pages 825–860. Elsevier.

Webber, B. G., Matthews, A. J., Heywood, K. J., and Stevens, D. P. (2012). Ocean rossby waves as a triggering mechanism for primary madden–julian events. *Quarterly Journal of the Royal Meteorological Society*, 138(663):514–527.

Weiss, J. (1991). The dynamics of enstrophy transfer in two-dimensional hydrodynamics. *Physica D: Nonlinear Phenomena*, 48(2-3):273–294.

Werner, F. E., Cowen, R. K., and Paris, C. B. (2007). Coupled biological and physical models: present capabilities and necessary developments for future studies of population connectivity. *Oceanography*, 20(3):54–69.

White, W. B. (2000). Coupled rossby waves in the indian ocean on interannual timescales. *Journal of physical oceanography*, 30(11):2972–2988.

Wicks, L. C., Hill, R., and Davy, S. K. (2010). The influence of irradiance on tolerance to high and low temperature stress exhibited by symbiodinium in the coral, pocillopora damicornis, from the high-latitude reef of lord howe island. *Limnology and Oceanography*, 55(6):2476–2486.

Wilkinson, C. and Hodgson, G. (1999). Coral reefs and the 1997-1998 mass bleaching and mortality. *Nature and Resources*, 35(2):16–25.

Wilkinson, C. C. et al. (2004). *Status of coral reefs of the world: 2004*. Australian Institute of Marine Science (AIMS).

Willis, B. L., Babcock, R. C., Harrison, P. L., and Oliver, J. K. (1985). Patterns in the mass spawning of corals on the Great Barrier Reef from 1981 to 1984. *Proceedings Of The Fifth International Coral Reef Congress*.

Wilson, J. and Harrison, P. L. (1998). Settlement-competency periods of larvae of three species of scleractinian corals. *Marine Biology*, 131(2):339–345.

Wood, S., Baums, I., Paris, C., Ridgwell, A., Kessler, W., and Hendy, E. (2016). El niño and coral larval dispersal across the eastern pacific marine barrier. *Nature Communications*, 7:12571.

Wood, S., Paris, C., Ridgwell, A., and Hendy, E. (2014). Modelling dispersal and connectivity of broadcast spawning corals at the global scale. *Global Ecology and Biogeography*, 23(1):1–11.

Wyrtki, K., Bennett, E., and Rochford, D. (1971). *Oceanographic Atlas of the International Indian Ocean Expedition*. National Science Foundation. https://books.google.co.za/books?id=T3fWMQEACAAJ.

Yamagata, T., Behera, S. K., Luo, J.-J., Masson, S., Jury, M. R., and Rao, S. A. (2004). Coupled ocean-atmosphere variability in the tropical indian ocean. *Earth's Climate*, pages 189–211. https://doi.org/10.1029/147GM12.

Appendix A

Model evaluation of the parent domain

The parent domain (31–85°E and 24°N–30°S) of the ROMS simulation designed to simulate the large oceanographic features in the western Indian Ocean region is compared with observational and satellite data in order to establish whether the salient features of the western Indian Ocean are realistically simulated.

Model spin-up

The model was initialised from January and run for a total period of 10 years to obtain a robust, repeating seasonal signal. The integrated properties show that statistical equilibriums reached after a spin-up of 36 months (Figure A.1). For all of the integrated variables, except volume-averaged salinity and temperature, the model exhibits no significant temporal drift after a spin-up period of about 1 year.

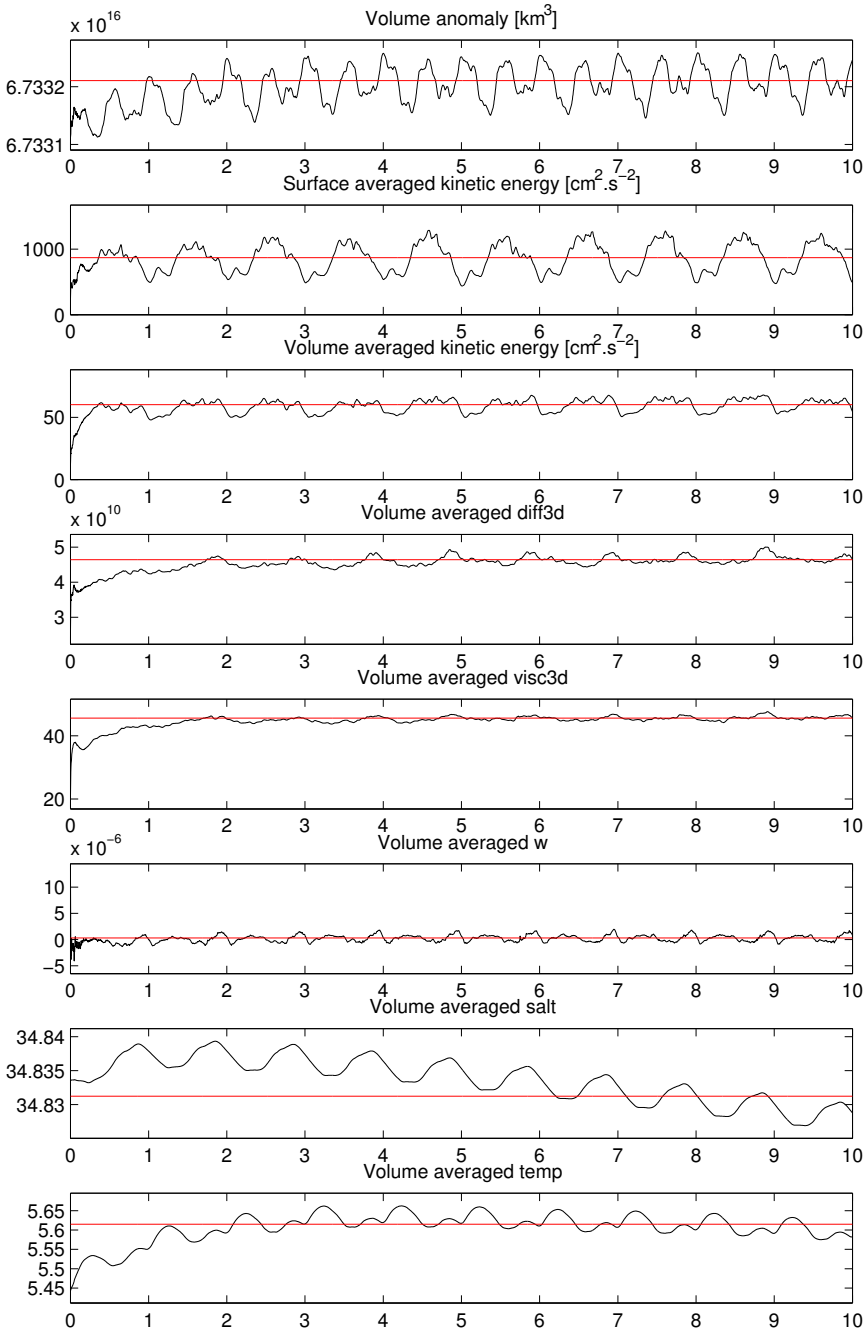

Fig. A.1 Time evolution of different integrated model variables: surface-averaged kinetic energy, volume averaged kinetic energy, volume averaged salinity and volume-averaged temperature

Surface tracer properties

The distribution of water properties in the model is governed by the incorporation of surface fluxes, the incoming signal form the lateral boundary conditions, and internal

physical processes. While the sea surface state may be largely driven by the atmosphere, the underlying thermocline properties are in part determined by the values of boundary conditions.

Comparison with observations shows that the parent domain exhibit a realistic SST pattern across the domain (Figure A.2). The surface heat fluxes and mixed layer depth driven by the surface winds during the monsoons play a great role in the SST distribution in the region. The warmest SST ($\sim$28°C) in the eastern tropical Indian Ocean in all seasons is indicative of the influx of warm Pacific waters via the ITF (Tomczak and Godfrey, 2003). The Indian Ocean domain is generally characterized by warm SSTs that ranges between 26°C south at about 30°S and 28°C at about 10°N during the DJF and MAM as evident by the model as well as in satellite data from TRMM. This period is characterised by moderate winds which reduces the wind-induced evaporative heat loss and vertical mixing. As the SW monsoon sets in, the tropical western Indian Ocean cools with SST value of $\sim$26°C west of about 60°E. Cooling of the region is attributed to the strong and steady monsoonal winds over the region which enhance both wind-induced evaporative cooling and vertical mixing. Both the model and satellite data shows the intense upwelling north of Somalia (about 10°N). The difference between the model and the satellite data shows that model is warmer/cooler although the bias is $\leq$1°C suggesting that part of this signal may be inherited from bias in the large scale solution.

The seasonal cycle of the sea surface salinity for the model is compared with that from the WOA2009 data (Figure A.3). In general the seasonal cycle of salinity in both the model and WOA data shows high values ($\geq$35 psu) in the Arabian Sea and south of 20°N. The spatial distribution of the surface salinity during the DJF and MAM show two distinct salinity tongues at the eastern boundary of the domain. The north-eastern tongue is relatively fresher, water with surface salinity of $\sim$34.5, and enters from the northeast sector of the domain, near 12°S, 75°E with typical characteristics of the Indian Ocean Tropical Surface Water (TSW). Its lower salinity has been associated with the excess of precipitation over evaporation in the tropics (Wyrtki et al., 1971; Tomczak and Godfrey, 1994). On the other hand, the southeastern tongue, near 30°S, 75°E, is saltier water, with surface salinity of $\sim$35.5 which exhibits typical characteristics of the Indian Ocean Subtropical Surface Water (STSW). Its higher salinity is known to be associated with the excess of evaporation over precipitation in the

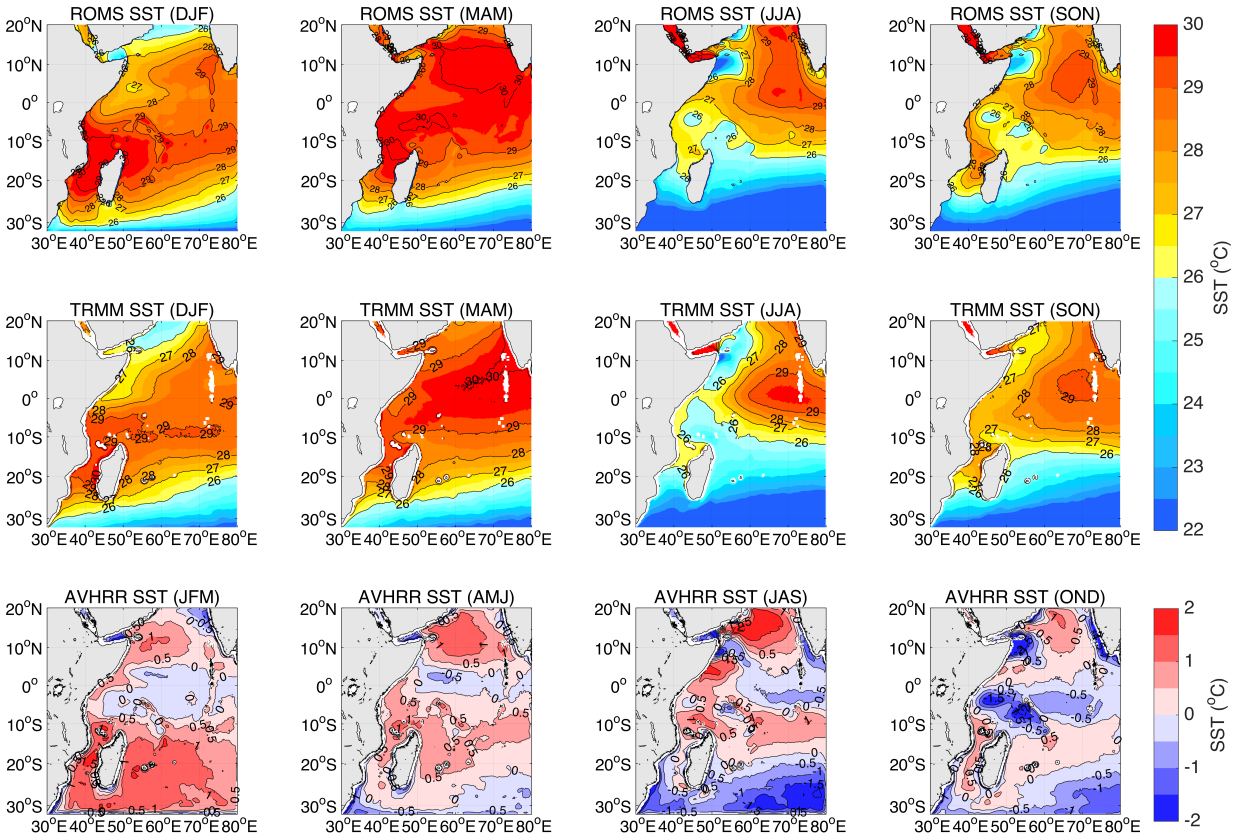

Fig. A.2 Seasonal SSTs (°C) for the parent model domain (upper panel), and TRMM (middle panel) where the contour interval is 1°C. The difference between the model and satellite are shown in the bottom panel, where the contour interval is 0.5°C. Positive (negative) values indicate an over-estimation (underestimation) of SSTs by parent model.

subtropics Wyrtki et al. (1971), within the subtropical gyre. The difference between the model and WOA09 data shows that the model is fresher (by ∼0.4 psu) in most of the domain and saline (by ∼0.6 psu) in the southern part of the Mozambique Channel.

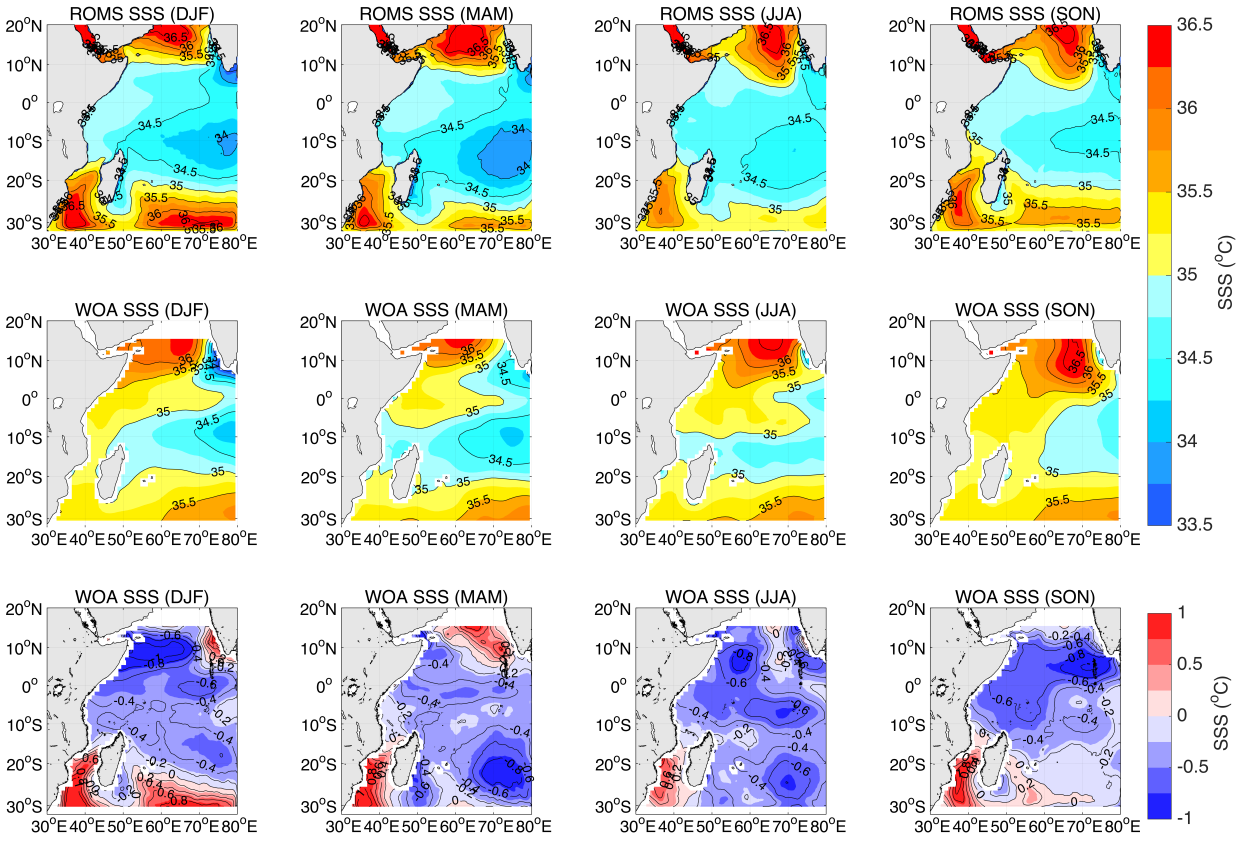

Fig. A.3 Seasonal surface salinity (psu) for the parent model domain (upper panel), and WOA09 (middle panel) where the contour interval is 1 psu. The difference between the model and observations from WOA09 are shown in the bottom panel, where the contour interval is 0.2°psu. Positive (negative) values indicate an over-estimation (underestimation) of surface salinity by parent model.

Sub-surface tracer distribution

Cross-section through the Indian Ocean show that the meridional distribution of upper ocean water masses is well captured. It is clear that although the temperature distribution is reasonably well simulated Figure A.4, the salinity at upper 200 m is less (∼0.2 psu) compared to observations Figure A.5.

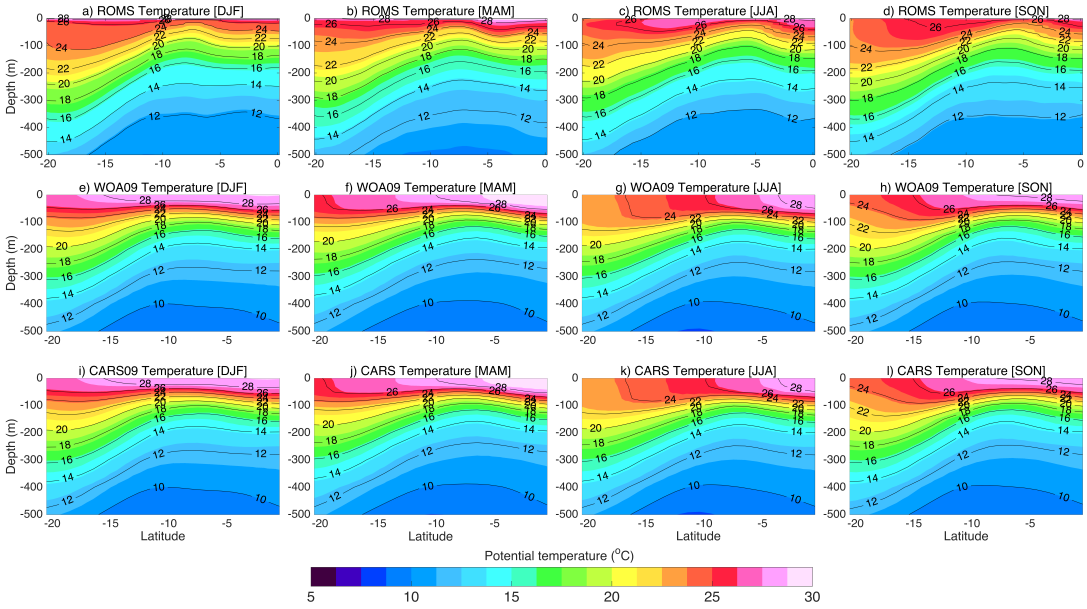

Fig. A.4 Vertical profile of the seasonal mean potential temperature along a meridional section in the parent domain (upper panel), WOA09 (middle panel) and CARS09 (bottom panel)

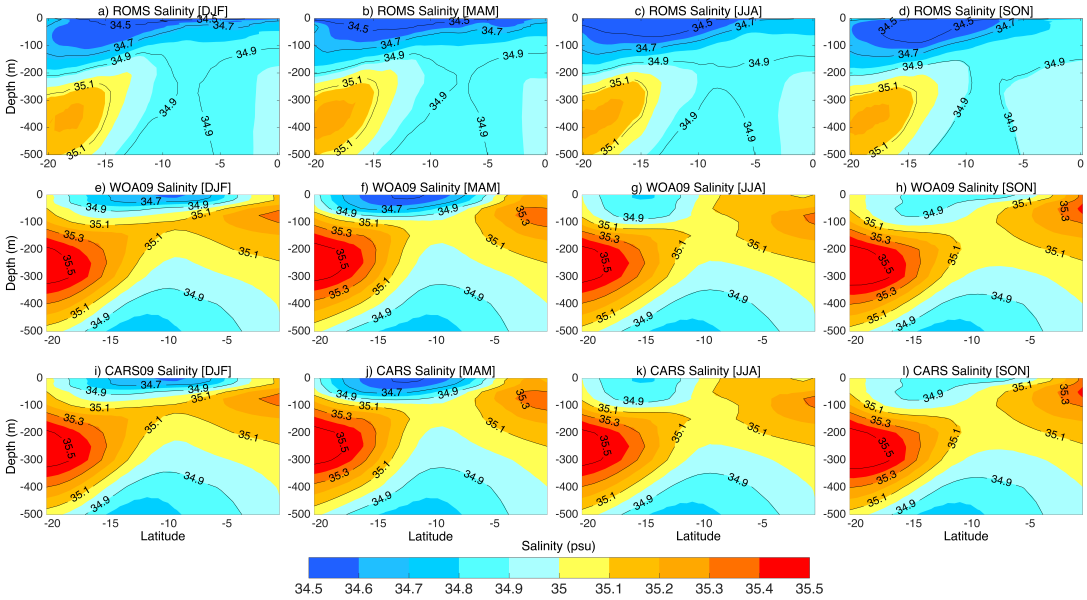

Fig. A.5 Vertical profile of the seasonal mean salinity along a meridional section in the parent domain (upper panel), WOA09 (middle panel) and CARS09 (bottom panel)

Water masses

Salinity as a function of potential temperature (T-S diagram), based on the annual water properties extracted from the meridional transect along the 60°E between 10° –

20°S (as representative of the SEC) from WOA09, CARS09 and model run is shown in Figure A.6. Most of the water masses present in the observational data can also be identified in the model including the Tropical Surface Water (TSW), Subtropical Surface Water (STSW), South Indian Central Water (SICW), Antarctic Intermediate Water (AAIW) and North Atlantic Deep Water.

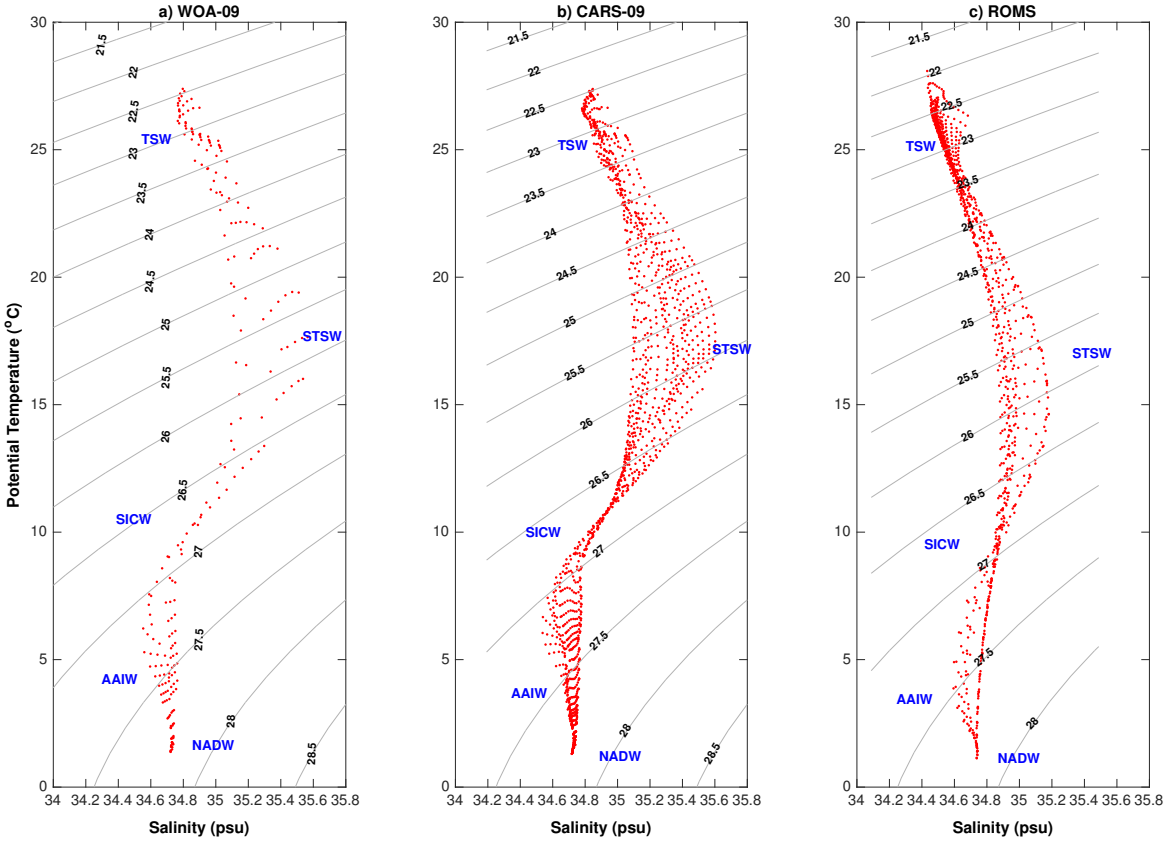

Fig. A.6 Water mass properties of the Indian Ocean sector along the SEC calculated from (a) WOA09, (b) CARS09 and (c) parent domain